american physiological society
PHYSIOLOGICAL REVIEWS
REVIEW ARTICLE

AXON INITIAL SEGMENT STRUCTURE AND FUNCTION IN HEALTH AND DISEASE

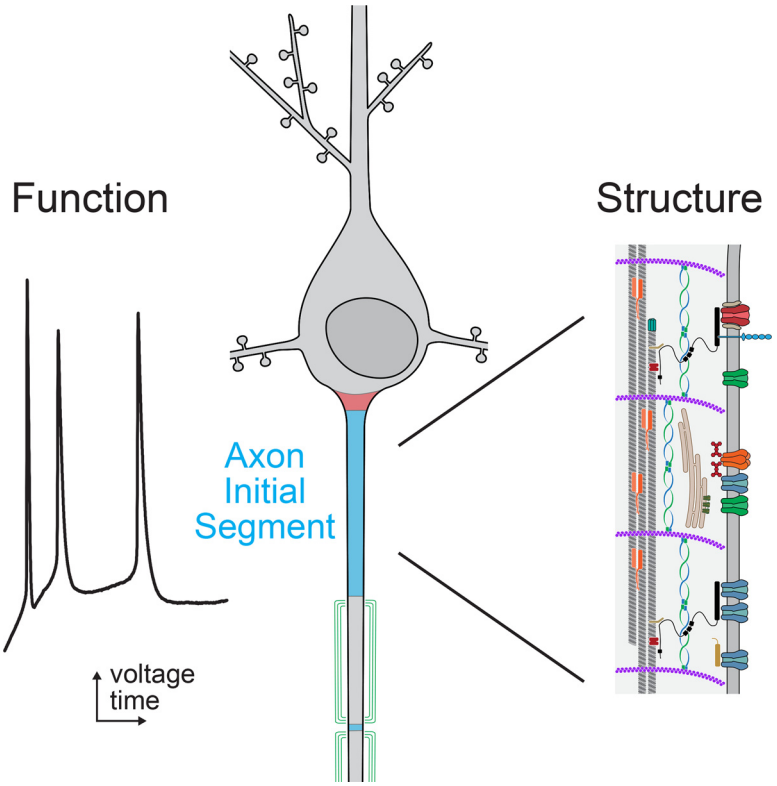

AUTHORS

Paul M. Jenkins, Kevin J. Bender

CORRESPONDENCE

pjenkins@umich.edu; kevin.bender@ucsf.edu

KEY WORDS

ankyrin; axon initial segment; excitability; ion channel; polarity

CLINICAL HIGHLIGHTS

The axon initial segment (AIS) is the site for action potential (AP) generation in most neurons owing to a high concentration of ion channels, transporters, and cell adhesion molecules. Dysfunction in many of the genes encoding these AIS proteins is implicated in neuropsychiatric and neurodevelopmental disorders, including epilepsy, intellectual disability, autism spectrum disorders, bipolar disorder, and others. AIS protein dysfunction can disrupt AP firing, neuronal communication, and network activity and likely contributes to the etiology of these diseases. In addition, there is growing evidence that other conditions, like neurodegenerative diseases, traumatic brain injury, and ischemia, are also associated with significant alterations in AIS structure and function. In this review, we discuss the cellular and molecular mechanisms of AIS formation and plasticity, the physiology of AIS-localized ion channels, and how brain disease could be caused by, or result in, changes in AIS structure and function.

JENKINS AND BENDER, 2025, *Physiol Rev* 105: 765–801
October 31, 2024; Copyright © 2025 the American Physiological Society.
https://doi.org/10.1152/physrev.00030.2024

american physiological society
PHYSIOLOGICAL REVIEWS
Physiol Rev 105: 765–801, 2025
First published October 31, 2024; doi:10.1152/physrev.00030.2024
REVIEW ARTICLE

AXON INITIAL SEGMENT STRUCTURE AND FUNCTION IN HEALTH AND DISEASE

Paul M. Jenkins[1] and Kevin J. Bender[2]

[1]Departments of Pharmacology and Psychiatry, University of Michigan Medical School, Ann Arbor, Michigan, United States and
[2]Department of Neurology, Weill Institute for Neurosciences, University of California, San Francisco, California, United States

Abstract

At the simplest level, neurons are structured to integrate synaptic input and perform computational transforms on that input, converting it into an action potential (AP) code. This process, converting synaptic input into AP output, typically occurs in a specialized region of the axon termed the axon initial segment (AIS). The AIS, as its name implies, is often contained to the first section of axon abutted to the soma and is home to a dizzying array of ion channels, attendant scaffolding proteins, intracellular organelles, extracellular proteins, and, in some cases, synapses. The AIS serves multiple roles as the final arbiter for determining if inputs are sufficient to evoke APs, as a gatekeeper that physically separates the somatodendritic domain from the axon proper, and as a regulator of overall neuronal excitability, dynamically tuning its size to best suit the needs of parent neurons. These complex roles have received considerable attention from experimentalists and theoreticians alike. Here, we review recent advances in our understanding of the AIS and its role in neuronal integration and polarity in health and disease.

ankyrin; axon initial segment; excitability; ion channel; polarity

CLINICAL HIGHLIGHTS

The axon initial segment (AIS) is the site for action potential (AP) generation in most neurons owing to a high concentration of ion channels, transporters, and cell adhesion molecules. Dysfunction in many of the genes encoding these AIS proteins is implicated in neuropsychiatric and neurodevelopmental disorders, including epilepsy, intellectual disability, autism spectrum disorders, bipolar disorder, and others. AIS protein dysfunction can disrupt AP firing, neuronal communication, and network activity and likely contributes to the etiology of these diseases. In addition, there is growing evidence that other conditions, like neurodegenerative diseases, traumatic brain injury, and ischemia, are also associated with significant alterations in AIS structure and function. In this review, we discuss the cellular and molecular mechanisms of AIS formation and plasticity, the physiology of AIS-localized ion channels, and how brain disease could be caused by, or result in, changes in AIS structure and function.

1. OVERALL STRUCTURE AND FUNCTION OF THE AIS

The axon initial segment (AIS) is a specialized membrane domain that extends 10–60 μm into the axon that was first described in the 1960s through a series of elegant electron microscopy studies (1, 2) (**FIGURE 1**). The studies described the AIS as a region of the axon past the axon hillock characterized by an electron-dense membrane undercoat and tightly bundled microtubules, called fascicles. In the decades that followed, the AIS was found to exhibit tight clustering of densely packed membrane proteins, including voltage-gated ion channels, cell adhesion molecules, and transporters (**FIGURE 2**). These proteins are interspersed within evenly spaced actin rings that decorate the AIS membrane (**FIGURE 3**). Subsequent electrophysiological studies demonstrated that, for most neurons, action potentials (APs) are first triggered in the AIS (see recent major reviews from Refs. 6–11).

Over the course of evolution, the AIS has continued to evolve unique and important functions. Invertebrates, like *Caenorhabditis elegans* and *Drosophila melanogaster*, possess an AIS that shares some common features with the more recently evolved mammalian AIS. For example, *Drosophila* ddaE neurons have an AIS-like diffusion barrier that separates the axon and somatodendritic compartments. Furthermore, some *Drosophila* neurons also have an AIS-like region that has an enrichment of ion channels and attendant scaffolding proteins (12). Similarly, *C. elegans* neurons show enrichment of ion channel scaffolds in the proximal axon and conserved functions of both intracellular vesicle filtering and membrane protein diffusion (13). However, for the purpose of this review, we will focus on the vertebrate AIS, which has evolved a number of

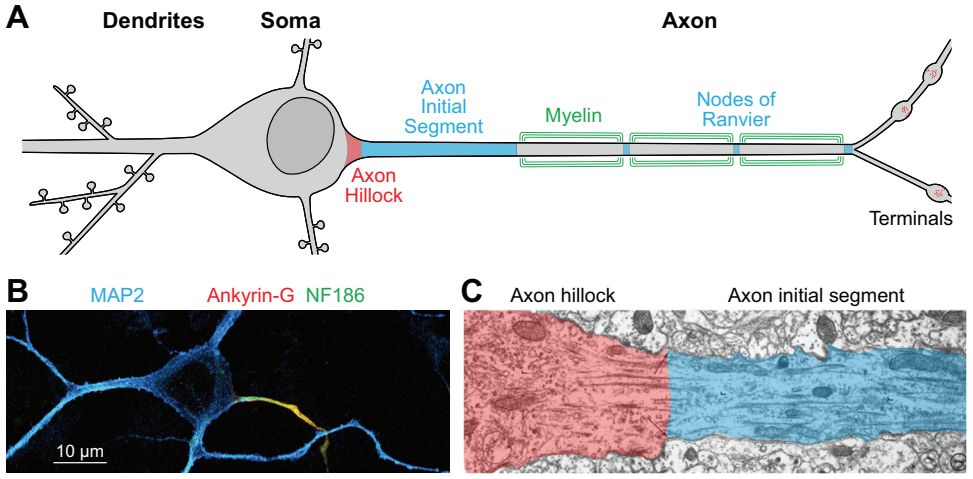

FIGURE 1. Basics of the axon initial segment. *A*: model of a neuron. In most neurons, the axon initial segment (AIS) begins just after the axon hillock, which is where the axon connects to the soma. In myelinated neurons, myelin (green) covers the axon between the nodes of Ranvier. The action potential is initiated within the AIS and propagates down the axon to the nerve terminals where neurotransmitters are released. *B*: representative images of cultured neocortical neuron at day in vitro 7 stained with MAP2 (cyan hot LUT), ankyrin-G (green), and neurofascin-186 (red). Created from unpublished data from Jenkins laboratory, related to Ref. 3. *C*: ultrastructure of the AIS. The AIS (blue) begins after the axon hillock (red) and is marked by a dense submembranous undercoat and microtubule fascicles. Adapted from Ref. 1; used with permission.

additional unique features. For example, convergent evolution of voltage-gated sodium channels (Na_Vs) and one class of potassium channels, KCNQ channels, led to the acquisition of an AIS scaffolding motif that further strengthened the clustering of these channels within the AIS through binding to the scaffolding protein ankyrin-G (14).

1.1. Mechanisms of AIS Formation and Maintenance

1.1.1. Ankyrin-G is the master organizer of the AIS.

The formation of the AIS is controlled by the intracellular scaffolding protein ankyrin-G, the gene product of *ANK3* (**FIGURE 2**). The vertebrate ankyrin gene family is composed of three homologous genes, *ANK1*, *ANK2*, and *ANK3*, that encode the proteins ankyrin-R (15–16), ankyrin-B (18, 19), and ankyrin-G (20, 21), respectively. In general, ankyrins act as intracellular scaffolds by binding a host of interacting partners, using their 24 NH_2-terminal ankyrin repeats and tethering them to the underlying actin cytoskeleton through interactions with β-spectrin, a component of the actin-associated tetrameric spectrin complex (22).

Ankyrin-G was shown to be necessary for initial formation of the AIS, as shRNA-mediated silencing or genetic deletion of *Ank3* in mice causes a complete loss of the AIS (23, 24). Ankyrin-G is widely expressed throughout the body as an ~190-kDa peptide. Outside the AIS, this

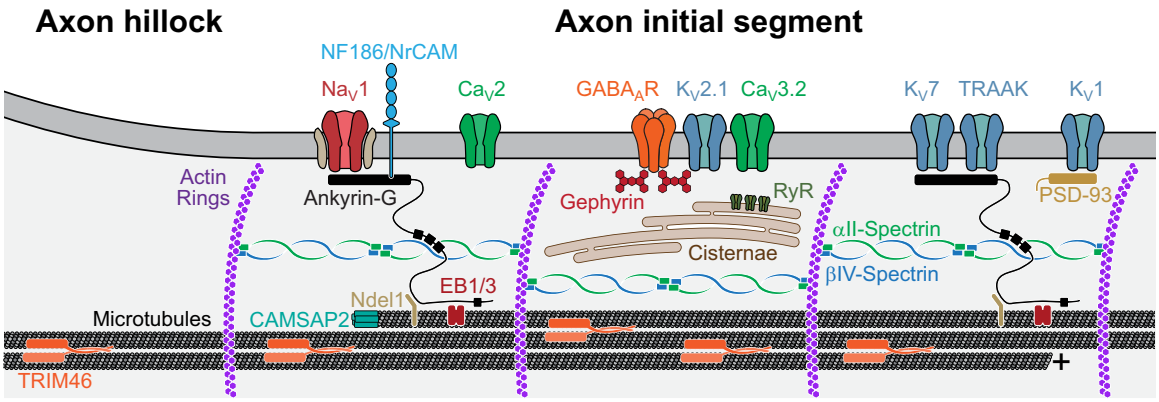

FIGURE 2. Molecular components of the axon initial segment (AIS). The axon initial segment is built by the scaffolding protein ankyrin-G, which binds to ion channels (Na_V1, Na_Vβ-subunits, K_V7), cell adhesion molecules (neurofascin-186, NrCAM), and others and links them to the actin cytoskeleton through interactions with βIV/αII-spectrin tetramers. Other AIS proteins, although ultimately dependent on ankyrin-G, localize to the AIS without binding directly to ankyrin-G. For example, K_V1 localizes through interactions with PSD-93. The AIS is also characterized by bundled, plus-end-out microtubule fascicles that host a number of critical microtubule-associated proteins (EB1/3, CAMSAP2, Ndel1, and TRIM46).

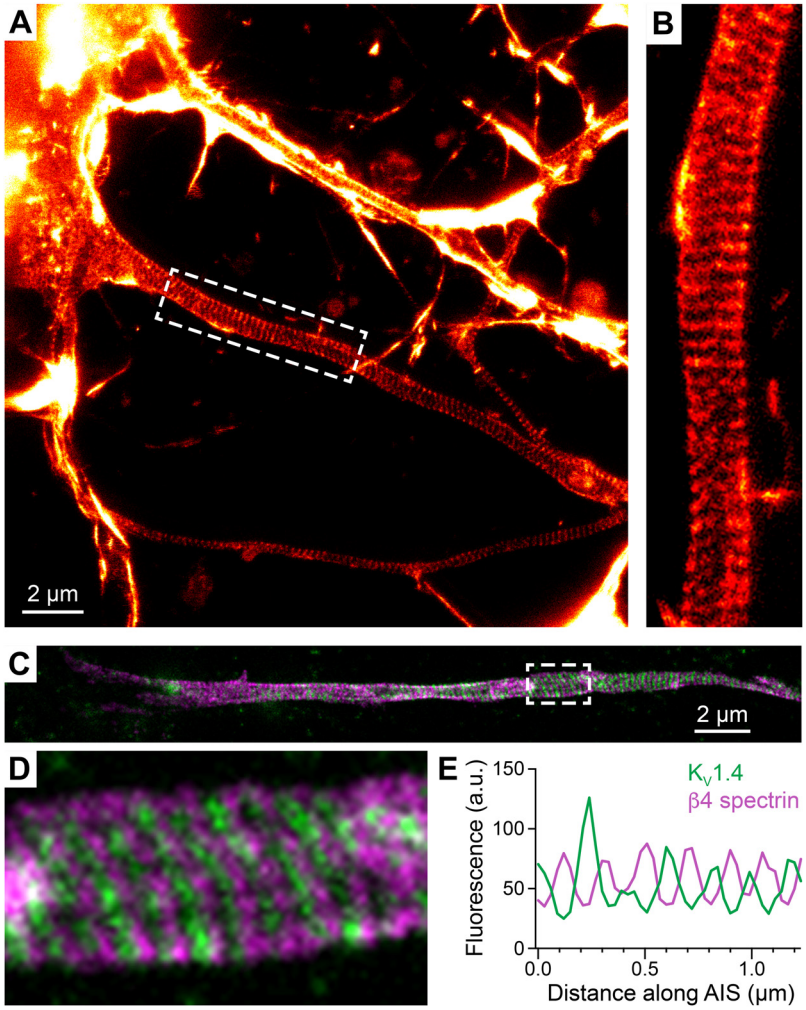

FIGURE 3. The axon initial segment (AIS) contains periodic, evenly spaced rings of actin and AIS proteins. *A*: representative image of cultured hippocampal neuron at day in vitro (DIV) 5 stained with SiR-actin captured by stimulated emission depletion (STED) microscopy. Image courtesy of Dr. Elisa D'Este (Max Planck Institute for Medical Research). Image adapted from Ref. 4; used with permission. *B*: higher magnification image of region of interest marked in *A* showing actin rings, originally described in Ref. 5. *C*: representative image of the AIS of a cultured hippocampal neuron at DIV22 stained with antibodies to Kv1.4 (green) and βIV-spectrin (magenta) captured by STED microscopy. Image courtesy of Dr. Elisa D'Este (Max Planck Institute for Medical Research). *D*: higher magnification image of region of interest marked in *C*. *E*: line fluorescence intensity measurement of *D* showing the nonoverlapping periodicity of K_V1.4 (green) and βIV-spectrin (magenta); a.u., arbitrary units. *C*–*E*: created from unpublished data from Elisa D'Este, related to Ref. 4.

isoform is localized to dendritic spines in cell-like neocortical pyramidal cells. There, it is important for stabilizing AMPA receptors within spines and overall spine structure and density (25). Alternative splicing of a large internal exon within the *ANK3* gene gives rise to giant 270- and 480-kDa isoforms of ankyrin-G (20, 26). Genetic deletion of the large exon or silencing of the 480-kDa isoform with shRNA completely abolishes the AIS and clustering of known ankyrin-dependent partners, including voltage-gated channels, cell adhesion molecules, and GABAergic synapses (27, 28). In neurons, the 480-kDa isoform of ankyrin-G interacts with βIV-spectrin-containing tetramers to link AIS proteins to the actin cytoskeleton (29, 30). In addition, ankyrin-G can interact with the microtubule cytoskeleton through the formation of a complex with the microtubule end-binding proteins EB1 and EB3, which help stabilize ankyrin-G at the AIS (28, 31).

While it is clear that ankyrin-G is strictly required for AIS formation, the exact mechanisms targeting ankyrin-G to the AIS remain incompletely understood. Work in wild-type cultured dorsal root ganglion neurons demonstrated that multiple domains of the 270-kDa isoform of ankyrin-G are required for proper clustering of ankyrin within the AIS, including the serine-rich and tail domains found within the giant exon (26). Further work using *Ank3* knockout-and-rescue in hippocampal neurons demonstrated that only the full-length 480-kDa isoform of ankyrin-G was able to fully recapitulate normal AIS length and position (27). In addition, shRNA targeting only the 480-kDa isoform of ankyrin-G causes a nearly complete loss of ankyrin-G immunoreactivity at the AIS and clustering of ankyrin-dependent AIS proteins (27, 28). Consistent with these results, genetic deletion of the giant *Ank3* exon results in a complete loss of the AIS (27). However, since this deletion results in the loss of both the 270- and 480-kDa forms of ankyrin-G, the possibility that 270-kDa ankyrin-G is also present at the AIS and is participating in protein clustering within this domain cannot be excluded.

The other two ankyrins have unique, mostly nonoverlapping functions within neurons (32). In forebrain neurons, ankyrin-B is found in distal axons, beyond the AIS, where it plays important roles in scaffolding proteins like the cell adhesion molecule L1CAM, which is important in the regulation of axon branching (33). In addition, ankyrin-B contributes to the transport of axonal cargoes through

interactions with dynactin (34). In neocortical pyramidal neurons, ankyrin-B also localizes to dendrites, where it scaffolds $Na_V1.2$ to regulate dendritic excitability (3). Ankyrin-R, which was thought to be predominantly expressed in erythrocytes, has been shown recently to be expressed in forebrain parvalbumin-positive interneurons and in cerebellar Purkinje neurons, where it scaffolds voltage-gated potassium channels (35, 36).

At the molecular level, ankyrins would be predicted to be cytoplasmic proteins owing to their lack of transmembrane domains. However, all three ankyrins are highly membrane-associated due to palmitoylation, which is the addition of the 16-carbon fatty acid palmitate to target protein cysteine residues (37–39). Ankyrin-G is palmitoylated at a single cysteine in the NH_2-terminal ankyrin repeats (C70), and mutation of that residue to a nonpalmitoylatable alanine blocks membrane association, formation of the AIS, and stabilization of GABAergic synapses (38, 40). Palmitoylation is catalyzed by a family of ~23 zinc finger Asp-His-His-Cys motif-containing (zDHHC) palmitoylacytransferase enzymes (41, 42). The 190-kDa isoform of ankyrin-G was shown to be palmitoylated in a functionally redundant manner by two enzymes, zDHHC5 and zDHHC8 (43). Whether these enzymes are responsible for palmitoylation of the giant neuronal isoforms remains unknown. Interestingly, related family member ankyrin-B is palmitoylated on four additional cysteine residues by a different zDHHC enzyme, zDHHC17 (39), which could contribute to the unique, mostly nonoverlapping subcellular localization of ankyrin-B and ankyrin-G in neurons (44, 45).

Another mechanism that has been proposed to regulate the AIS localization of ankyrin-G is the formation of a distal axonal "fence" composed of ankyrin-B and the underlying αII/βII-spectrin cytoskeleton (45). In this model, a distal axonal barrier assembles first and controls the positioning of ankyrin-G within the axon by sterically blocking its movement distally. Several results supported these conclusions: first, ankyrin-B and βII-spectrin appear in the axon of cultured hippocampal neurons before accumulation of ankyrin-G at the AIS. Second, silencing of *Ank2* or associated spectrins caused ankyrin-G to spill from the AIS and become diffusely distributed throughout the axon. Third, overexpression of ankyrin-B causes the position of this fence to shift toward the soma and causes a corresponding shortening of ankyrin-G localization and AIS length.

However, if the ankyrin-B fence is necessary to set the position of the AIS, then one would expect changes in the AIS in *Ank2* null conditions. While this is seen in vitro, *Ank2* null mice show no difference in the number or length of the AIS (23), suggesting that there are potential compensatory mechanisms that protect from AIS loss in vivo. Another possibility is that plasticity-related modulation of the AIS length in response to altered neuronal excitability contributed to these results. Decreases in neuronal excitability are often accompanied by an increase in AIS length, while hyperexcitability causes shortening of the AIS (46). Recent work demonstrated that heterozygous deletion of *Ank2* disrupts the scaffolding of dendritic Na_V channels, resulting in neuronal hypoexcitability (3). This raises the possibility that AIS lengthening in *Ank2* null cultured neurons may reflect more complex, homeostatic efforts to adjust overall excitability. Similarly, overexpression of ankyrin-B may result in excess surface expression of Na_Vs in dendritic domains. If this is true, it may result in excess excitability that may, in turn, promote the shortening of the AIS. Future experiments are needed to understand the exact mechanisms by which ankyrin-B and ankyrin-G cooperate to position the AIS.

1.1.2. Other proteins contribute to the formation and maintenance of the AIS.

While the role of ankyrin-G in the initial establishment of the AIS is well established, it is becoming clear that other resident AIS proteins contribute to the formation and maintenance of the AIS (**FIGURE 2**). Multiple Na_Vs are expressed in central nervous system (CNS) neurons, with mature forebrain excitatory neurons expressing $Na_V1.2$ and $Na_V1.6$ and inhibitory neurons predominantly expressing $Na_V1.1$ and $Na_V1.6$, although exceptions can be found (47–50). Early developmental shRNA-mediated silencing of multiple Na_Vs in cultured spinal motor neurons, cultured hippocampal neurons, or organotypic slices causes reductions in the number of AISs that are positive for ankyrin-G and the intensity of ankyrin-G staining within the AIS (51, 52). By contrast, homozygous deletion of *Scn2a* ($Na_V1.2$) after postnatal day 30 has no effect on ankyrin-G localization or AIS length in the neocortex (53). These seemingly disparate results could be potentially explained by the timing of the Na_V deletion, with early deletion causing deficits in AIS formation (51, 52) and later deletion sparing AIS formation and maintenance (53). Another possibility is that the shRNA targeting multiple Na_V family members has a larger effect on AIS formation than the genetic deletion of a single gene. Deletion of *Scn8a* ($Na_V1.6$) similarly had no effect on ankyrin-G localization or AIS length in neocortical neurons. However, in those cells, $Na_V1.2$ remained localized to the AIS to a much higher extent than in control mice (54). Thus this residual $Na_V1.2$ may be sufficient to maintain normal ankyrin-G localization.

The cell adhesion molecule neurofascin (*Nfasc*) exists as two predominant splice variants, a 155-kDa

isoform found in glial cells and a 186-kDa isoform (NF186) that is found in neurons. Like other AIS proteins, NF186 relies on ankyrin-G for its AIS localization, as deletion of ankyrin-G causes a complete loss of clustering of NF186 in the proximal axon (24, 25). However, NF186 itself may contribute to ankyrin-G clustering at the AIS. For example, shRNA-mediated silencing of NF186 in cultured hippocampal neurons does not block the initial formation of the AIS, as measured by the percentage of cells that exhibit AIS clustering of ankyrin-G, but instead prevents normal clustering of the extracellular matrix protein brevican at the AIS (55). However, using an identical shRNA-silencing approach, Leterrier et al. (51) showed that depletion of NF186 caused an ~40% decrease in clustering of ankyrin-G at the AIS upon assembly as well as alterations on long-term maintenance of the AIS. Genetic deletion of *Nfasc* does not disrupt the formation of the AIS in cerebellar Purkinje neurons or clustering of most AIS components, with the exception of NrCAM (56). However, extended organotypic cultures from these mice cause a progressive loss of AIS components (56).

Ankyrins tether membrane protein complexes to the underlying actin cytoskeleton by binding to the tetrameric spectrin complex (22). Spectrins are obligate heteroteramers that comprise two α-subunits and two β-subunits. There is only one α-subunit found in neurons, αII-spectrin (product of *Sptan1*), which is found in both axonal and somatodendritic compartments (57, 58). While there are multiple β-spectrin proteins in neurons, βIV-spectrin (product of *Sptbn4*) predominates at the AIS (59). Silencing of βIV-spectrin levels using shRNA did not reduce the fraction of cultured neurons that were positive for AIS-clustered ankyrin-G (55). Genetic deletion of *Sptbn4* caused a destabilization of the AIS, resulting in reduced or fragmented staining for AIS proteins, including ankyrin-G (29, 60). Similarly, deletion of *Sptan1* causes disruptions in the AIS clustering of ankyrin-G and disruption of the associated cytoskeleton (57, 58).

The microtubule and end-binding proteins EB1 and EB3 are clustered at high levels within the AIS through interaction with the ankyrin-G tail domain (28, 31). Silencing of ankyrin-G expression causes a marked increase in EB1 and EB3 comets throughout the cells, reduced EB1/3 accumulation at the AIS, and alterations in microtubule polarity in the proximal AIS. Likewise, silencing of EB1 or EB3 causes a decrease in AIS localization of ankyrin-G, an increase in ankyrin-G mobility within the AIS, and an apparent mislocalization to non-axonal processes (28, 31). Ankyrin-G also interacts with the tripartite motif containing (TRIM) protein TRIM46 at the AIS, which plays a key role in axon specification and the formation of parallel microtubule bundles (61). Knockdown of ankyrin-G has been shown to disrupt the accumulation of TRIM46 at the AIS (61). Similarly, the deletion of ankyrin-G prevents AIS accumulation of TRIM46 but does not affect the accumulation of TRIM46 in the proximal 100 μm of the axon (62), suggesting that TRIM46 has ankyrin-G- and AIS-independent mechanisms for axonal localization. The results from TRIM46 silencing or deletion have been more variable. Silencing of TRIM46 expression with shRNA causes a significant decrease in ankyrin-G accumulation at the AIS (61, 63). By contrast, TRIM46 knockout mice exhibit normal axon specification, ankyrin-G AIS accumulation, AIS structure, and neuronal function (62). Perhaps the differences between paradigms are reflective of compensation from unknown protein(s) in the TRIM46 knockout mouse that does not occur in acute knockdown conditions.

Taken together, these results highlight that, while ankyrin-G is the organizer of the AIS, both its initial levels at the AIS and the long-term stability of the structure rely on the full complement of AIS proteins.

1.1.3. Expanding the AIS proteome.

Given its critical role in neuronal polarity and excitability, there has been great interest in finding pathways that would allow manipulation of the AIS, either experimentally or therapeutically. To date, much of the focus has been on identifying candidate proteins and pathways based on homology to other ankyrin/spectrin complexes, like those found in erythrocytes or at nodes of Ranvier. Other candidate discovery approaches, like yeast-two-hybrid screens, have been used to identify novel interacting partners for resident AIS proteins, like ankyrin-G (40, 64). However, these assays are often limited by the size and/or behavior of the bait protein chimera, which must fold properly and enter the nucleus for the assay to work. In addition, since these chimeras include nonnative proteins, there is an added concern that normal posttranslational modification, which can be required for binding, may not occur. Similarly, immunoprecipitation-mass spectrometry experiments are often limited by the relative insolubility and sensitivity to proteolysis of many AIS protein complexes.

To overcome these limitations, recent work has focused on the use of proximity labeling approaches with promiscuous biotin ligases fused to resident AIS proteins. These approaches, in which biotin is added to lysine residues of putative interacting proteins within a short radius (~10 nm), have the advantage that they can detect transient or weak interactions and do not rely on detergent solubilization and detection approaches described above. The addition of the

biotin ligase BirA* to multiple AIS proteins, including NF186, Ndel1, and TRIM46, allowed the proximity mapping of the AIS at multiple depths relative to the plasma membrane, with the NF186 cytoplasmic domain being very close to the plasma membrane and Ndel1 and TRIM46 being closer to the cytoplasmic microtubule bundles found deeper in the axoplasm (65). This screen identified multiple known AIS proteins, including αII- and βIV-spectrin, ankyrin-G, NF186, and $Na_V1.2$, but also failed to detect other known AIS proteins, including $Na_V1.6$, NrCAM, KCNQ2/3, Caspr2, and PSD-93. This indicates that a failure to detect a particular protein does not necessarily mean that it is missing from the AIS, as a lack of identification could reflect spatial restrictions relative to the AIS protein-BirA* fusion or a developmental window that missed these potential interactions. Multiple novel AIS proteins were also identified, including proteins likely to be involved with protein trafficking and sorting, cytoskeletal remodeling, and neuronal polarity (65).

Similar approaches were used to examine the extracellular proteome of the AIS by targeting horseradish peroxidase-coupled secondary antibodies to the AIS by binding to primary antibodies directed against the extracellular domain of NF186. The addition of biotin-tyramide and hydrogen peroxide creates biotin phenoxyl radicals that allow proximity biotin labeling of proteins within ~250 nm of the secondary antibody-fused horseradish peroxidase (66, 67). Using this approach, Ogawa and colleagues (68) identified a novel cell adhesion molecule, contactin-1, which is a widely expressed glycosylphosphatidyl inositol (GPI)-anchored cell adhesion molecule. Contactin-1 was shown to be clustered at the AIS by CRISPR-mediated epitope tagging of the native *Cntn1* gene, and this localization was dependent on binding to the L1 cell adhesion molecules NF186 and NrCAM. Knockout of *Cntn1* impaired extracellular matrix formation at the AIS and led to significant decreases in axo-axonic innervation at both Purkinje neurons in the cerebellum and somatosensory cortex pyramidal neurons (68). Thus a range of approaches have helped to begin to unravel the proteome at the AIS, which may provide insight into novel regulatory mechanisms for the control of AIS formation and maintenance.

1.2. Molecular Functions of the AIS

1.2.1. Regulation of neuronal polarity.

The AIS is a key landmark that separates the somatodendritic compartment from the axon, and this domain has been proposed to be a key regulator of neuronal polarity. This idea has been supported by work showing that removal of the AIS causes the proximal axon to exhibit features normally seen in dendrites (**FIGURE 4**). For example, shRNA-mediated silencing of *Ank3* causes loss of the AIS and mislocalization of the somatodendritic proteins MAP2, the K^+/Cl^- cotransporter KCC2, and β1-integrin into the axonal compartment (23, 69). Similarly, genetic deletion of the giant isoforms of *Ank3* causes MAP2 mislocalization into the proximal axon (27). In addition to protein mislocalization, in the absence of an AIS, the proximal portion of the neurite that eventually becomes the axon exhibits structural features that are consistent with dendritic identity, like dendritic spines (23, 27, 70).

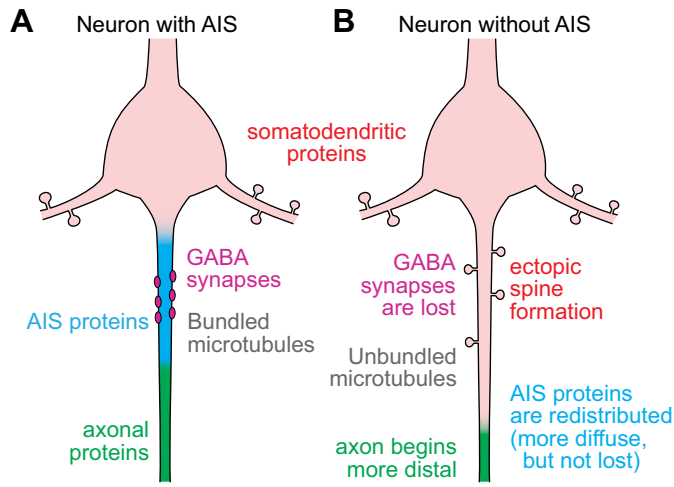

FIGURE 4. Effects of axon initial segment (AIS) loss on neuronal structure. *A*: neurons that have a normal AIS are characterized by separation of axonal and somatodendritic compartments, high levels of clustering of AIS proteins, and GABAergic cartridge synapses arising from chandelier cells. *B*: neurons that lose their AIS through manipulations like genetic deletion of ankyrin-G exhibit multiple kinds of cellular dysfunction. Dendritic proteins are able to enter the proximal part of the axon causing development of ectopic dendritic spines. The interface between the axon and somatodendritic compartment moves distally within the neurite that is to become the axon. AIS protein clustering within the AIS is lost and proteins are redistributed within the cell. GABAergic synapses at the AIS are lost.

While it is clear that the molecular composition and structural identity of the proximal axon are highly regulated by the AIS, additional AIS-independent mechanisms exist to maintain the separation of the somatodendritic and axonal compartments. For example, while deletion of *Ank3* causes MAP2 mislocalization into the proximal axon, this dendritic protein is eventually excluded from the axon, and separation of axon and dendrite resumes, although the interface is further from the cell body than normally seen in neurons possessing an AIS (27). Similarly, the relative distribution of the transferrin receptor and TGN38, proteins normally found in the dendritic compartment, is unchanged upon removal of the AIS when comparing the dendrites to the distal axon (>50 μm from the soma) (27), suggesting that the axon-dendrite interface is shifting positions within the cell. Similar results were seen with the dendritic spine phenotype,

where distal axons lose dendritic spines and acquire normal axonal features like the presence of neurofilament (27, 70). The ankyrin-G- and AIS-independent maintenance of axon specification and polarity was also seen with shRNA-mediated silencing of *Ank3* in rat neocortex, where axons that lacked ankyrin-G and an AIS still crossed the corpus callosum into the contralateral cortex despite the proximal neurite acquiring dendritic characteristics (45). Together, these results demonstrate that the AIS is important for the maintenance of the axonal character of the proximal axon but not for the overall specification of the axon or distal axonal polarity, suggesting that additional AIS-independent mechanisms exist for the maintenance of neuronal polarity.

1.2.2. Regulation of polarized distribution of proteins.

Neurons rely on the polarized distribution of proteins between the somatodendritic and axonal compartments for the proper processing of signaling inputs and subsequent output to downstream cells. The AIS contributes to this polarized distribution of proteins through multiple mechanisms, including serving as a site for the sorting of molecular motor-bound vesicles and acting as a membrane and cytoplasmic barrier.

The unique subcellular distribution of somatodendritic and axonal proteins is achieved, in part, through polarized transport of cargoes onto motor-driven vesicles bound for these cellular compartments (reviewed in Ref. 71). As nascent membrane proteins transit the rough endoplasmic reticulum and Golgi network, they are loaded onto vesicles associated with specific kinesin and dynein motors that utilize the microtubule cytoskeleton to traffic these proteins to their ultimate destinations. Vesicles containing axon-bound cargoes freely enter both the axonal and dendritic compartments, although they enter the axon with a greater frequency (72, 73). By contrast, vesicles containing somatodendritic cargoes are excluded from the axon (72, 74–76). Multiple mechanisms have been proposed for this polarized transport process, including recruitment of axon-specific motor proteins to axonal microtubules and an active removal of mistargeted dendrite-bound vesicles from the axon (77).

Axonal transport of cargo along microtubules is accomplished, in large part, by the kinesin-1 (KIF5A-C) family of microtubule motors (73, 78). Axon-bound kinesin motors exhibit a striking change in movement during early neuronal development between developmental *stages 2* and *3*, when neurons transition from having multiple immature neurites (*stage 2*) to a single long neurite that becomes the axon (*stage 3*) (79) (**FIGURE 5**). For example, a fluorescently labeled and truncated form of KIF5C equally samples multiple neurites during *stage 2* but redirects almost exclusively to the axon as the growth cone emerges and the axon growth rate increases (80). This recruitment occurs through preferential binding of microtubules within the AIS (73). These processes occur as the axon is being specified and well before the establishment of the AIS.

In some cases, vesicles bound for the somatodendritic compartment travel along microtubules that direct them toward the axon. However, once they reach the proximal axon, the vesicles stop and are returned to the somatodendritic compartment. Given the position of the AIS between these two compartments, a great deal of work has focused on the retrieval of somatodendritic cargoes from the AIS, which relies on actin- and myosin-

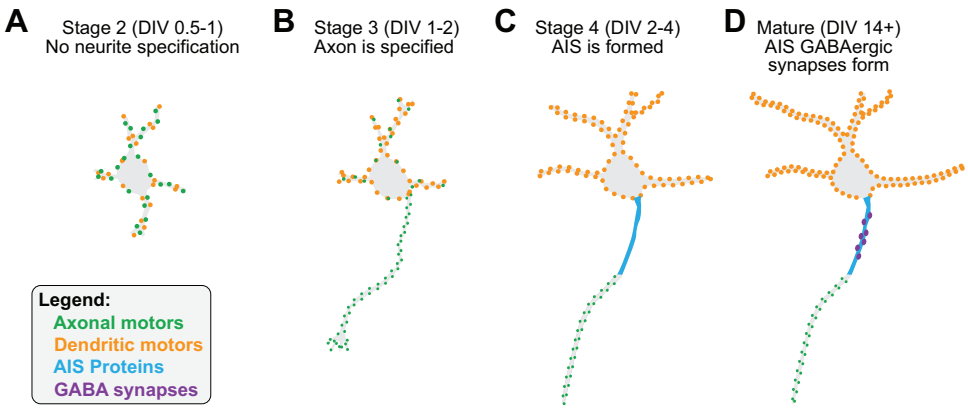

FIGURE 5. Developmental stages of axon initial segment (AIS) formation in cultured neurons. *A*: in stage 2 neurons (12–24 hours after plating), multiple immature neurites form. Axonal (green) and dendritic (orange) molecular motors equally sample each neurite. *B*: as neurons reach *stage 3* [days in vitro (DIV) 1 and 2], 1 neurite undergoes a growth spurt, eventually becoming the axon. At this point, before the AIS has formed, axonal motors begin to exhibit strong preference for the axonal neurite and dendritic motors begin to show dendrite-specific transport. *C*: during *stage 4* (DIV2–4), ankyrin-G begins to assemble the AIS (blue). AIS proteins are clustered with ankyrin-G and form a multiprotein complex necessary for maintenance of AIS structure and function. *D*: as neurons mature (DIV14+), chandelier cells form GABAergic cartridge synapses on the AIS (purple). Neurodevelopmental stages based on Ref. 79.

based vesicle capture and retrieval process (**FIGURE 6**). In this process, vesicles are first halted through interactions between the cytoplasmic domain of somatodendritic cargo proteins and myosin V motors, which interact with actin patches in the AIS to prevent further procession of the vesicles (81–85). Once arrested, these vesicles are then removed from the proximal axon by minus-end-directed dynein motors, which are activated by the Ndel1-LIS1 complex (86, 87) or through a Rab5 and FHF-dependent process (88). Interestingly, it was shown that the sorting of most somatodendritic cargoes occurs proximal to the AIS, within the axon hillock, in a zone termed the preaxon exclusion zone (PAEZ) (76). The PAEZ serves as a recognition site for axon-bound kinesin motors, which utilize acetylated microtubules to pass through the PAEZ into the axon (**FIGURE 6**). Consistent with this idea, conferring KIF5 binding to somatodendritic cargoes allowed them to bypass the PAEZ and enter the axon. On the other hand, axonal entry was blocked with a KIF5 dominant-negative peptide (76). This sorting process occurred even in neurons lacking an AIS, as ankyrin-G shRNA treatment did not block exclusion of the somatodendritic transferrin receptor from the axon (76), consistent with results seen in ankyrin-G null mice (27).

Given these results, how do we reconcile the role of the AIS in neuronal polarity and polarized sorting of cargo? On one hand, motors and cargoes show a preference for their respective compartments before the establishment of the AIS, and AIS deletion alone does not remove the barrier for somatodendritic proteins entering the axon proper. On the other hand, the proximal axon certainly acquires dendritic characteristics, including the presence of dendritic spines and entry of somatodendritic proteins (at least proximally) when the AIS is deleted (**FIGURE 4**). This suggests a similar situation to what we see with protein clustering at the AIS. In that case, ankyrin-G establishes the AIS and recruits other critical binding partners, like ion channels, cytoskeletal proteins, and cell adhesion molecules. These binding partners then play a key supportive role in AIS maintenance. In the case of neuronal polarity, the initial specification of the axon and establishment of polarized cargo sorting occurs first, before formation of the AIS. However, it is clear that the AIS is necessary for maintaining the normal function of these processes, as deletion of the AIS shifts the position of the separation between these compartments.

1.2.3. Cytoplasmic filter and diffusion barrier.

In addition to participating in the polarized sorting of motor-driven cargo, the AIS limits the diffusion of cytoplasmic and plasma membrane proteins as well as plasma membrane lipids (89–91). For example, cultured hippocampal neurons develop a cytoplasmic “filter” that reduces the entry of fluorescently labeled 70-kDa dextran between 3 and 5 days after being plated [days in vitro (DIV) 3–5], during the time when the AIS is forming (92). Pharmacological disruption of F-actin reduced the ability of the filter to exclude dextran, as did ankyrin-G depletion (92). Multiple studies have demonstrated a similar restriction of membrane protein and lipid movement within the AIS, termed the AIS diffusion barrier. The transmembrane protein L1CAM, as well as the membrane outer leaflet GPI-anchored protein Thy1, showed significant restriction of mobility within the AIS but not in the distal axon (89). When fluorescent lipids were fused with the axons of DIV14 hippocampal neurons, the lipids

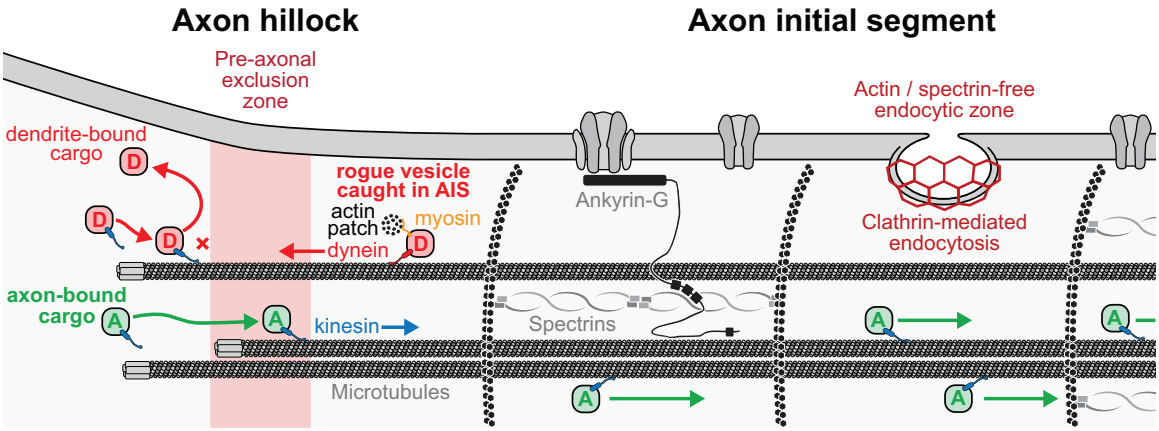

FIGURE 6. Axon initial segment (AIS) function in protein sorting and trafficking. Vesicles containing axonal cargo (green) are recruited to the axon at the preaxon exclusion zone (PAEZ), where they traffic into the axon on plus end-out microtubules. Vesicles containing dendritic cargo (red) are turned back at the PAEZ. Those that inappropriately enter the AIS are retrieved and returned to the soma through the activity of actin-based myosin motors. Within the AIS proper, areas devoid of the submembranous actin-spectrin mesh serve as sites for clathrin-mediated endocytosis within the AIS. The tight clustering of proteins within the AIS and their tethering to the actin cytoskeleton serve as a diffusion barrier that limits protein and lipid mobility within the plane of the membrane and in the axoplasm.

were restricted to the axon and did not diffuse into the somatodendritic compartment, suggesting the presence of a lipid diffusion barrier (90). However, a subsequent study argued that insufficient time was allowed for the lipids to reach the hillock (93). To directly address this question, Nakada et al. (91) used single-molecule imaging of dioleoylphosphatidylethanolamine (DOPE) phospholipids in DIV10 hippocampal neurons and found that the diffusion rate was reduced 800-fold in the AIS compared to the surrounding membranes. This decrease in lipid mobility was proposed to be the result of highly concentrated membrane proteins at the AIS and their subsequent anchoring to the dense submembranous cytoskeleton. In this model, membrane proteins act as "pickets" bound to an actin "fence" that restricts the movement of proteins and lipids that encounter the fence (94).

While the AIS is widely accepted to act as a diffusion barrier, a major challenge has been testing the functional necessity of this barrier in the separation of axonal and somatodendritic compartments. For example, pharmacological disruption of the actin cytoskeleton increases the lateral mobility of L1CAM and Thy1 within the AIS and further disrupts the polarized localization of NgCAM (89). This raises the question of whether this is due to disruption of the AIS diffusion barrier or due to disruption of the actin-based protein sorting machinery within the AIS (83). Similarly, protein and lipid diffusion are high in young neurons that lack an AIS or in cells where the AIS has been removed by ankyrin-G depletion. Yet, neurons without an AIS still exhibit separation of the somatodendritic and axonal compartments, albeit in a different location, despite the loss of highly clustered AIS proteins. This raises the question of whether a more distal diffusion barrier separates these domains in the absence of an AIS.

1.2.4. Control of microtubule organization.

Since the initial descriptions of the AIS were based on electron microscopy studies from Palay et al. (1) and Peters et al. (2), the AIS was defined by tightly bundled fascicles of microtubules. These bundled microtubules rely on the presence of ankyrin-G as *Ank3* null mice exhibit a loss of both the microtubule bundles and the dense membranous undercoat that are identifying features of the AIS (70). Recent work has shed light on the mechanisms that contribute to microtubule bundle formation within the AIS. Multiple microtubule-associated proteins are found at the AIS, including EB1/EB3, Ndel1, CAMSAP2, and TRIM46 (28, 31, 63, 86, 95) (**FIGURE 2**). Ankyrin-G interacts with EB1 and EB3 through motifs found in the tail domain (28), and these complexes help anchor microtubule bundles to the AIS plasma membrane (28, 31). In addition, ankyrin-G interacts with TRIM46, thereby promoting the formation of stable microtubule parallel bundles (61, 63). This TRIM46 accumulation occurs during the transition from *stage 3* to *stage 4* of neuronal development, preceding clustering of ankyrin-G, and extends proximal to the AIS into the presumed PAEZ (96). Similar localization is seen with microtubule-affinity regulating kinase 2 (MARK2) (97), which plays a key role in regulating tau association with microtubules (98). Thus the AIS and PAEZ work together to serve as a major microtubule organizing center, arranging the microtubule cytoskeleton and its associated proteins to maintain separation of axonal and somatodendritic compartments.

1.2.5. Regulation of endocytosis.

Given that the AIS membrane is densely packed with proteins, it was generally assumed that little membrane endocytosis occurred here. The dense membranous "undercoat" (**FIGURE 1**), tightly spaced actin rings (**FIGURE 3**), and highly clustered ankyrin/spectrin complexes (**FIGURE 2**) are all positioned in ways that could make membrane access for endocytic machinery difficult. However, evidence has emerged in just the past few years indicating that endocytosis does occur at the AIS and, in fact, contributes markedly to overall neuronal structure and function.

The first role of AIS-localized endocytosis is related to protein trafficking. Axonal and somatodendritic proteins that are incorrectly targeted to the AIS are rapidly cleared by endocytosis and sent to late endosomes for degradation (13). Shockingly, some proteins seem to utilize AIS insertion and endocytosis as a normal part of their trafficking pathway. For example, after neuroligin 1 is released from the endoplasmic reticulum, it is first inserted into the AIS plasma membrane after which it rapidly relocalizes to dendritic spines (99). Second, conditions that induce long-term synaptic depression drive Na_V endocytosis, demonstrating that regulated endocytosis within the AIS controls neuronal excitability (100). This is seen during development, where nuclear mitotic apparatus protein 1 (NuMA1) transiently localizes to the AIS during development to block endocytosis of multiple AIS membrane proteins, thus promoting their stability (101).

How is the process of endocytosis regulated at the AIS? The inner leaflet of the AIS membrane is covered with ankyrin-G and the underlying spectrin/actin cytoskeleton, which would presumably make access by the endocytic machinery more challenging. In polarized epithelial cells, ankyrin-G and spectrin similarly coat the lateral membrane but are patterned into nonuniform microdomains that move within the plane of the membrane to sweep away the endocytic machinery, thus slowing the rate of endocytosis (102). Strikingly, recent

work suggests that similar mechanisms occur within the AIS. Using a combination of superresolution microscopy and platinum replica electron microscopy, Wernert et al. (103) showed that clathrin-coated pits form on patches of AIS membrane devoid of spectrin and actin (**FIGURE 6**) in areas between the actin rings (**FIGURE 3**). Disruption of the spectrin scaffold or spectrin depletion increased the formation of clathrin-coated pits. Although not directly associated with an increased rate of endocytosis, these pits exhibit a long lifetime on the plasma membrane. They are therefore positioned to act as long-lived access sites for endocytic machinery, allowing for the removal of appropriate proteins like those that are no longer interacting with scaffolds like ankyrin-G (103). Further work is necessary to identify signaling pathways that regulate AIS endocytosis.

1.3. AIS-Localized Ion Channels and Neuronal Excitability

1.3.1. Sodium channels.

Action potentials (APs) are triggered in the AIS of most cells that have axons, largely due to the high expression of voltage-dependent sodium channels (Na_Vs) in this region (104–111). Indeed, the AIS has such a high concentration of Na_Vs that one can define the AIS based solely on Na_V localization (112). It is these channels, combined with the small size of the AIS that requires minimal charge to depolarize, that make it easier to initiate an AP here than in any other region (113). Decades of work have explored how these channels concentrate to the AIS, which Na_V isoforms localize to the AIS of different cell classes, and how the biophysical properties of Na_Vs expressed in different regions of the AIS affect different aspects of AP initiation and propagation. From these studies, certain themes have emerged.

After early embryogenesis, three main sodium channels are expressed in neurons of the central nervous system (CNS): $Na_V1.1$, $Na_V1.2$, and $Na_V1.6$ (**FIGURE 7**). They are expressed to varying degrees depending on cell type, with $Na_V1.6$ being expressed almost ubiquitously across all neurons. They can function as protein monomers, with each α-subunit capable of fluxing sodium in isolation. However, in vivo, they exist in a complex with a host of other proteins, including ankyrins, Na_V β-subunits β1–4, and fibroblast growth factor homologous factors (FGF/FHFs). Each pore-forming α-subunit complexes with two β-subunits, either a β1 or β3, and then either a disulfide-linked β2 or β4 (114). These β-subunits play important roles in modulation of Na_V channel properties, including surface localization, gating, and kinetics (115). Beyond the modulation of Na_V α-subunits, the β-subunits function independently as Ig-superfamily cell adhesion molecules, playing key roles in cell migration, neurite outgrowth and pathfinding, and cell migration.

As the AIS is established in early development, certain Na_Vs localize first. In excitatory pyramidal cells in neocortex, $Na_V1.2$ is the first Na_V localized to the AIS (116). After the first postnatal week, corresponding roughly to the first year in humans, $Na_V1.2$ is displaced by $Na_V1.6$ (**FIGURE 7**). This displacement occurs most markedly in the distal AIS where newly inserted $Na_V1.6$ is immediately stabilized by interactions with ankyrin-G and potassium channels (117). Similar observations were first made in retinal ganglion cells (118). In parvalbumin-expressing neocortical interneurons, parallel changes appear to occur with $Na_V1.1$ and $Na_V1.6$, with $Na_V1.1$ being more critical for AP initiation in early development. Notably, the switch from $Na_V1.1$-dependent to $Na_V1.1$-independent AP initiation appears to occur later in these cells than in pyramidal cells, extending into the third postnatal week in mice. After this period, the likelihood of lethal seizures associated with heterozygous loss of function in $Na_V1.1$ diminishes as interneurons can more readily initiate APs via $Na_V1.6$ (48, 119).

Similar rules apply in other brain regions. In mature systems, $Na_V1.6$ is expressed almost ubiquitously in CNS neurons and is often the Na_V isoform localized to the distal AIS and responsible for AP initiation (47, 49, 112, 120–125). One notable exception is midbrain dopaminergic neurons, which appear to express $Na_V1.2$ exclusively in the AIS (126).

Why do AIS Na_V isoforms change over development? In neocortical pyramidal cells, one theory is that the voltage-dependent properties of $Na_V1.2$ are more appropriate for AP initiation during early development. When examined in native systems (dorsal root ganglion cells) in the presence of auxiliary subunits, $Na_V1.2$ channels have more depolarized voltage-dependent activation and inactivation properties compared to $Na_V1.6$ (127). Developing neurons have few potassium channels and, as such, have high membrane resistance and depolarized resting membrane potentials (128, 129). With resting membrane potential so depolarized, cells would be unlikely to hyperpolarize sufficiently to relieve $Na_V1.6$ channels from steady-state inactivation. $Na_V1.2$ channels, by contrast, have more depolarized voltage-dependent properties and can cycle through opening and closure without becoming locked in inactivated states in these developing neurons (127). In addition, developmentally regulated splicing in $Na_V1.2$ depolarizes voltage-dependent gating properties even further in early development (130, 131), supporting the idea that developing cells have specializations that allow for electrogenesis in this depolarized voltage range.

The displacement of $Na_V1.2$ from the AIS by $Na_V1.6$ appears to be an active process. In mice that conditionally lack $Na_V1.6$ (Scn8a-/-) in pyramidal cells, $Na_V1.2$

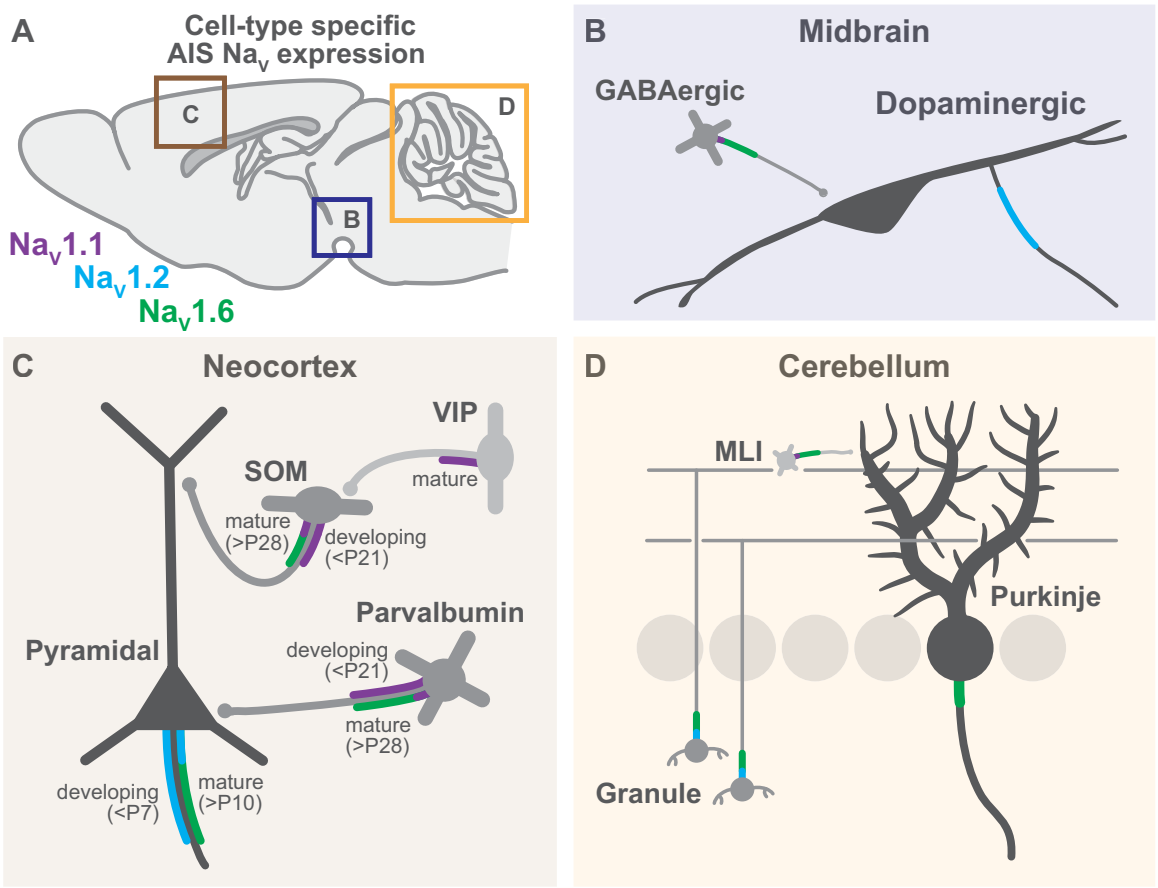

FIGURE 7. Developmental localization patterns of Na$_V$s in the central nervous system. *A*: schematic representation of the rodent brain regions examined in *B*–*D*. Na$_V$1.1 is in purple, Na$_V$1.2 is in cyan, Na$_V$1.6 is in green. *B*: in midbrain, dopaminergic neurons predominantly express Na$_V$1.2 localized in the axon initial segment (AIS). GABAergic interneurons that synapse onto the dopaminergic cells express Na$_V$1.1 in the proximal AIS and Na$_V$1.6 in the distal AIS. *C*: in the neocortex, localization patterns change during development. In developing glutamatergic pyramidal neurons (<P7), Na$_V$1.2 is localized throughout the AIS. In maturing pyramidal neurons, Na$_V$1.2 is restricted to the proximal AIS and Na$_V$1.6 occupies the majority of the AIS, including distal AP initiation regions responsible for AP generation. In developing parvalbumin (PV)-expressing GABAergic neurons (<P21), Na$_V$1.1 is the main Na$_V$ localized to the AIS. In mature PV neurons, Na$_V$1.1 is largely replaced by Na$_V$1.6 in most of the AIS, and Na$_V$1.1 is restricted to the proximal AIS. Somatostatin (SOM)-expressing neurons exhibit a similar change in localization as PV neurons. *D*: in the cerebellum, Purkinje cells express Na$_V$1.6 in the AIS. Molecular layer interneurons (MLIs) and granule cells have initial segments that mimic those found in mature neocortical parvalbumin and pyramidal cells, respectively, with Na$_V$1.1 or Na$_V$1.2 in the proximal AIS and Na$_V$1.6 in the distal AIS.

never leaves. These mature neurons that express only Na$_V$1.2 still initiate APs in the AIS but exhibit a threshold for AP initiation that is depolarized relative to cells that instead have Na$_V$1.6 (54). These neurons that lack Na$_V$1.6 have reduced persistent sodium current, a noninactivating component of the total sodium current that is active at subthreshold membrane potentials, indicating that this aspect of AIS function is largely due to Na$_V$1.6 alone (54, 122). Of note, this persistent current has repeatedly been attributed to Na$_V$1.6 channels localized to the AIS, placing it in an ideal position to regulate pacemaking in a variety of cell classes (132–135).

Throughout life, Na$_V$1.2 remains expressed in the proximal AIS of pyramidal cells (Ref. 47, but see Refs. 52, 136–138) (**FIGURE 7**). Proximally located channels are thought to activate at potentials more depolarized than those in the distal AIS and are therefore activated after APs initiate in the distal AIS. These proximally localized Na$_V$s are thus thought to serve an important role, helping boost APs as they backpropagate and invade the somatic region, which can act as a large current sink. Initial experiments in layer 5 rat somatosensory cortex pyramidal cells suggested that these Na$_V$1.2 channels were required for successful backpropagation; if they were missing, somatic Na$_V$s would never be recruited, and backpropagation would fail (47). Subsequent direct tests of this where *Scn2a* was conditionally knocked out of pyramidal cells still observed successful backpropagation, despite complete loss of Na$_V$1.2 (53). However, these results should be interpreted with caution. Knockout was done in mouse prefrontal layer 5 pyramidal cells, which have smaller somata than the layer 5 pyramidal cells originally studied in rat somatosensory cortex. Thus backpropagation may be maintained in this cell

class since the current sink imposed by the size of the soma is smaller. Furthermore, modest compensatory changes in $Na_V1.6$ AIS expression were evident in cells that lost $Na_V1.2$, potentially allowing for successful backpropagation. Ideally, future experiments that would allow for acute, potent block of $Na_V1.2$ without affinity for $Na_V1.6$ would be able to test these ideas with more precision. This could be done pharmacologically if truly isoform-specific inhibitors were developed. One possibility may lie in refinements to aryl sulfonimide-based compounds, as these compounds can be tuned to block particular Na_V isoforms (139). Indeed, refinements within this class of molecules have already revealed a use-dependent inhibitor that is 100-fold more potent for $Na_V1.6$ than any other Na_V (140).

The density of Na_Vs in the AIS, relative to densities in other neuronal compartments, continues to be a subject of debate. Initial electrophysiological analyses of Na_Vs present in patches of membrane excised from the soma and AIS suggested that the Na_V density was comparable between the two compartments and suggested that the voltage-dependent properties of channels in the AIS were primarily responsible for AP initiation (141, 142). This observation was at odds with immunostaining, which clearly shows an excess density of Na_Vs in the AIS. Why would densities be comparable when making electrophysiological assessments but far from comparable when staining for channels? The answer was in the approaches used. Excised patches of membrane incorporate channels that can be pulled from the cell. However, if a channel is anchored strongly to a submembranous cytoskeleton, they are far less likely to be pulled into a patch. Such is the case for Na_Vs (and select potassium channels) in the AIS. Subsequent experiments depolymerized the actin cytoskeleton, leading to a new estimate that Na_Vs were 50 times more densely packed in the AIS than the proximal dendrite (143). Similarly, recordings from axon blebs, a patchable swelling of the axon that forms at the surface of an acute brain slice when cut with a vibratome, showed similar ratios (19 times), in part because the cytoskeleton is absent from these blebs (47). Similar ratios (39 and 36 times for AIS versus soma and proximal dendrite, respectively) were found when comparing freeze-fracture immunogold labeling of individual $Na_V1.6$ channels in hippocampal pyramidal cells (144). Notably, this may represent the full complement of Na_Vs in these compartments, as hippocampal pyramidal cells differ from neocortical pyramidal cells in that they lack $Na_V1.2$ in their somata and dendrites (53, 128, 138, 144).

While these density ratios suggest a large difference in AIS and somatic Na_V density, direct imaging of sodium influx during APs draws different conclusions. Here, sodium influx appears to be only 3 times higher in the AIS than the soma and 12 times higher than the proximal dendrite of neocortical pyramidal cells (133, 143, 145). Several possibilities could account for the lower ratio observed with AP-evoked imaging. First is the complement of Na_V isoforms in these different compartments. While the distal AIS rests at a slightly more hyperpolarized membrane potential than the soma (146), it is also far more enriched with $Na_V1.6$ channels that exhibit a more hyperpolarized voltage dependence for inactivation compared to the $Na_V1.2$ channels enriched in the soma and proximal dendrite (33, 147, 148). Sodium imaging experiments, typically performed at physiological resting membrane potentials, are thus likely done in conditions in which a larger fraction of the Na_V pool is subject to steady-state inactivation in the distal AIS than the soma. By contrast, voltage-clamp protocols used to determine overall Na_V density in the two compartments typically evoke Na_V currents from very hyperpolarized potentials (−100 to −120 mV; Refs. 45, 143). This relieves both $Na_V1.2$ and $Na_V1.6$ channels from steady-state inactivation completely before assessing Na_V currents. Thus the mismatch between total channels and those assayed with AP-evoked sodium imaging may be due in part to differences in the proportion of channels available for sodium flux in the different experimental designs.

Second is the fact that all channel activation is stochastic and not all Na_Vs are activated with each AP, in part due to processes like slow inactivation (149). Furthermore, individual channels that were activated must then recover from fast inactivation, which can limit the total number of channels available to support another AP if it should occur within a small timeframe. Many axons therefore express Na_Vs far in excess of what is required for single APs to ensure that APs can be initiated and propagated during periods of sustained, high-frequency firing (150). Again, this contrasts with voltage-clamp experiments that are typically designed to maximally recruit all channels from a closed state.

Third, one might consider how Na_Vs are recruited in the distal AIS and soma during an AP. Whole cell recordings from the soma and AIS reveal different membrane voltage kinetics near the AP threshold. In the AIS, depolarization gradually rises until the threshold is reached, triggering an AP that propagates both down the axon and back to the soma (113, 151). Because the soma is the recipient, rather than the instigator, of this AP, it experiences a far more sudden change in voltage and the faster membrane depolarization occurs, the more effectively Na_Vs are recruited (152–154). Thus a combination of these three factors, availability, stochasticity, and recruitment, may account for the apparent mismatch

between total Na_V channel density in the AIS and the proportion of channels recruited during APs.

The fast rise of the AP, as measured in the soma, has received considerable attention. Some have argued that the change in voltage at the AP threshold is so sharp that it cannot be accounted for by a Hodgkin-Huxley (HH)-based gating model (**FIGURE 8**). Instead, it has been proposed to reflect the cooperative activation of Na_Vs in the AIS (155, 156). In this model, physical coupling between Na_Vs is thought to lead to coordinated channel opening, where the activation of one channel hyperpolarizes the voltage dependence of activation of its coupled neighbor, in theory accounting for the sharpness of AP initiation. Similar concepts have been proposed for cardiac sodium channels, at least when recorded in expression systems (157). However, this theory has been challenged by others (158, 159). In the case of the AIS, the most direct assessments have been direct recordings of APs in the axon, which reveal smooth voltage depolarization near the threshold (47, 113), consistent with HH models of independently activated channels (**FIGURE 8**). Further support came from the examination of Na_V voltage dependence in the presence of subsaturating concentrations of the pore blocker tetrodotoxin (TTX). If channel cooperativity exists, then blocking some channels with TTX should shift the voltage dependence of the remaining pool. This was not observed (47).

What then accounts for the sharp rise of the AP in the soma? This voltage component of the AP occurs before the recruitment of somatic Na_Vs, so it cannot be explained by their recruitment. Instead, it appears to be due to the way in which current flows from the site of AP initiation in the AIS to the soma, both axially, within the cell, and through a large current loop that also takes into consideration current flow within the extracellular space. In this way, the soma and AIS act as the two ends of an electrical dipole (**FIGURE 9**), with the soma functioning as a large current sink, and the sudden rise of the AP can be accounted for if one is observing AP from the point of view of a current sink that is physically larger than the site of AP initiation (160, 161).

1.3.2. Potassium channels.

Potassium channels are a diverse class of channels, equally diverse in functional properties. Multiple isoform subclasses contribute to the resting membrane potential, AP repolarization, and membrane dynamics between APs (162). These channels are expressed across neuronal compartments, and, often, a complement of channels in and outside the AIS contributes to AP waveform and subthreshold membrane potential (163). Here, we focus on those with known expression in the AIS and their roles in the function of AIS.

Delayed rectifier currents arising from K_V1-family potassium channels account for a major fraction of the total outward current in the AIS of pyramidal cells. In neocortical and hippocampal pyramidal cells, K_V1 delayed rectifiers are expressed at high levels and account for ~75% of the AIS outward current (112, 164–166). While K_V1s appear to be expressed throughout pyramidal cell axons, their expression is restricted to the AIS in cerebellar stellate cells (105) and is completely absent from cerebellar Purkinje cell initial segments (167). Universally, block of K_V1s slows the repolarization phase of the AP (105, 164, 165), but in

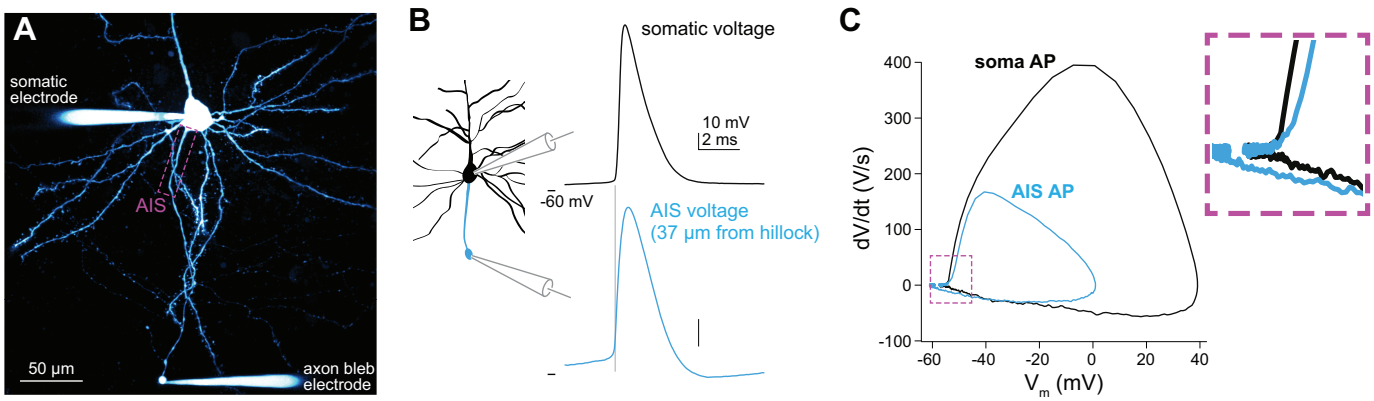

FIGURE 8. Action potential (AP) voltage waveform is affected by recording site. *A*: representative 2-photon z-stack of a layer 5b thick tufted pyramidal neuron with 2 whole cell recording electrodes, 1 at the soma and 1 at the axon bleb. Note: data in *B* and *C* are not from this representative cell. *B*: cartoon representation of recording electrode positions and representative traces of the voltage changes during the action potential as measured on the soma (black) and at the axon bleb (cyan). In this recording, the bleb recording was made from a region of axon 37 µm from the axon hillock, likely near the distal axon initial segment (AIS). *C*: phase plane plots of APs in *B* in the soma and bleb. Note that AIS AP peak voltage is smaller than at the soma in part due to higher resistance of recording electrodes necessary for bleb recording. Area in magenta is expanded in *inset*. Note smooth rise of AP [first derivative (dV/d*t*)] in axonal bleb recording, contrasting with sharp rise of AP dV/d*t* in soma. This latter sharpness may be explained by soma-AIS dipole coupling. Data collected by Spratt et al. (*B* and *C*) as part of Ref. 53. All images and data are unpublished in the format shown, data from the Bender Laboratory, related to Spratt et al. (53).

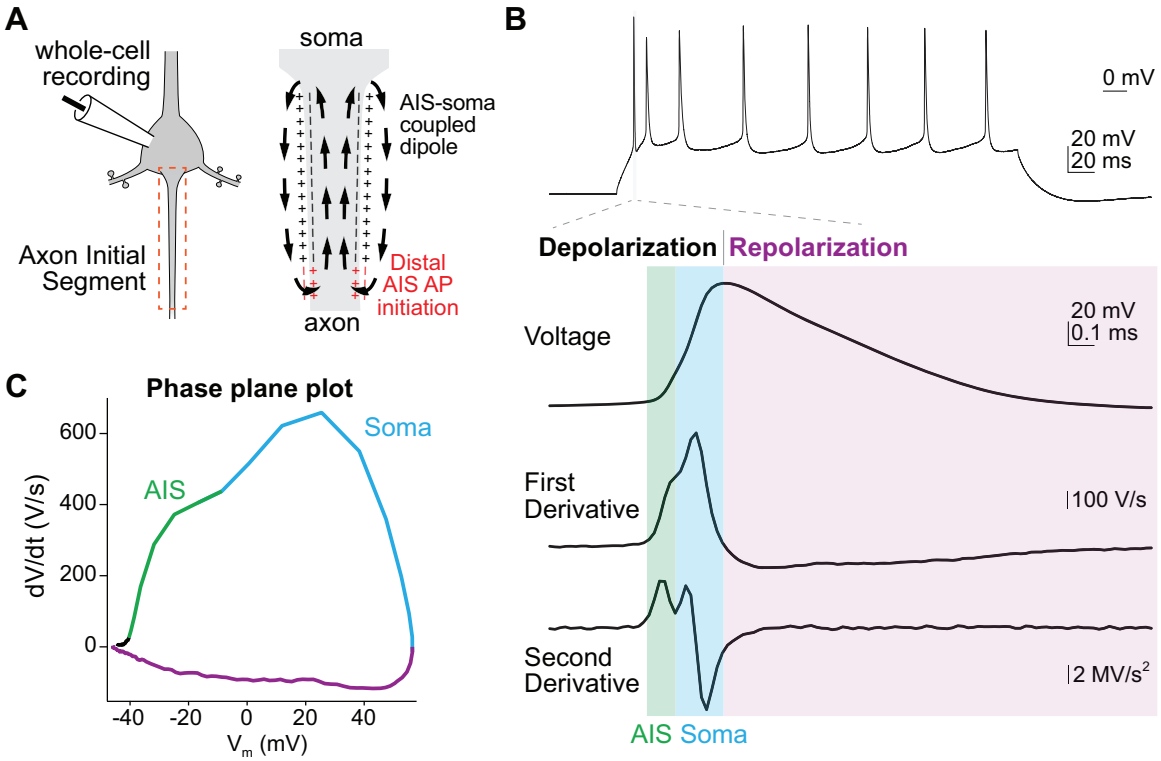

FIGURE 9. Electrical components of action potential (AP) electrogenesis in somatic whole cell recordings. *A*: typical measurements of APs are made at the soma, which is part of an electrical dipole coupled with the axon initial segment (AIS) during AP initiation. APs initiate in the distal AIS, with local positive current influx. Arrows denote current flux of dipole. *B*, *top*: Somatic current injection produces a series of APs. The first AP is expanded in time below. *B*, *bottom*: AP voltage, voltage speed (first derivative), and voltage acceleration (second derivative) plotted vs. time. Shaded areas correspond to AIS (green) and somatic (cyan) components of the rising phase of the AP, and the repolarization (purple) phase of the AP. Note inflection point in voltage acceleration dividing AIS and somatic components. *C*: plot of voltage vs. voltage speed [first derivative (dV/d*t*)], termed a phase plane plot. Different components of AP are color coded as in *B*. Created from unpublished data [Spratt et al. (53)] from Bender laboratory.

some interneuron classes, they exert additional effects on excitability. These channels can begin to activate in some cells as they reach the AP threshold, giving these cells a characteristic "delayed onset" spiking phenotype (168, 169).

A second family of delayed rectifier channels, K_V2s, are also localized to the AIS but have different functions than K_V1s. Rather than being broadly distributed in the membrane, $K_V2.1$s form clusters in neocortical and hippocampal pyramidal cell initial segments. These clusters colocalize with sites of GABAergic input and with the $GABA_A$ receptor scaffold gephyrin (170). Furthermore, they appear at sites where intracellular calcium cisternae are in close proximity to the membrane, reminiscent of studies of K_V2 clusters in the soma that appear to not conduct potassium but instead serve as scaffolds for intracellular calcium stores (171). The K_V2 clusters in the AIS may be similarly nonconducting, as the application of K_V2-specific channel antagonists has no effect on AP waveform, at least as measured from the soma (162). Thus these channels may be more important for AIS structure than electrogenesis, helping to carve out space in the AIS membrane for GABAergic input. Consistent with this idea, cell classes that lack AIS GABAergic input have no K_V2 immunostaining in their initial segments (172).

$K_V7.2$ and 7.3 channels, also known as KCNQ2 and KCNQ3, are also expressed at high densities in the AIS, especially the distal AIS (173–175). In contrast to K_V1s that open quickly in response to depolarization, K_V7s have slow kinetics and their activity can be regulated by calcium through calmodulin-dependent signaling (176). They therefore act to temper sustained firing, with K_V7 antagonists promoting high-frequency burst firing (173, 177, 178). Furthermore, a small fraction of K_V7s are active at hyperpolarized potentials, helping set the AIS resting membrane potential (173, 178).

In addition to voltage-dependent potassium channels, some cells also appear to express calcium-activated potassium channels in the AIS. Small-conductance channels (SK, $K_{Ca}2$) have been localized to the AIS of cultured hippocampal pyramidal cells, where their density is regulated in a PKA-dependent manner (179). Big-conductance channels (BK, $K_{Ca}1$) may contribute to AP repolarization in pyramidal cell initial segments, likely through interactions with Ca_V2 channels (Ref. 180, but see Ref. 181). In addition, most recently, the stretch-sensitive leak potassium channel TRAAK was identified in the AIS (182, 183). What role it

has in AIS membrane excitability is unclear, but similar channels localized to nodes of Ranvier appear critical for membrane repolarization during an AP (184).

1.3.3. Calcium channels.

AP-evoked calcium influx in the AIS was first observed in the early days of calcium imaging in ex vivo slice preparations (185, 186), but the source of this influx was not investigated for some time. Initial studies in auditory brainstem cartwheel cells found that calcium influx was mediated by $Ca_V2.3$ and $Ca_V3.2$ in these cells and provided some evidence through application of the $Ca_V3.2$-preferring antagonist nickel that similar channel types were also present in neocortical pyramidal cells and cerebellar Purkinje cells (187–189). Similarly, in the hippocampus, immunoelectron microscopy and calcium imaging paired with pharmacology have shown that Ca_V3 channels are localized to dentate granule cell initial segments (190, 191). Direct whole cell recordings from the axon initial segment confirmed the presence of Ca_V3 in pyramidal cells (146).

Ca_V3s support multiple roles in the AIS. These channels activate at subthreshold membrane potentials and contribute to local membrane depolarization. They inactivate slowly compared to Na_Vs, remaining active over the course of several APs. Thus they both make it easier to generate an AP and sustain AP activity in high-frequency bursts in multiple cell classes (187–190, 192). In some cells, Ca_V3s interact with AIS-localized potassium channels, regulating their activity (191).

More recent studies showed that additional calcium sources contribute to AIS calcium signaling to varying degrees, depending on cell class. Proximity biotinylation approaches suggest that $Ca_V2.1$ and 2.2 are present in developing cultured hippocampal pyramidal cells (193). $Ca_V2.1$, and $Ca_V2.2$ channels are also present and support the bulk of AP-evoked calcium influx in mouse and ferret prefrontal cortex pyramidal neurons (108, 180, 192). Interestingly, Ca_V2s appear to be diffusely distributed along the AIS membrane, whereas Ca_V3s appear localized to hotspots that may correspond to sites of GABAergic input and $K_V2.1$ localization described above (108). Here, Ca_V3s couple to ryanodine-sensitive intracellular calcium stores, suggesting an interplay between GABA, calcium influx, and store-based signaling. In some somatosensory cortical layer 5 pyramidal cells, intracellular stores occupy a considerable portion of AIS cytosol (194), contributing up to half of the total AP-evoked calcium signal as measured by calcium-sensitive fluorophores (195). The reason for this diversity and overall function of intracellular signaling at the AIS remains unresolved but could relate to a range of activity-dependent regulatory processes, including calcium-dependent kinase signaling, synapses onto the AIS, and some aspects of AIS structural plasticity (196–199). Unraveling this may be best done in the somatosensory cortex, since layer 5 pyramidal cells containing giant cisternal organelles are interdigitated here with other cells that lack organelles (194).

More recently, some reports have challenged the idea that Ca_Vs and stores are the sole source of calcium signaling in the AIS, suggesting that $Na_V1.2$ channels are an additional source (181, 195). This was put forth in part due to an inability to block AP-evoked AIS calcium influx completely with Ca_V antagonists. However, considerations toward Ca_V antagonist mechanism of action may explain these results. Traditional divalent blockers like cobalt and cadmium (but not nickel) transiently block channel pores but then permeate into the cytosol where they bind calcium indicators and eliminate their sensitivity to calcium entry (200, 201). This leaves peptide toxins and other small molecules, which each interact with Ca_Vs differently. Some antagonists, such as ω-agatoxin IV, act as gating modifiers, shifting voltage-dependent activation by more than +50 mV (202). Thus, if an AP is used to probe for calcium influx, $Ca_V2.1$ may be transiently unblocked, as an AP is associated with changes in membrane potential exceeding 80 mV. Other Ca_V antagonists, like ω-conotoxin MVIIC (CTx), exhibit voltage-independent binding to a pore domain of $Ca_V2.1$ and 2.2 but exhibit differential off rates from these two channel isoforms. Notably, CTx exhibits a relatively fast off rate from $Ca_V2.2$ (203), making experiments where toxins are applied transiently difficult to interpret. Finally, some compounds that interact with Ca_V3 channels appear highly lipophilic and have a binding that is strongly affected by membrane potential, requiring careful consideration of experimental time course and design (204, 205).

1.3.4. Hyperpolarization-activated cyclic nucleotide-gated cation channels.

Hyperpolarization-activated cyclic nucleotide-gated cation (HCN) channels, as their name implies, are voltage-dependent channels that are open when cells are hyperpolarized, close with marked depolarization, and permeate cations in proportion to their regulation by cyclic adenosine monophosphate (cAMP) (206). These features, in addition to their slow kinetics for opening and closing, imbue cells with interesting membrane properties, including the ability to fluctuate voltage more strongly at certain frequencies. In many cell types, this membrane resonance depends on dendritic HCN expression. Indeed, differential dendritic HCN expression can be used to classify different neocortical pyramidal cell classes (207). While HCN is expressed at high levels in neocortical pyramidal cell dendrites, it

appears absent in the AIS (146). By contrast, other cell types have marked AIS and axonal HCN expression, even when these same cells lack HCN expression in somatodendritic domains (208). To date, AIS HCN function has been examined in three cell classes: hippocampal granule and basket cells and medial superior olivary neurons in the auditory brainstem (208–210). In basket cells, HCN channels, presumably localized to the AIS, help stabilize the AP threshold during high-frequency, repetitive firing. The mechanism for this effect is unclear but is not due simply to the inward current contributed by HCN (208). In granule cells, AIS HCN can support persistent firing independent of synaptic inputs. Here, increased HCN activity, mediated in part through neuromodulatory control of HCN itself, depolarizes the AIS sufficiently to evoke APs over long periods (209). In olivary neurons, HCN appears to depolarize AIS local resting potential and decrease the likelihood of initiating an AP, an effect ascribed to reduced Na_V channel availability. Of note, serotonergic signaling strongly shifted the voltage dependence of these AIS-localized HCN channels, leading to an increase in AP initiation probability (210). Taken together, these data suggest that HCN can exert cell-type specific actions on the AIS that may depend on the types of computations performed within each cell class.

1.4. GABAergic Synapses at the AIS

The AIS of most neurons lacks direct synaptic input; however, there are special cases where the AIS is inhibited. AIS inhibition is most commonly focused on principal cells within a circuit, including neocortical, hippocampal, and amygdalar pyramidal cells, and cerebellar Purkinje cells. In some cases, like in Purkinje cells, the AIS receives somewhat diffuse input from the same cells that synapse onto the soma (167). In others, like neocortex, hippocampus, and amygdala, specialized interneurons synapse exclusively onto the AIS. These cells, termed chandelier cells, are more commonly found in associative regions than sensory regions and, interestingly, are more numerous in primate cortex than murine species (211). Their development and plasticity have been detailed in recent reviews (212–214); here, we briefly describe their function at the AIS.

Initial studies into chandelier cell-mediated GABA signaling made a surprising discovery. $GABA_A$ synapses typically hyperpolarize the membrane potential, with chloride flowing into cells, following their normal electrochemical gradient. Chandelier inputs, when first studied, were instead found to depolarize the AIS of neocortical pyramidal cells (215), raising the possibility that these synapses function to excite postsynaptic neurons. This aligns with observations more distal in the axon, where GABAergic synapses near transmitter release sites are consistently found to depolarize the membrane relative to resting conditions (216–218). However, studies of putative chandelier inputs in hippocampal pyramidal cells found the opposite: GABAergic signaling was inhibitory on all somatodendritic and initial segment targets onto hippocampal pyramidal cells (219). These discrepancies were not a result of the circuit being studied but rather its developmental stage. Subsequent studies that measured chloride electrochemical gradients in the AIS versus the proximal dendrites found that synapses in dendritic regions were inhibitory by the start of the second postnatal week in the mouse. At this developmental time point, identical to that studied originally, AIS-targeted synapses instead depolarized the local membrane. It was only after several more weeks of development in the mouse that synapses onto the AIS matured to inhibit the AIS (220). Thus chandelier cells are unique in that they depolarize the AIS from resting potentials at later stages in development than more typically found for GABAergic synapses onto dendritic regions. However, ultimately, they do develop to inhibit the AIS (221–225). This inhibition is critical for regulating overall network function. In the hippocampus, for example, chandelier inputs have been shown to actively suppress pyramidal cell output. When chandelier cells are silenced, pyramidal cells begin to form inappropriate representations of an animal's space, forming place fields when they otherwise would not (221). This delayed development of inhibition in the AIS has consequences for circuits that continue to mature into periadolescence. Chandelier synapses undergo a period of elaboration just before adolescence and experimentally induced changes in network activity can regulate their density. If network activity is increased, chandelier synapse density decreases. This same manipulation, if done after adolescence, leads to an increase in chandelier synapse density (226). These changes make sense if considered in a homeostatic framework. In preadolescence, a system aiming for a certain overall firing rate may suppress the formation of another "excitatory" input if network activity is already elevated. By contrast, more chandelier input would help temper excess network activity when these synapses mature to inhibit the AIS. Remarkably, this regulation is bidirectional also on the postsynaptic side. If chandelier inputs are silenced or excised, the AIS adapts to retune its excitability in light of this lost inhibitory input (225).

2. MODULATION OF AIS FUNCTION AND STRUCTURE

The way in which changes in chandelier cell input shape the function of the AIS is part of a much larger conceptual

framework that has emerged in the last decade. Studies of short- and long-term modulation and plasticity have primarily focused on synapses (227–230), but it is now clear that AIS function and structure are similarly modulated to tune overall neuronal excitability. This includes neuromodulatory and trafficking mechanisms that retune the biophysics or density of individual ion channels or changes in AIS structure that alter the way in which synaptic inputs are converted into AP output.

2.1. *Short-Term Neuromodulation of AIS Excitability*

A host of ion channel classes present in the AIS appear subject to neuromodulation by G-protein coupled receptor signaling pathways. G_i-coupled D2 and D3 dopamine receptors regulate different aspects of $Ca_V3.2$ biophysical properties to suppress AP output. Activation of D2 receptors expressed by entorhinal cortex stellate cells increases the AP threshold by depolarizing Ca_V3 voltage dependence of activation without altering inactivation properties. This effect was mimicked by blocking protein kinase A (PKA), suggesting that D2 receptors act to suppress constitutive PKA signaling, presumably allowing for dephosphorylation of $Ca_V3.2$ via phosphatases. Consistent with this concept, the experiments appeared to require an intact cytosolic milieu, as all voltage-clamp measurements were done in a perforated-patch configuration that limits the degree to which the intracellular solution is disturbed (231). What particular phosphorylation site, or sites, on $Ca_V3.2$ are the target of such modulation in stellate cells remains unclear. Prior work in heterologous expression systems noted that alteration of phosphorylation states of several residues can produce similar effects to voltage-dependent activation but not in isolation; voltage-dependent inactivation properties are also altered (232).

The modulatory pathway identified in entorhinal stellate cells appeared to affect Ca_V3 function across the cell, as changes in biophysical properties were evident from somatic voltage-clamp recording (231). Therefore, the relative contribution of AIS versus dendritic Ca_V3s modulation remains unclear in this cell class. By contrast, D3 receptors have been shown to modulate AIS $Ca_V3.2$ selectively in auditory brainstem cartwheel cells, D3-expressing prefrontal pyramidal cells, and hippocampal pyramidal cells (187, 189, 192, 233, 234). Whole cell Ca_V3 current, dominated by channels localized to the dendrite, is not altered by D3 receptor signaling. Simultaneous calcium imaging through the AIS and dendrite showed that AIS signals are suppressed with no change in dendritic regions in either cell class (192, 233). This appeared to be due to associations between D3 and $Ca_V3.2$ being somehow restricted to the AIS membrane, as the signaling pathway could be reconstituted and studied biophysically in heterologous expression systems. There, the dominant effect observed was a D3-dependent hyperpolarization in steady-state voltage-dependent inactivation. This shift reduces the number of channels available to be recruited by depolarizing synaptic input, effectively reducing the total Ca_V3 current. The net effect of this modulation was a reduction in AP output, especially when such activity occurred in high-frequency bursts (189, 192, 233).

Similar to the D2 receptor function described above, D3 receptor signaling appears to be dynamically regulated by membrane-scaffolded kinases and, presumably, diffusible phosphatases. Evidence for this comes from different recording configurations: in whole cell recordings, induction of D3 receptor $Ca_V3.2$ modulation is irreversible, presumably because phosphatases that could reverse channel phosphorylation have been dialyzed from the cytosol (233). By contrast, changes in AP bursting activity could be reversed in cell-attached recordings of APs that did not alter the intracellular milieu (189), similar to perforated-patch approaches used in studies in D2-dependent pathways. D3-dependent modulation was found to require PKC activation, which was puzzling, as G_i-coupled receptors like D3 receptors do not signal via PKC. Subsequent experiments revealed that this PKC dependence was only part of the puzzle. D3 receptors are a class of receptors that must be phosphorylated by PKC to recruit effectors downstream of arrestin, a component of the receptor internalization and degradation pathway that also drives its own signaling independent of G_α-subunits (235, 236). Consistent with this signaling scheme, AIS D3 receptors could not regulate $Ca_V3.2$ in the absence of arrestin (187, 234). This is interesting, since G-protein receptors can engage G-protein and arrestin differentially depending on the ligand bound to the receptor. For D3 signaling, this has implications for the treatment of neuropsychiatric disease. Here, different classes of second-generation antipsychotic medications, all thought to act as antagonists of D2 and D3 receptor G-protein signaling, differentially engaged D3 receptors at the AIS, with some acting as agonists for D3-arrestin signaling (234). Thus the regulation of AIS calcium, and the regulation of AP burst activity, may be an important consideration in antipsychotic efficacy.

AIS potassium channels can also be regulated downstream of Ca_V3. In hippocampal granule cells, cholinergic signaling leads to a hyperpolarization of the voltage dependence of $Ca_V3.2$ activation. This allowed Ca_V3 to flux calcium at resting membrane potential, which dampened calcium-dependent K_V7 activity (191). As described below, the overall potassium channel density in the AIS can be regulated by activity on even longer time scales.

While Ca_V3s are a primary target of neuromodulatory signaling in the AIS, sodium channels are also subject to regulation. Serotonin regulates Na_Vs in neocortical pyramidal cells, suppressing the current density of $Na_V1.2$ with apparent alterations in backpropagation efficacy (237). Similarly, serotonin can suppress total Na_V current in spinal cord motorneurons from turtles, which could account for motor fatigue known to be due to serotonergic signaling (238).

Beyond these observations, there are additional ways in which AIS channels can be modified. Na_Vs are targets for posttranslational modifications (PTMs), including phosphorylation, ubiquitination, palmitoylation, nitrosylation, glycosylation, and SUMOylation, as detailed in recent reviews (239–241). Generally, these PTMs have been studied in the context of channel trafficking or biophysical properties, but there are hints to suggest that PTMs may play an important role in the modulation of AIS plasticity. Among the PTMs, phosphorylation has been most heavily studied (reviewed in Ref. 241), and there is clear evidence that phosphorylation modulates Na_V binding to ankyrin and thus AIS localization. Na_Vs bind to ankyrin using the large intracellular loop between the second and third set of transmembrane domains (II-III loop) (242, 243), and CK2-mediated phosphorylation of key serine residues within this loop is necessary for high affinity binding to ankyrin-G (244). One of the major players in AIS plasticity is the serine and threonine phosphatase calcineurin, which is necessary for activity-dependent modulation of AIS position downstream of calcium influx through Ca_Vs (245). While the inhibition of calcineurin blocks activity-dependent AIS repositioning, the exact molecular targets of calcineurin remain unknown. While ankyrin-G is repositioned during AIS plasticity, suggesting that cytoskeletal rearrangement could be sufficient to explain AIS plasticity, it remains possible that modulation of Na_V binding to ankyrin could also play an important role in this process. For example, direct dephosphorylation of the II-III loop of Na_Vs would be expected to weaken affinity for ankyrin and could help drive Na_V endocytosis necessary for AIS plasticity (100).

Phosphorylation-dependent regulation of AIS Na_Vs likely goes beyond modulation of channel localization. For example, $Na_V1.6$ was shown to be a target of the serine and threonine kinase Ca^{2+}/CaM-dependent protein kinase II (CaMKII) (246). Inhibition of CaMKII in heterologous cells causes a >70% decrease in $Na_V1.6$ currents and a 5.8-mV rightward shift in the voltage dependence of activation. Consistent with these findings, inhibition of CaMKII in acutely dissociated Purkinje neurons reduced sodium currents by ~90% (246). It is possible that the effects of CaMKII inhibition are limited to modulation of channel biophysical properties, since the predicted phosphorylation sites are found within the I-II loop and not the ankyrin-binding II-III loop. However, it is also possible that other phosphorylation sites were not represented due to technical limitations on peptide coverage of many of the intracellular domains of $Na_V1.6$ (246). Nevertheless, phosphorylation of other intracellular domains of the channel could contribute to alterations in channel localization. For example, recent work demonstrated that the I-II loop contributes to axonal trafficking of Na_Vs (138).

Na_Vs are also subject to regulation by palmitoylation, which is the reversible covalent addition of the fatty acid palmitate to cysteine residues in target proteins through a labile thioester bond (42, 44). Palmitoylation is added to target proteins through the activity of the zDHHC family of palmitoylacyltransferases and removed by a growing list of protein thioesterases (42). In the case of Na_Vs, the addition of palmitate occurs very early in the biosynthesis of the channel (247), suggesting that this PTM may be critical for normal channel function and/or localization. $Na_V1.6$ was shown to be palmitoylated on three cysteine residues, one on the COOH-terminal tail and two within the ankyrin-binding II-III loop (248). Global inhibition of palmitoylation with the broad palmitoylation inhibitor 2-bromopalmitate decreased $Na_V1.6$ current density and caused a hyperpolarized shift in the voltage dependence of inactivation in heterologous cells (248). Stimulation of global palmitoylation using palmitic acid caused an increase in $Na_V1.6$ current density but no change in channel inactivation (248). One of the challenges of global modulation of palmitoylation is that many other Na_V-interacting proteins that are necessary for localization and function are also subject to palmitoylation, including Na_V β-subunits (249) and ankyrins (38, 39). Thus several key questions remain. Is channel palmitoylation regulated by activity and does it play a role in AIS plasticity as has been seen for synaptic plasticity (250)? What are the palmitoylacyltransferases and thioesterases involved in the regulation of Na_V palmitoylation and do they participate in AIS plasticity? Do the effects of Na_V channel palmitoylation go beyond promoting surface localization and modulating channel biophysical properties?

Other PTMs and interacting partners have been proposed to modulate channel properties, but work was hampered by a relative paucity of tools for studying the effects of these modifications on channel localization during AIS plasticity. The development of tagged channel constructs (33) or CRISPR-based tagging approaches (100, 138) that allow normal developmental subcellular localization patterns should help tease apart the contribution of these PTMs to channel localization.

2.2. *Long-Term Modification of AIS Structure and Excitability*

AIS structure determines neuronal excitability; the longer the AIS, the more sodium channels present and the

easier it is to initiate an AP. While it is generally accepted that AIS structure varies across cell classes, the malleability of AIS structure in single cells was first demonstrated only recently in 2010 by two landmark studies. This new form of plasticity appears to be homeostatic in nature, acting to normalize AP output in response to long-term changes in synaptic drive.

In cultured hippocampal neurons, increasing excitability through chronic chemical depolarization shifted the location of the AIS, moving it further from the soma without altering its overall length (251). This change in the AIS position was reversible, with the AIS reverting to its original position upon return to baseline excitability levels. Similar movements occurred when optogenetically driving cells to fire in high-frequency bursts. These manipulations both engaged Ca_V1 channels necessary for structural plasticity (245). Oddly, this is the only Ca_V isoform that has not been functionally localized to the AIS, suggesting that the structural plasticity rheostat is localized elsewhere, perhaps in the Cav1-enriched somatic compartment (252).

The first account of AIS structural plasticity in vivo was in the auditory brainstem (253). Here, cells within the nucleus magnocellularis (NM) were studied. These cells are the first to receive input from the auditory nerve and can fire APs at very high frequencies, tracking auditory hair cell input (254). These excitatory inputs can be silenced effectively by removing the cochlea, and magnocellularis neurons were found to respond to this loss of synaptic input by expanding the area of the initial segment. This occurred without any change in the AIS position relative to the soma, although it should be noted that the AIS already abuts the soma under normal excitability levels. This expansion of the AIS area, despite necessarily occurring on the distal end of the AIS, increased overall neuronal excitability by increasing total Na_V current density and lowering the AP threshold (253).

What is becoming clear is that the structural plasticity at the AIS is occurring on shorter time scales than originally realized, with plasticity occurring in hours or even minutes (255, 256). This plasticity appears driven by overall neuronal activity, engaging calcium-dependent signaling cascades that promote AIS reorganization. The early stages of AIS plasticity involve calcium influx through L-type Ca_V1 channels and downstream activation of the calcium-dependent serine/threonine phosphatase, calcineurin (245). The target of calcineurin remains unknown, but inhibition of calcineurin blocks repositioning of both ankyrin-G and $Na_V1.2$ (100). Clathrin-mediated endocytosis of $Na_V1.2$ from the distal AIS plays a key role in AIS plasticity (100). In addition to repositioning of Na_Vs at the AIS, voltage-gated potassium channels (K_Vs) are repositioned and the relative expression of specific K_V subtypes is changed in response to neuronal activity (257–259). AIS plasticity, much like synaptic potentiation, also requires the actin-based motor protein myosin II, although the exact function for this motor protein in plasticity remains elusive (260, 261). Induction of AIS plasticity also increased the number of longitudinal actin fibers within the AIS, and blockade of actin polymerization prevented AIS plasticity (262). In addition to actin-based mechanisms, microtubule-dependent pathways contribute to AIS plasticity. For example, microtubule reorganization at the AIS though cyclin-dependent kinase 5 (CDK5), a widely expressed serine/threonine kinase, is necessary for normal AIS plasticity (263). While many of these mechanisms of AIS plasticity are shared between different neurons, there are some unique mechanisms to drive AIS relocalization. For example, inhibition of M-current in cultured hippocampal neurons drives repositioning of a complex of FGF14, Na_Vs, and KV7 but not ankyrin-G, suggesting that these processes involved in AIS plasticity may be separable (264).

These first excitability manipulations used to evoke AIS plasticity were somewhat extreme. Subsequent studies showed that similar plasticity can occur in response to a wide array of conditions, including epilepsy (265–267), focal stroke (268, 269), traumatic brain injury (270), tauopathy (271, 272), inflammatory pain (273), and amyotrophic lateral sclerosis (274). Combined, it is now clear that AIS plasticity is a common mechanism engaged in pathological conditions, but whether AIS plasticity is a normal part of brain function has been harder to demonstrate. A key approach to address this question is a method to label and track AIS in living tissue, rather than relying on post hoc immunofluorescent labeling of constituent parts.

2.3. Methods for Live Labeling the AIS

Multiple methods have been utilized to attempt to live image the AIS, with varying degrees of success. Most of these approaches have relied on labeling native AIS proteins with antibodies or (over) expressing tagged members of the AIS protein complex. For example, antibodies directed against the extracellular domain of the cell adhesion molecule neurofascin or ectopic expression of neurofascin-green fluorescent protein (GFP) have been used to label the AIS (**FIGURE 10**). While antibodies directed against the extracellular side of neurofascin label the AIS, these tagged neurofascins fail to move with the AIS during structural plasticity (275). By contrast, overexpressed neurofascin-GFP can spill into domains beyond the AIS, including the soma and

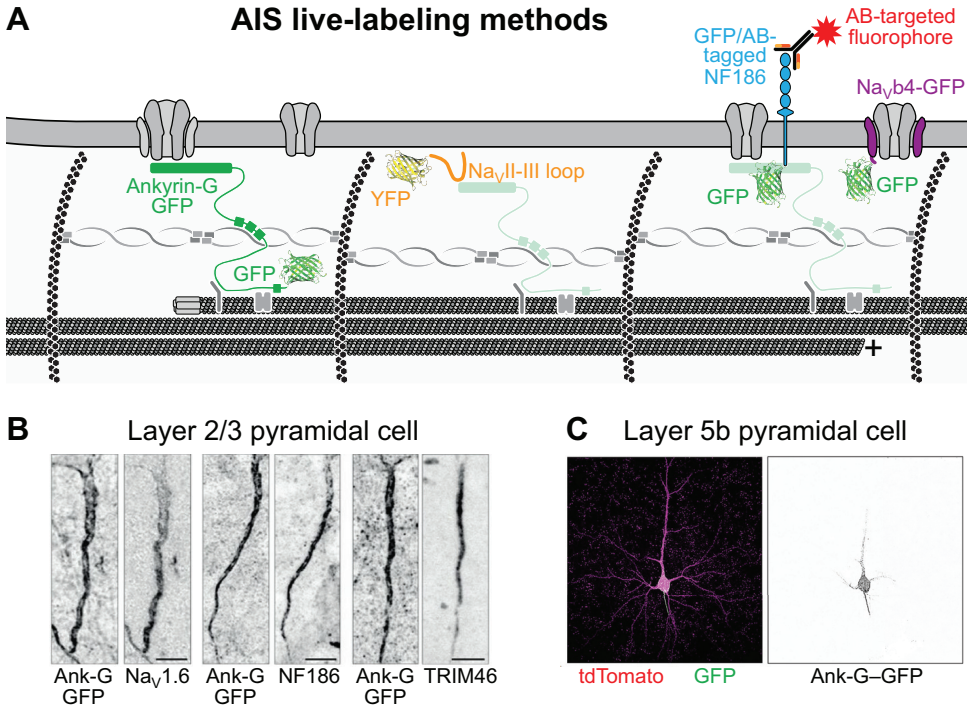

FIGURE 10. Live imaging of axon initial segment (AIS) structure. *A*: representation of methods that have been used to live label the AIS. Overexpression of green fluorescent protein (GFP)-tagged neurofascin-186, Na$_V$β4-GFP, and 270-kDa ankyrin-G-GFP (not shown) fails to report the accurate position of the AIS. Labeling of native neurofascin with antibodies directed against the extracellular domain accurately labels the AIS but fails to report AIS plasticity. Overexpression of the II-III loop of Na$_V$1.2 fused to YFP effectively reports the position of the AIS and reflects AIS plasticity but with some temporal delay. Labeling of endogenous ankyrin-G with a Cre-dependent GFP tag reports the position of the AIS and allows detection of AIS plasticity in real time. *B*: representative images of layer II/III somatosensory pyramidal neurons from *Ank3*:GFP x CamkII Cre mice. Intrinsic GFP was shown along with staining for Na$_V$1.6 (*left*), neurofascin-186 (*middle*), and TRIM46 (*right*). Bars = 10 μm. Created with data from Dr. Maren Engelhardt; adapted from Ref. 256; used with permission. *C*, *left*: isolated layer II/III somatosensory from *Ank3*:GFP mouse transduced with sparse synapsin-Cre-tdTomato AAV. Ankyrin-G-GFP is shown in green, and TdTomato is shown in magenta. Bar = 10 μm. *C*, *right*: ankyrin-G-GFP signal shown as greyscale demonstrating that ankyrin-G localizes to the soma and dendrites of mature pyramidal neurons, in addition to identifying the position of the AIS. Created from unpublished data.

dendrites, rendering it ineffective for identifying the AIS in living cells (275). Similar results were obtained with overexpression of Na$_V$β4-GFP or 270-kDa ankyrin-G-GFP, where these constructs exhibit localization outside of the AIS (275). This was observed with either overexpression of a 270-kDa ankyrin-G-GFP or even when native ankyrin-G was knocked out and replaced by this exogenous 270-kDa ankyrin-G-GFP. More biologically appropriate localization was observed with the knockout of endogenous ankyrin-G and rescue with a full-length 480-kDa ankyrin-G-GFP construct, rather than the 270-kDa construct but only in a narrow expression window (27). Even slight overexpression of this 480-kDa construct, similar to the 270-kDa construct, results in spillover of ankyrin-G into compartments that normally do not see 480-kDa ankyrin-G, like distal dendrites.

Other approaches for labeling the AIS have relied on the expression of chimeric constructs that contain ankyrin-G-binding domains from resident AIS proteins. One promising candidate has been the II-III loop of Na$_V$1.2, identified in 2003 as the ankyrin-G binding site of the channel (242, 243). This domain has been fused to multiple proteins to label the AIS, including CD4 (242), fluorescent proteins (242, 275), and Kv2.1 (242). In particular, the YFP-Na$_V$1.2 II-III loop showed promise in live labeling the AIS where it specifically labeled the AIS in living dentate granule cells (275) (**FIGURE 10**). However, a few challenges remain with this construct. First, although the construct does report on AIS plasticity, it takes hours to catch up to the underlying ankyrin-G cytoskeleton (275). Second, some studies report changes in sodium currents that likely reflect a dominant-negative effect of the II-III loop chimera outcompeting native sodium channels within the AIS (242), although that effect is not seen in all cell types or expression levels (275). Third, methods are still needed to deliver this construct in vivo that may ultimately disrupt the normal physiology of neurons, especially under conditions of prolonged expression.

Thus the optimal tool for live labeling the AIS would do so without disrupting localization and function of other AIS proteins and would accurately reflect activity-dependent plasticity in real time. To generate this tool, we recently created a Cre-dependent *Ank3*:GFP mouse line that places a GFP tag on the COOH terminus of the native *Ank3* allele after Cre recombination

(256) (**FIGURE 10**). By labeling the native *Ank3* allele, we avoided the problems associated with ankyrin-G overexpression, while the Cre dependence allows expression in genetically defined cell types, which is critical since *Ank3* is nearly ubiquitously expressed in the body. To minimize problems with the GFP tag interfering with protein function, we used the same linker-GFP sequence that is used in the 480-kDa ankyrin-G-GFP plasmid, which has been used in knockout-and-rescue studies to rescue normal clustering of Na_Vs, neurofascin, and βIV-spectrin (27), as well as the formation of GABAergic synapses (40). The addition of the GFP tag to the native *Ank3* allele does not affect the AIS (ultra)structure, molecular composition of the AIS, or electrophysiological properties of neurons (256). Importantly, this live labeling approach allows the detection of activity-dependent AIS plasticity in real time, with AIS repositioning occurring in within 10 minutes of application of 15 mM KCl (256). In addition, AISs (and nodes of Ranvier) can be imaged in live animals over multiple weeks (256). Thus this tool will allow the monitoring of AIS plasticity in real time and in response to more physiologically relevant stimuli and to be able to track the effects of these changes using electrophysiology. Although the ankyrin-G-GFP mouse provides an excellent marker for the AIS, it is important to note that ankyrin-G subcellular localization is developmentally regulated, with accumulation on the soma and proximal dendrites of forebrain pyramidal neurons occurring in mice after the first 2 weeks of life (33, 40, 256). This can be clearly seen in isolated ankyrin-G-GFP-expressing neurons (**FIGURE 10**). Nevertheless, even if neurons exhibit somatodendritic ankyrin-G, the AIS can clearly be identified by its significantly higher concentration of ankyrin-G.

2.4. AIS Plasticity under More Physiological Conditions

Given these new methods, we are now starting to appreciate that AIS structural plasticity occurs not just in pathological conditions but as part of normal brain function. For example, AIS length in the barrel cortex is plastic during normal development. Starting from birth, AISs within the barrel cortex continue to lengthen up until postnatal *day 13*, the time when active whisking and exploration begin (276). After the onset of whisking behavior, the AIS shortens in response to neuronal activity, a process that can be blocked by sensory deprivation (i.e., whisker trimming) (276). Similar results are seen in the visual cortex, where the AIS undergoes stimulus-dependent plasticity (277). Disruption of the excitatory/inhibitory (E/I) balance with early-life NMDA receptor blockade causes a shortening of the AIS in the prefrontal cortex, which can be blocked by environmental enrichment (278). Induction of long-term potentiation with high-frequency electrical stimulation results in a rapid reduction in AIS length in dentate gyrus granule cells (279). Even normal aging processes can impact AIS plasticity. For example, layer II/III neurons in the visual cortex show significant increases in neuronal activity in aged rats, resulting in reductions in AIS length and density of $Na_V1.6$, presumably an attempt to maintain homeostasis (280). Multiple neocortical areas showed similar age-related changes in AIS length in marmosets, suggesting that activity-dependent refinement of AIS length is a common process in brain development and aging (281). Interestingly, opposite effects on AIS plasticity are seen in inhibitory interneurons. Olfactory bulb dopaminergic interneurons respond to hyperexcitability by lengthening the AIS, an effect that is opposite what is seen in excitatory neurons (282). This sets up a system where an increase in the E/I balance causes opposite, but complementary, effects on the AIS: shortening of the AIS in excitatory neurons to increase their threshold and lengthening of the AIS in inhibitory neuron to decrease their threshold, resulting in restoration of E/I balance.

In many neurons, the AIS forms just distal to the axon hillock where it serves to integrate dendritic inputs into an action potential. In some cases, however, the AIS arises from a basal dendrite where privileged input onto this axon-carrying dendrite (AcD) elicits APs with a lower threshold than other dendrites (283). The proportion of AcD cells varies across brain regions and between organisms, with rodents possessing more AcD cells than primates or humans (284, 285). Interestingly, recent work has shown that cells are able to modulate the position of axon origin in response to neuronal activity within a few days (286), adding a new layer of complexity to our understanding of neuronal plasticity.

3. DYSFUNCTION OF THE AIS IN DISEASE

Given its role in determining neuronal excitability, it is not surprising that dysfunction in the AIS is implicated in disorders of excitability (287–289). What is perhaps more surprising is how common AIS dysfunction is observed across other neurological and neuropsychiatric disorders (290, 291). With a few notable exceptions, the latter observations have focused on AIS structure and argue that AIS structural alterations are common in disease. However, given how common structural plasticity appears to be, it is now an open question whether these structural changes are causal to disease or instead an effort to compensate for changes in cellular or network excitability that have other origins. Disentangling these possibilities will require considerable effort.

3.1. Epilepsy

Dysfunction in AIS-localized ion channels has long been implicated in epilepsy (292). Indeed, de novo variation in ion channels is a major contributor to genetic epilepsies. Early infantile epileptic encephalopathy (EIEE), seizures that begin within the first days or weeks of life, are often linked to changes in the genes *SCN2A* and *KCNQ2*. These genes encode the sodium channel $Na_V1.2$ and the potassium channel $K_V7.2$, two channels that increase expression early in development and are the first to incorporate into the AIS (293, 294). Different forms of genetic variation in these genes give rise to EIEE. In *SCN2A*, missense variants that enhance the activity of $Na_V1.2$ channels, so-called gain-of-function (GoF) variants, render developing neurons hyperexcitable. By contrast, variations that dampen $K_V7.2$ function, either through protein truncation of *KCNQ2* or missense variants that render channels less excitable, produce a loss-of-function (LoF) in this potassium channel. This, too, leads to hyperexcitability, as one of the main channels responsible for hyperpolarization is impaired.

Other AIS-localized channels are associated with later-onset epilepsy, largely due to their delayed developmental expression. *SCN8A* expression increases during the first postnatal year in humans, and seizures associated with *SCN8A* GoF similarly tend to manifest, on average, at 5 months. Dravet syndrome, often associated with *SCN1A* LoF, also tends to have seizures with onset after the first few months of life. Because $Na_V1.1$ channels are preferentially expressed in inhibitory interneurons in the neocortex, *SCN1A* LoF results in a disinhibition of networks. These seizures are often coincident with a fever, as elevated temperature can exacerbate network dysfunction associated with alterations in excitability (295). This is because sodium channels, like all ion channels, have voltage-dependent properties that can be modulated markedly by temperature.

Dysfunction in other classes of potassium channels, including those in the K_V1, K_V3, and K_V4 classes, also results in epilepsy (296). Many of these can be due to changes in AIS excitability, but K_V expression and interactions with other ion channels in non-AIS compartments can also contribute to hyperexcitability. For example, the loss of $Na_V1.2$ in mature neocortical pyramidal cell dendrites, after $Na_V1.2$ is displaced from the AIS by $Na_V1.6$, fails to fully depolarize dendrites and recruit voltage-dependent potassium channels. This leads to hyperexcitability because the AIS cannot properly repolarize between APs (53). This consideration for other neuronal compartments is likely even more important for calcium and HCN channels. While both can be expressed in the AIS to varying degrees, they are better thought of as modulators of excitability, in contrast to sodium and potassium channels, which are true drivers of AP firing. Instead, their expression in other compartments in particular cell classes may be more critical. One clear example is in thalamic neurons, where Ca_V3 channels expressed at high levels in dendrites contribute markedly to burst spiking phenotypes (297).

Ion channel auxiliary subunits can also contribute to disease. The sodium channel β1-subunit, a product of *SCN1B*, has a particularly strong association with epilepsy. Monoallelic *SCN1B* variants have been found in patients with Generalized Epilepsy with Febrile Seizures plus (GEFS+) (298, 299). Biallelic recessive variants in *SCN1B* cause Dravet syndrome, a severe and intractable pediatric epileptic encephalopathy (300–302). The β1-dysfunction likely causes epilepsy via dysregulation of Na_V α-subunits, ultimately leading to changes in neuronal firing and network desynchronization (303). However, given the myriad effects of β1 dysfunction, it is possible that other non-AIS defects are contributing to disease, like alterations in neuronal structure (304).

Another family of Na_V-modulating proteins that are associated with epilepsy is the fibroblast growth factor homologous factor (FGF/FHF) family. FGF/FHFs bind to the COOH-terminal tail of Na_Vs to modulate channel gating and current density (305). FGF12 is tightly coupled to $Na_V1.2$ and clustered within the AIS (305). De novo missense variants and copy number variation in *FGF12*, also known as *FHF1*, have been found in developmental and epileptic encephalopathy patients (306, 307). These GoF variants cause a strong depolarizing shift in the voltage dependence of inactivation of $Na_V1.6$ (306).

Given the strong association of Na_V α- and β-subunits with epilepsy and their dependence on ankyrin-G for AIS localization, it is perhaps unsurprising that seizure disorders are seen in patients with *ANK3* variants. A recent study of 27 patients with *ANK3* variants found that 50% of patients with biallelic variants and 25% of patients with monoallelic variants exhibit epilepsy, as well as many other comorbid conditions (308). Among three patients homozygous for a frame-shift variant that is predicted to disrupt the 480-kDa isoform of ankyrin-G, one developed severe seizures at age 12 (309). This has been modeled effectively in mice. Genetic deletion of *Ank3* exon 1b, which deletes ankyrin-G from the cerebellum and from parvalbumin-expressing GABAergic neurons in the forebrain, causes loss of the AIS from parvalbumin neurons resulting in disinhibition, seizures, and sudden death (310).

Temporal lobe epilepsy has been linked to changes in AIS structure. Here, initial segments of adult-born dentate granule cells were both shorter in length and farther from the soma (267). Similarly, a mouse model of

absence epilepsy exhibited an increase in distance between the AIS and soma with no change in overall length (266). These effects are often linked to reductions in excitability, suggesting that these types of AIS structural refinement are compensatory in nature.

3.2. Intellectual Disability and Autism Spectrum Disorder

Disruption of the *ANK3* gene is strongly associated with the development of intellectual disability (ID) and autism spectrum disorder (ASD). Among patients with biallelic *ANK3* variants, 91% (10/11) exhibited ID and 100% showed language delay (308). The three patients described above with biallelic frameshift in *ANK3* exhibited moderate ID (309). This phenotype does seem to show gene dose dependence, as patients with monoallelic variants were less likely to exhibit ID (69%) or language delay (87.5%) (308).

LoF variants in both of the predominant Na_Vs in pyramidal neurons, $Na_V1.2$ and $Na_V1.6$, are associated with ASD and ID (148, 289, 311–313). These cases largely stem from de novo protein truncating variation in *SCN2A* and *SCN8A*, but missense variants have also been associated with ASD/ID. Typically, these variants dampen channel activity, but at times they introduce completely new biophysical properties. In one child, a variant affected an amino acid localized to the $Na_V1.2$ pore selectivity filter (314). This variant switched the polarity of an amino acid localized to the selectivity filter, replacing a lysine with a glutamic acid (K1422E). Evolutionarily, this imparts a reversion of the selectivity filter to that found in Ca_V3 channels from which Na_Vs evolved (315). K1422E channels thus switch from channels selective for sodium into channels with mixed selectivity for multiple cations, including calcium (137, 316, 317). Consistent with these changes in permeability, a mouse model carrying this variant exhibited changes in calcium dynamics at the AIS of neocortical pyramidal cells. AP-evoked calcium influx occurred during both the depolarizing and repolarizing phases of the AP in the proximal AIS, an area enriched with $Na_V1.2$ (47), whereas, in normal conditions, calcium influx was only observed during AP repolarization (137). Similarly, direct recordings of channel currents in heterologous expression systems showed pronounced calcium currents from K1422E-containing $Na_V1.2$ channels whereas wild-type channels exhibited none (137, 316).

While the AIS is clearly affected in these disorders, it is also important to consider non-AIS functions of proteins in ASD and ID. For example, the dendritic localization of $Na_V1.2$ in neocortical pyramidal cells may be the most critical aspect of its function in relation to ASD and ID (128, 318). Understanding diverse roles in different neuronal compartments, as well as understanding why particular missense variants that change channel biophysics in unique ways are associated with a particular set of comorbid phenotypes, will be critical questions to address in the coming years (e.g., Ref. 319).

3.3. Migraine

Migraine is characterized by recurrent headache, often with aura and difficulty processing sensory information. Alterations in several genes have been implicated, including *CACNA1A* ($Ca_V2.1$) and subclasses of purinoreceptors (320, 321). Several missense variants in *SCN1A* are associated with familial hemiplegic migraine, although it is unclear whether dysfunction of $Na_V1.1$ in the AIS is causative. All known variants are missense, in contrast to protein truncating variants often observed in Dravet syndrome (322, 323). For example, the first variant discovered to be associated with migraines, G1489K, speeds $Na_V1.1$ recovery from fast inactivation (324). However, it should be noted that the variant was studied in *SCN5A*, not *SCN1A*, due to issues associated with generating stable $Na_V1.1$ protein in heterologous systems. The root cause of this expression issue, which is common to many sodium channels, was recently identified. Sodium channel genes contain nucleotide sequences that resemble cryptic prokaryotic promoters that lead to the expression of mRNA toxic to bacteria (325). Codon optimization approaches that eliminate these cryptic promoters allow for more stable expression, likely allowing for higher throughput studies of how different Na_V variants contribute to diverse neurodevelopmental disorders.

3.4. Neuropsychiatric Conditions

The *ANK3* locus on chromosome 10 has been implicated as a significant risk locus for bipolar disorder, and possibly schizophrenia, with some of the highest significance and largest effect sizes (odds ratios of up to 1.4) in a genome-wide association study (326–333). In addition, patients who are homozygous for an *ANK3* variant that results in a frameshift and a premature stop codon specifically in the 480-kDa isoform exhibit a severe neurological phenotype that includes intellectual disability (IQ $<$50), hypotonia, and spasticity, highlighting the critical importance of *ANK3* in normal brain function (309). *Ank3* LoF mice exhibit multiple behaviors consistent with psychiatric disease, including increased hyperactivity, decreased anxiety-like behavior, and sleep dysfunction (334–337). A subset of these behaviors is modulated by the frontline bipolar disorder therapeutics lithium and valproate (335–337). Alterations in AIS length are seen in rodent models with drug-induced ADHD-like behaviors, although it is not clear if these changes are causal or a result of

activity-induced plasticity in response to altered network activity (338).

3.5. Neurodegenerative Conditions

Multiple neurodegenerative mechanisms appear to affect neuronal excitability by altering AIS structure. Amyloid precursor protein (APP), implicated in Alzheimer's disease, regulates AIS position via its nonpathological functions, interacting directly with ankyrin-G and βIV spectrin. Increasing glutamate concentration in cultures activates APP production and leads to a shortening and distal movement of the AIS. Similar effects are observed with APP overexpression. This suggests that its function is sufficient to drive AIS plasticity, but whether APP is necessary remains unclear (339). Similar effects are observed within mouse models where the tau protein, which interacts with microtubules, is subject to excess phosphorylation, as seen in Alzheimer's disease and frontotemporal dementia (340). Hippocampal pyramidal cells in these mouse models have dampened excitability, in part due to a distal movement of the AIS (271). The addition of toxic extracellular tau oligomers to cultured hippocampal neurons causes a partial disruption of the AIS structure that is dependent on intracellular tau (341). Increased expression of the microRNA miR-342-5p is seen in mouse models of Alzheimer's disease and causes decreases in ankyrin-G expression and subsequent disruptions in AIS functions (342, 343).

In amyotrophic lateral sclerosis (ALS), apparent nonhomeostatic changes in AIS structure are observed. In human-derived motor neuron models of ALS, the AIS was longer than normal and motor neurons were hyperexcitable. The AIS from these motor neurons was insensitive to activity manipulations that normally drive structural plasticity, suggesting that impairments in plasticity may be central to ALS etiology (274). Similarly, long initial segments were observed in a mouse model of ALS (344), and in post mortem human tissue, the AIS has been found to be larger in diameter via electron microscopy imaging that likely could not quantify overall length (345). In multiple sclerosis, by contrast, AIS length increases were observed only in layer 5/6 neocortical pyramidal cells associated with myelin loss (346).

3.6. Traumatic Brain Injury

Blunt force trauma leads to circuit restructuring, with effects on initial segments. Several observations suggest that these are apparent neuroprotective effects to compensate for aberrant hyperexcitability, at least with mild cases, but that neurodegenerative issues can arise with more severe trauma. For example, blast force trauma experienced by an animal within a tube decreases AIS length in neocortical and hippocampal pyramidal cells in rats. These animals also exhibited deficits in novel object recognition following trauma (347). Focused "mild" concussive events, delivered directly to the exposed neocortical dura in mouse, also reduce AIS length, with a corresponding reduction in the AIS component of the AP waveform (270). Molecularly, traumatic events that damage cells and axons appear to do so via activation of calpain. Calpain targets major AIS scaffolds, including ankyrin-G and βIV spectrin, and can, at times, lead to the complete elimination of the AIS (348). With increasing trauma, other issues arise, including axotomy that is preceded by an accumulation of APP (349–351) and the recruitment of microglia that normally never target the AIS (352). This suggests that similar cellular mechanisms are shared across trauma and degeneration.

3.7. Concluding Thoughts on the AIS in Disease

It is becoming increasingly clear that the AIS is altered in a growing number of human diseases, but it remains a major challenge to disentangle causation from plasticity-induced changes. Variants in resident AIS proteins also tend to cause complicated and variable phenotypes with multiple comorbidities. For example, biallelic variants in the AIS organizing protein ankyrin-G cause a broad spectrum of phenotypes, including ID, language delay, motor delay, psychiatric disorders, epilepsy, sleep dysfunction, hypotonia, ataxia, and autism spectrum disorder (308, 309). Additionally, ankyrin-G has multiple functions in neurons beyond the AIS, including scaffolding channels in proximal dendrites, stabilizing GABAergic synapses, and modulating excitatory synapses in dendritic spines. Similar complexities in function exist for other AIS proteins, including Na_Vs, neurofascin, α-spectrin, and others. Continued efforts to fully understand the AIS and its unique function in neuronal excitability, polarity, and cellular signaling will not only help illuminate its role in health but also in a range of disease states.

CORRESPONDENCE

P. M. Jenkins (pjenkins@umich.edu); K. J. Bender (kevin.bender@ucsf.edu).

ACKNOWLEDGMENTS

We thank Dr. Elisa D'Este (Max Planck Institute for Medical Research, Heidelberg, Germany) and Dr. Maren Engelhardt (Johannes Kepler University, Linz, Austria) for providing images. We also thank Drs. Ryan Alexander and Vanessa Bender (University of California, San Francisco) for critical review of the manuscript.

GRANTS

This work was supported by grants from the National Institutes of Health (R01MH126960 to K.J.B. and P.M.J; R01MH125978 to K.J.B.), SFARI (4551 and 899599 to K.J.B.), a Hodgkin Huxley Research Award from FamilieSCN2A (to K.J.B.), and a Million Dollar Bike Ride award from the Orphan Disease Center at the University of Pennsylvania and FamilieSCN2A (to P.M.J.).

DISCLOSURES

No conflicts of interest, financial or otherwise, are declared by the authors.

AUTHOR CONTRIBUTIONS

P.M.J. and K.J.B. prepared figures; P.M.J. and K.J.B. drafted manuscript; P.M.J. and K.J.B. edited and revised manuscript; P.M.J. and K.J.B. approved final version of manuscript.

REFERENCES

1. Palay SL, Sotelo C, Peters A, Orkand PM**.** The axon hillock and the initial segment. **J Cell Biol** 38: 193–201, 1968. doi:10.1083/jcb.38.1.193.
2. Peters A, Proskauer CC, Kaiserman-Abramof IR**.** The small pyramidal neuron of the rat cerebral cortex. The axon hillock and initial segment. **J Cell Biol** 39: 604–619, 1968. doi:10.1083/jcb.39.3.604.
3. Nelson AD, Catalfio AM, Gupta JP, Min L, Caballero-Floran RN, Dean KP, Elvira CC, Derderian KD, Kyoung H, Sahagun A, Sanders SJ, Bender KJ, Jenkins PM**.** Physical and functional convergence of the autism risk genes Scn2a and Ank2 in neocortical pyramidal cell dendrites. **Neuron** 112: 1133–1149.e6, 2024. doi:10.1016/j.neuron.2024.01.003.
4. D'Este E, Kamin D, Göttfert F, El-Hady A, Hell SW**.** STED nanoscopy reveals the ubiquity of subcortical cytoskeleton periodicity in living neurons. **Cell Rep** 10: 1246–1251, 2015. doi:10.1016/j.celrep.2015.02.007.
5. Xu K, Zhong G, Zhuang X**.** Actin, spectrin, and associated proteins form a periodic cytoskeletal structure in axons. **Science** 339: 452–456, 2013. doi:10.1126/science.1232251.
6. Grubb MS, Shu Y, Kuba H, Rasband MN, Wimmer VC, Bender KJ**.** Short- and long-term plasticity at the axon initial segment. **J Neurosci** 31: 16049–16055, 2011. doi:10.1523/JNEUROSCI.4064-11.2011.
7. Huang CY, Rasband MN**.** Axon initial segments: structure, function, and disease. **Ann N Y Acad Sci** 1420: 46–61, 2018. doi:10.1111/nyas.13718.
8. Leterrier C**.** The axon initial segment: an updated viewpoint. **J Neurosci** 38: 2135–2145, 2018. doi:10.1523/JNEUROSCI.1922-17.2018.
9. Bender KJ, Trussell LO**.** The physiology of the axon initial segment. **Annu Rev Neurosci** 35: 249–265, 2012. doi:10.1146/annurev-neuro-062111-150339.
10. Kole MH, Stuart GJ**.** Signal processing in the axon initial segment. **Neuron** 73: 235–247, 2012. doi:10.1016/j.neuron.2012.01.007.
11. Nelson AD, Jenkins PM**.** Axonal membranes and their domains: assembly and function of the axon initial segment and node of Ranvier. **Front Cell Neurosci** 11: 136, 2017. doi:10.3389/fncel.2017.00136.
12. Jegla T, Nguyen MM, Feng C, Goetschius DJ, Luna E, van Rossum DB, Kamel B, Pisupati A, Milner ES, Rolls MM**.** Bilaterian giant ankyrins have a common evolutionary origin and play a conserved role in patterning the axon initial segment. **PLoS Genet** 12: e1006457, 2016. doi:10.1371/journal.pgen.1006457.
13. Eichel K, Uenaka T, Belapurkar V, Lu R, Cheng S, Pak JS, Taylor CA, Südhof TC, Malenka R, Wernig M, Özkan E, Perrais D, Shen K**.** Endocytosis in the axon initial segment maintains neuronal polarity. **Nature** 609: 128–135, 2022. doi:10.1038/s41586-022-05074-5.
14. Pan Z, Kao T, Horvath Z, Lemos J, Sul JY, Cranstoun SD, Bennett V, Scherer SS, Cooper EC**.** A common ankyrin-G-based mechanism retains KCNQ and NaV channels at electrically active domains of the axon. **J Neurosci** 26: 2599–2613, 2006. doi:10.1523/JNEUROSCI.4314-05.2006.
15. Bennett V, Stenbuck PJ**.** The membrane attachment protein for spectrin is associated with band 3 in human erythrocyte membranes. **Nature** 280: 468–473, 1979. doi:10.1038/280468a0.
16. Bennett V, Stenbuck PJ**.** Human erythrocyte ankyrin. Purification and properties. **J Biol Chem** 255: 2540–2548, 1980.
17. Lux SE, John KM, Bennett V**.** Analysis of cDNA for human erythrocyte ankyrin indicates a repeated structure with homology to tissue-differentiation and cell-cycle control proteins. **Nature** 344: 36–42, 1990. doi:10.1038/344036a0.
18. Davis JQ, Bennett V**.** Brain ankyrin. A membrane-associated protein with binding sites for spectrin, tubulin, and the cytoplasmic domain of the erythrocyte anion channel. **J Biol Chem** 259: 13550–13559, 1984. doi:10.1016/S0021-9258(18)90728-3.
19. Otto E, Kunimoto M, McLaughlin T, Bennett V**.** Isolation and characterization of cDNAs encoding human brain ankyrins reveal a family of alternatively spliced genes. **J Cell Biol** 114: 241–253, 1991. doi:10.1083/jcb.114.2.241.
20. Kordeli E, Lambert S, Bennett V**.** AnkyrinG. A new ankyrin gene with neural-specific isoforms localized at the axonal initial segment and node of Ranvier. **J Biol Chem** 270: 2352–2359, 1995. doi:10.1074/jbc.270.5.2352.
21. Peters LL, John KM, Lu FM, Eicher EM, Higgins A, Yialamas M, Turtzo LC, Otsuka AJ, Lux SE**.** Ank3 (epithelial ankyrin), a widely distributed new member of the ankyrin gene family and the major ankyrin in kidney, is expressed in alternatively spliced forms, including forms that lack the repeat domain. **J Cell Biol** 130: 313–330, 1995. doi:10.1083/jcb.130.2.313.
22. Bennett V, Lorenzo DN**.** Spectrin- and ankyrin-based membrane domains and the evolution of vertebrates. **Curr Top Membr** 72: 1–37, 2013. doi:10.1016/B978-0-12-417027-8.00001-5.
23. Hedstrom KL, Ogawa Y, Rasband MN**.** AnkyrinG is required for maintenance of the axon initial segment and neuronal polarity. **J Cell Biol** 183: 635–640, 2008. doi:10.1083/jcb.200806112.
24. Zhou D, Lambert S, Malen PL, Carpenter S, Boland LM, Bennett V**.** AnkyrinG is required for clustering of voltage-gated Na channels at axon initial segments and for normal action potential firing. **J Cell Biol** 143: 1295–1304, 1998. doi:10.1083/jcb.143.5.1295.
25. Smith KR, Kopeikina KJ, Fawcett-Patel JM, Leaderbrand K, Gao R, Schurmann B, Myczek K, Radulovic J, Swanson GT, Penzes P**.** Psychiatric risk factor ANK3/ankyrin-G nanodomains regulate the

structure and function of glutamatergic synapses. **Neuron** 84: 399–415, 2014. doi:10.1016/j.neuron.2014.10.010.

26. Zhang X, Bennett V. Restriction of 480/270-kD ankyrin G to axon proximal segments requires multiple ankyrin G-specific domains. **J Cell Biol** 142: 1571–1581, 1998. doi:10.1083/jcb.142.6.1571.

27. Jenkins PM, Kim N, Jones SL, Tseng WC, Svitkina TM, Yin HH, Bennett V. Giant ankyrin-G: a critical innovation in vertebrate evolution of fast and integrated neuronal signaling. **Proc Natl Acad Sci USA** 112: 957–964, 2015. doi:10.1073/pnas.1416544112.

28. Freal A, Fassier C, Le Bras B, Bullier E, De Gois S, Hazan J, Hoogenraad CC, Couraud F. Cooperative interactions between 480 kDa ankyrin-G and EB proteins assemble the axon initial segment. **J Neurosci** 36: 4421–4433, 2016. doi:10.1523/JNEUROSCI.3219-15.2016.

29. Komada M, Soriano P. [Beta]IV-spectrin regulates sodium channel clustering through ankyrin-G at axon initial segments and nodes of Ranvier. **J Cell Biol** 156: 337–348, 2002. doi:10.1083/jcb.200110003.

30. Yang Y, Ogawa Y, Hedstrom KL, Rasband MN. betaIV spectrin is recruited to axon initial segments and nodes of Ranvier by ankyrinG. **J Cell Biol** 176: 509–519, 2007. doi:10.1083/jcb.200610128.

31. Leterrier C, Vacher H, Fache MP, d'Ortoli SA, Castets F, Autillo-Touati A, Dargent B. End-binding proteins EB3 and EB1 link microtubules to ankyrin G in the axon initial segment. **Proc Natl Acad Sci USA** 108: 8826–8831, 2011. doi:10.1073/pnas.1018671108.

32. Stevens SR, Rasband MN. Pleiotropic ankyrins: scaffolds for ion channels and transporters. **Channels (Austin)** 16: 216–229, 2022. doi:10.1080/19336950.2022.2120467.

33. Yang R, Walder-Christensen KK, Kim N, Wu D, Lorenzo DN, Badea A, Jiang YH, Yin HH, Wetsel WC, Bennett V. ANK2 autism mutation targeting giant ankyrin-B promotes axon branching and ectopic connectivity. **Proc Natl Acad Sci USA** 116: 15262–15271, 2019. doi:10.1073/pnas.1904348116.

34. Lorenzo DN, Badea A, Davis J, Hostettler J, He J, Zhong G, Zhuang X, Bennett V. A PIK3C3-ankyrin-B-dynactin pathway promotes axonal growth and multiorganelle transport. **J Cell Biol** 207: 735–752, 2014. doi:10.1083/jcb.201407063.

35. Stevens SR, van der Heijden ME, Ogawa Y, Lin T, Sillitoe RV, Rasband MN. Ankyrin-R links Kv3.3 to the spectrin cytoskeleton and is required for purkinje neuron survival. **J Neurosci** 42: 2–15, 2022. doi:10.1523/JNEUROSCI.1132-21.2021.

36. Stevens SR, Longley CM, Ogawa Y, Teliska LH, Arumanayagam AS, Nair S, Oses-Prieto JA, Burlingame AL, Cykowski MD, Xue M, Rasband MN. Ankyrin-R regulates fast-spiking interneuron excitability through perineuronal nets and Kv3.1b K+ channels. **eLife** 10: e66491, 2021. doi:10.7554/eLife.66491.

37. Staufenbiel M. Ankyrin-bound fatty acid turns over rapidly at the erythrocyte plasma membrane. **Mol Cell Biol** 7: 2981–2984, 1987. doi:10.1128/mcb.7.8.2981-2984.1987.

38. He M, Jenkins P, Bennett V. Cysteine 70 of ankyrin-G is S-palmitoylated and is required for function of ankyrin-G in membrane domain assembly. **J Biol Chem** 287: 43995–44005, 2012. doi:10.1074/jbc.M112.417501.

39. Gupta JP, Jenkins PM. Ankyrin-B is lipid-modified by S-palmitoylation to promote dendritic membrane scaffolding of voltage-gated sodium channel Na(V)1.2 in neurons. **Front Physiol** 14: 959660, 2023. doi:10.3389/fphys.2023.959660.

40. Tseng WC, Jenkins PM, Tanaka M, Mooney R, Bennett V. Giant ankyrin-G stabilizes somatodendritic GABAergic synapses through opposing endocytosis of GABAA receptors. **Proc Natl Acad Sci USA** 112: 1214–1219, 2015. doi:10.1073/pnas.1417989112.

41. Fukata Y, Fukata M. Protein palmitoylation in neuronal development and synaptic plasticity. **Nat Rev Neurosci** 11: 161–175, 2010. doi:10.1038/nrn2788.

42. Mesquita FS, Abrami L, Linder ME, Bamji SX, Dickinson BC, van der Goot FG. Mechanisms and functions of protein S-acylation. **Nat Rev Mol Cell Biol** 25: 488–509, 2024. doi:10.1038/s41580-024-00700-8.

43. He M, Abdi KM, Bennett V. Ankyrin-G palmitoylation and betaII-spectrin binding to phosphoinositide lipids drive lateral membrane assembly. **J Cell Biol** 206: 273–288, 2014. doi:10.1083/jcb.201401016.

44. Philippe JM, Jenkins PM. Spatial organization of palmitoyl acyl transferases governs substrate localization and function. **Mol Membr Biol** 35: 60–75, 2019. doi:10.1080/09687688.2019.1710274.

45. Galiano MR, Jha S, Ho TS, Zhang C, Ogawa Y, Chang KJ, Stankewich MC, Mohler PJ, Rasband MN. A distal axonal cytoskeleton forms an intra-axonal boundary that controls axon initial segment assembly. **Cell** 149: 1125–1139, 2012. doi:10.1016/j.cell.2012.03.039.

46. Yamada R, Kuba H. Structural and functional plasticity at the axon initial segment. **Front Cell Neurosci** 10: 250, 2016. doi:10.3389/fncel.2016.00250.

47. Hu W, Tian C, Li T, Yang M, Hou H, Shu Y. Distinct contributions of Na(v)1.6 and Na(v)1.2 in action potential initiation and backpropagation. **Nat Neurosci** 12: 996–1002, 2009. doi:10.1038/nn.2359.

48. Li T, Tian C, Scalmani P, Frassoni C, Mantegazza M, Wang Y, Yang M, Wu S, Shu Y. Action potential initiation in neocortical inhibitory interneurons. **PLoS Biol** 12: e1001944, 2014. doi:10.1371/journal.pbio.1001944.

49. Tian C, Wang K, Ke W, Guo H, Shu Y. Molecular identity of axonal sodium channels in human cortical pyramidal cells. **Front Cell Neurosci** 8: 297, 2014. doi:10.3389/fncel.2014.00297.

50. Yamagata T, Ogiwara I, Mazaki E, Yanagawa Y, Yamakawa K. Nav1.2 is expressed in caudal ganglionic eminence-derived disinhibitory interneurons: mutually exclusive distributions of Nav1.1 and Nav1.2. **Biochem Biophys Res Commun** 491: 1070–1076, 2017. doi:10.1016/j.bbrc.2017.08.013.

51. Leterrier C, Clerc N, Rueda-Boroni F, Montersino A, Dargent B, Castets F. Ankyrin G membrane partners drive the establishment and maintenance of the axon initial segment. **Front Cell Neurosci** 11: 6, 2017. doi:10.3389/fncel.2017.00006.

52. Xu X, Shrager P. Dependence of axon initial segment formation on Na+ channel expression. **J Neurosci Res** 79: 428–441, 2005. doi:10.1002/jnr.20378.

53. Spratt PW, Alexander RP, Ben-Shalom R, Sahagun A, Kyoung H, Keeshen CM, Sanders SJ, Bender KJ. Paradoxical hyperexcitability from Na(V)1.2 sodium channel loss in neocortical pyramidal cells. **Cell Rep** 36: 109483, 2021. doi:10.1016/j.celrep.2021.109483.

54. Katz E, Stoler O, Scheller A, Khrapunsky Y, Goebbels S, Kirchhoff F, Gutnick MJ, Wolf F, Fleidervish IA. Role of sodium channel subtype in action potential generation by neocortical pyramidal neurons. **Proc Natl Acad Sci USA** 115: E7184–E7192, 2018. doi:10.1073/pnas.1720493115.

55. Hedstrom KL, Xu X, Ogawa Y, Frischknecht R, Seidenbecher CI, Shrager P, Rasband MN. Neurofascin assembles a specialized extracellular matrix at the axon initial segment. **J Cell Biol** 178: 875–886, 2007. doi:10.1083/jcb.200705119.

56. Zonta B, Desmazieres A, Rinaldi A, Tait S, Sherman DL, Nolan MF, Brophy PJ**.** A critical role for Neurofascin in regulating action potential initiation through maintenance of the axon initial segment. **Neuron** 69: 945–956, 2011. doi:10.1016/j.neuron.2011.02.021.

57. Huang CY, Zhang C, Ho TS, Oses-Prieto J, Burlingame AL, Lalonde J, Noebels JL, Leterrier C, Rasband MN**.** αII spectrin forms a periodic cytoskeleton at the axon initial segment and is required for nervous system function. **J Neurosci** 37: 11311–11322, 2017. doi:10.1523/JNEUROSCI.2112-17.2017.

58. Wang Y, Ji T, Nelson AD, Glanowska K, Murphy GG, Jenkins PM, Parent JM**.** Critical roles of alphaII spectrin in brain development and epileptic encephalopathy. **J Clin Invest** 128: 760–773, 2018. doi:10.1172/JCI95743.

59. Berghs S, Aggujaro D, Dirkx R Jr, Maksimova E, Stabach P, Hermel JM, Zhang JP, Philbrick W, Slepnev V, Ort T, Solimena M**.** βIV spectrin, a new spectrin localized at axon initial segments and nodes of Ranvier in the central and peripheral nervous system. **J Cell Biol** 151: 985–1002, 2000. doi:10.1083/jcb.151.5.985.

60. Lacas-Gervais S, Guo J, Strenzke N, Scarfone E, Kolpe M, Jahkel M, De Camilli P, Moser T, Rasband MN, Solimena M**.** BetaIVSigma1 spectrin stabilizes the nodes of Ranvier and axon initial segments. **J Cell Biol** 166: 983–990, 2004. doi:10.1083/jcb.200408007.

61. van Beuningen SF, Will L, Harterink M, Chazeau A, van Battum EY, Frias CP, Franker MA, Katrukha EA, Stucchi R, Vocking K, Antunes AT, Slenders L, Doulkeridou S, Sillevis Smitt P, Altelaar AF, Post JA, Akhmanova A, Pasterkamp RJ, Kapitein LC, de Graaff E, Hoogenraad CC**.** TRIM46 controls neuronal polarity and axon specification by driving the formation of parallel microtubule arrays. **Neuron** 88: 1208–1226, 2015. doi:10.1016/j.neuron.2015.11.012.

62. Melton A, Palfini V, Ogawa Y, Rasband MN**.** TRIM46 is not required for axon specification or axon initial segment formation in vivo (Preprint). **bioRxiv** 2024.2005.2023.595556, 2024. doi:10.1101/2024.05.23.595556.

63. Fréal A, Rai D, Tas RP, Pan X, Katrukha EA, van de Willige D, Stucchi R, Aher A, Yang C, Altelaar AF, Vocking K, Post JA, Harterink M, Kapitein LC, Akhmanova A, Hoogenraad CC**.** Feedback-driven assembly of the axon initial segment. **Neuron** 104: 305–321.e8, 2019. doi:10.1016/j.neuron.2019.07.029.

64. Yoon S, Myczek K, Penzes P**.** cAMP signaling-mediated phosphorylation of diacylglycerol lipase α regulates interaction with ankyrin-G and dendritic spine morphology. **Biol Psychiatry** 90: 263–274, 2021. doi:10.1016/j.biopsych.2021.03.023.

65. Hamdan H, Lim BC, Torii T, Joshi A, Konning M, Smith C, Palmer DJ, Ng P, Leterrier C, Oses-Prieto JA, Burlingame AL, Rasband MN**.** Mapping axon initial segment structure and function by multiplexed proximity biotinylation. **Nat Commun** 11: 100, 2020. doi:10.1038/s41467-019-13658-5.

66. Rees JS, Li XW, Perrett S, Lilley KS, Jackson AP**.** Selective proteomic proximity labeling assay using tyramide (SPPLAT): a quantitative method for the proteomic analysis of localized membrane-bound protein clusters. **Curr Protoc Protein Sci** 88: 19.27.1–19.27.18, 2017. doi:10.1002/cpps.27.

67. Oakley JV, Buksh BF, Fernández DF, Oblinsky DG, Seath CP, Geri JB, Scholes GD, MacMillan DW**.** Radius measurement via super-resolution microscopy enables the development of a variable radii proximity labeling platform. **Proc Natl Acad Sci USA** 119: e2203027119, 2022. doi:10.1073/pnas.2203027119.

68. Ogawa Y, Lim BC, George S, Oses-Prieto JA, Rasband JM, Eshed-Eisenbach Y, Hamdan H, Nair S, Boato F, Peles E, Burlingame AL, Van Aelst L, Rasband MN**.** Antibody-directed extracellular proximity biotinylation reveals that Contactin-1 regulates axo-axonic innervation of axon initial segments. **Nat Commun** 14: 6797, 2023. doi:10.1038/s41467-023-42273-8.

69. Franssen EH, Zhao RR, Koseki H, Kanamarlapudi V, Hoogenraad CC, Eva R, Fawcett JW**.** Exclusion of integrins from CNS axons is regulated by Arf6 activation and the AIS. **J Neurosci** 35: 8359–8375, 2015. doi:10.1523/JNEUROSCI.2850-14.2015.

70. Sobotzik JM, Sie JM, Politi C, Del Turco D, Bennett V, Deller T, Schultz C**.** AnkyrinG is required to maintain axo-dendritic polarity in vivo. **Proc Natl Acad Sci USA** 106: 17564–17569, 2009. doi:10.1073/pnas.0909267106.

71. Bentley M, Banker G**.** The cellular mechanisms that maintain neuronal polarity. **Nat Rev Neurosci** 17: 611–622, 2016. doi:10.1038/nrn.2016.100.

72. Burack MA, Silverman MA, Banker G**.** The role of selective transport in neuronal protein sorting. **Neuron** 26: 465–472, 2000. doi:10.1016/s0896-6273(00)81178-2.

73. Nakata T, Hirokawa N**.** Microtubules provide directional cues for polarized axonal transport through interaction with kinesin motor head. **J Cell Biol** 162: 1045–1055, 2003. doi:10.1083/jcb.200302175.

74. Jensen CS, Watanabe S, Rasmussen HB, Schmitt N, Olesen SP, Frost NA, Blanpied TA, Misonou H**.** Specific sorting and post-Golgi trafficking of dendritic potassium channels in living neurons. **J Biol Chem** 289: 10566–10581, 2014. doi:10.1074/jbc.M113.534495.

75. Jenkins B, Decker H, Bentley M, Luisi J, Banker G**.** A novel split kinesin assay identifies motor proteins that interact with distinct vesicle populations. **J Cell Biol** 198: 749–761, 2012. doi:10.1083/jcb.201205070.

76. Farias GG, Guardia CM, Britt DJ, Guo X, Bonifacino JS**.** Sorting of dendritic and axonal vesicles at the pre-axonal exclusion zone. **Cell Rep** 13: 1221–1232, 2015. doi:10.1016/j.celrep.2015.09.074.

77. Nirschl JJ, Ghiretti AE, Holzbaur EL**.** The impact of cytoskeletal organization on the local regulation of neuronal transport. **Nat Rev Neurosci** 18: 585–597, 2017. doi:10.1038/nrn.2017.100.

78. Huang CF, Banker G**.** The translocation selectivity of the kinesins that mediate neuronal organelle transport. **Traffic** 13: 549–564, 2012. doi:10.1111/j.1600-0854.2011.01325.x.

79. Dotti CG, Sullivan CA, Banker GA**.** The establishment of polarity by hippocampal neurons in culture. **J Neurosci** 8: 1454–1468, 1988. doi:10.1523/JNEUROSCI.08-04-01454.1988.

80. Jacobson C, Schnapp B, Banker GA**.** A change in the selective translocation of the kinesin-1 motor domain marks the initial specification of the axon. **Neuron** 49: 797–804, 2006. doi:10.1016/j.neuron.2006.02.005.

81. Lewis TL Jr, Mao T, Svoboda K, Arnold DB**.** Myosin-dependent targeting of transmembrane proteins to neuronal dendrites. **Nat Neurosci** 12: 568–576, 2009. doi:10.1038/nn.2318.

82. Al-Bassam S, Xu M, Wandless TJ, Arnold DB**.** Differential trafficking of transport vesicles contributes to the localization of dendritic proteins. **Cell Rep** 2: 89–100, 2012. doi:10.1016/j.celrep.2012.05.018.

83. Watanabe K, Al-Bassam S, Miyazaki Y, Wandless TJ, Webster P, Arnold DB**.** Networks of polarized actin filaments in the axon initial segment provide a mechanism for sorting axonal and dendritic proteins. **Cell Rep** 2: 1546–1553, 2012. doi:10.1016/j.celrep.2012.11.015.

84. Balasanyan V, Watanabe K, Dempsey WP, Lewis TL Jr, Trinh LA, Arnold DB. Structure and function of an actin-based filter in the proximal axon. **Cell Rep** 21: 2696–2705, 2017. doi:10.1016/j.celrep.2017.11.046.

85. Janssen AF, Tas RP, van Bergeijk P, Oost R, Hoogenraad CC, Kapitein LC. Myosin-V induces cargo immobilization and clustering at the axon initial segment. **Front Cell Neurosci** 11: 260, 2017. doi:10.3389/fncel.2017.00260.

86. Kuijpers M, van de Willige D, Freal A, Chazeau A, Franker MA, Hofenk J, Rodrigues RJ, Kapitein LC, Akhmanova A, Jaarsma D, Hoogenraad CC. Dynein regulator NDEL1 controls polarized cargo transport at the axon initial segment. **Neuron** 89: 461–471, 2016. doi:10.1016/j.neuron.2016.01.022.

87. Klinman E, Tokito M, Holzbaur EL. CDK5-dependent activation of dynein in the axon initial segment regulates polarized cargo transport in neurons. **Traffic** 18: 808–824, 2017. doi:10.1111/tra.12529.

88. Guo X, Farías GG, Mattera R, Bonifacino JS. Rab5 and its effector FHF contribute to neuronal polarity through dynein-dependent retrieval of somatodendritic proteins from the axon. **Proc Natl Acad Sci USA** 113: E5318–E5327, 2016. doi:10.1073/pnas.1601844113.

89. Winckler B, Forscher P, Mellman I. A diffusion barrier maintains distribution of membrane proteins in polarized neurons. **Nature** 397: 698–701, 1999. doi:10.1038/17806.

90. Kobayashi T, Storrie B, Simons K, Dotti CG. A functional barrier to movement of lipids in polarized neurons. **Nature** 359: 647–650, 1992. doi:10.1038/359647a0.

91. Nakada C, Ritchie K, Oba Y, Nakamura M, Hotta Y, Iino R, Kasai RS, Yamaguchi K, Fujiwara T, Kusumi A. Accumulation of anchored proteins forms membrane diffusion barriers during neuronal polarization. **Nat Cell Biol** 5: 626–632, 2003. doi:10.1038/ncb1009.

92. Song AH, Wang D, Chen G, Li Y, Luo J, Duan S, Poo MM. A selective filter for cytoplasmic transport at the axon initial segment. **Cell** 136: 1148–1160, 2009. doi:10.1016/j.cell.2009.01.016.

93. Futerman AH, Khanin R, Segel LA. Lipid diffusion in neurons. **Nature** 362: 119, 1993. doi:10.1038/362119a0.

94. Fujiwara T, Ritchie K, Murakoshi H, Jacobson K, Kusumi A. Phospholipids undergo hop diffusion in compartmentalized cell membrane. **J Cell Biol** 157: 1071–1081, 2002. doi:10.1083/jcb.200202050.

95. Akhmanova A, Hoogenraad CC. Microtubule minus-end-targeting proteins. **Curr Biol** 25: R162–171, 2015. doi:10.1016/j.cub.2014.12.027.

96. Ichinose S, Ogawa T, Jiang X, Hirokawa N. The spatiotemporal construction of the axon initial segment via KIF3/KAP3/TRIM46 transport under MARK2 signaling. **Cell Rep** 28: 2413–2426.e7, 2019. doi:10.1016/j.celrep.2019.07.093.

97. Mendoza CS, Plowinske CR, Montgomery AC, Quinones GB, Banker G, Bentley M. Kinesin regulation in the proximal axon is essential for dendrite-selective transport. **Mol Biol Cell** 35: ar81, 2024. doi:10.1091/mbc.E23-11-0457.

98. Thies E, Mandelkow EM. Missorting of tau in neurons causes degeneration of synapses that can be rescued by the kinase MARK2/Par-1. **J Neurosci** 27: 2896–2907, 2007. doi:10.1523/JNEUROSCI.4674-06.2007.

99. Bourke AM, Schwartz SL, Bowen AB, Kleinjan MS, Winborn CS, Kareemo DJ, Gutnick A, Schwarz TL, Kennedy MJ. zapERtrap: a light-regulated ER release system reveals unexpected neuronal trafficking pathways. **J Cell Biol** 220: e202103186, 2021. doi:10.1083/jcb.202103186.

100. Fréal A, Jamann N, Ten Bos J, Jansen J, Petersen N, Ligthart T, Hoogenraad CC, Kole MH. Sodium channel endocytosis drives axon initial segment plasticity. **Sci Adv** 9: eadf3885, 2023. doi:10.1126/sciadv.adf3885.

101. Torii T, Ogawa Y, Liu CH, Ho TS, Hamdan H, Wang CC, Oses-Prieto JA, Burlingame AL, Rasband MN. NuMA1 promotes axon initial segment assembly through inhibition of endocytosis. **J Cell Biol** 219: e201907048, 2019. doi:10.1083/jcb.201907048.

102. Jenkins PM, He M, Bennett V. Dynamic spectrin/ankyrin-G microdomains promote lateral membrane assembly by opposing endocytosis. **Sci Adv** 1: e1500301, 2015. doi:10.1126/sciadv.1500301.

103. Wernert F, Moparthi SB, Pelletier F, Lainé J, Simons E, Moulay G, Rueda F, Jullien N, Benkhelifa-Ziyyat S, Papandréou MJ, Leterrier C, Vassilopoulos S. The actin-spectrin submembrane scaffold restricts endocytosis along proximal axons. **Science** 385: eado2032, 2024. doi:10.1126/science.ado2032.

104. Meeks JP, Mennerick S. Action potential initiation and propagation in CA3 pyramidal axons. **J Neurophysiol** 97: 3460–3472, 2007. doi:10.1152/jn.01288.2006.

105. Rowan MJ, Tranquil E, Christie JM. Distinct Kv channel subtypes contribute to differences in spike signaling properties in the axon initial segment and presynaptic boutons of cerebellar interneurons. **J Neurosci** 34: 6611–6623, 2014. doi:10.1523/JNEUROSCI.4208-13.2014.

106. Khaliq ZM, Raman IM. Relative contributions of axonal and somatic Na channels to action potential initiation in cerebellar Purkinje neurons. **J Neurosci** 26: 1935–1944, 2006. doi:10.1523/JNEUROSCI.4664-05.2006.

107. Shu Y, Duque A, Yu Y, Haider B, McCormick DA. Properties of action-potential initiation in neocortical pyramidal cells: evidence from whole cell axon recordings. **J Neurophysiol** 97: 746–760, 2007. doi:10.1152/jn.00922.2006.

108. Lipkin AM, Cunniff MM, Spratt PW, Lemke SM, Bender KJ. Functional microstructure of Ca(V)-mediated calcium signaling in the axon initial segment. **J Neurosci** 41: 3764–3776, 2021. doi:10.1523/JNEUROSCI.2843-20.2021.

109. Filipis L, Canepari M. Optical measurement of physiological sodium currents in the axon initial segment. **J Physiol** 599: 49–66, 2021. doi:10.1113/JP280554.

110. Palmer LM, Stuart GJ. Site of action potential initiation in layer 5 pyramidal neurons. **J Neurosci** 26: 1854–1863, 2006. doi:10.1523/JNEUROSCI.4812-05.2006.

111. Foust A, Popovic M, Zecevic D, McCormick DA. Action potentials initiate in the axon initial segment and propagate through axon collaterals reliably in cerebellar Purkinje neurons. **J Neurosci** 30: 6891–6902, 2010. doi:10.1523/JNEUROSCI.0552-10.2010.

112. Lorincz A, Nusser Z. Cell-type-dependent molecular composition of the axon initial segment. **J Neurosci** 28: 14329–14340, 2008. doi:10.1523/JNEUROSCI.4833-08.2008.

113. Kole MH, Stuart GJ. Is action potential threshold lowest in the axon? **Nat Neurosci** 11: 1253–1255, 2008. doi:10.1038/nn.2203.

114. Catterall WA. Voltage-gated sodium channels at 60: structure, function and pathophysiology. **J Physiol** 590: 2577–2589, 2012. doi:10.1113/jphysiol.2011.224204.

115. Bouza AA, Isom LL. Voltage-gated sodium channel towardsubunits and their related diseases. **Handb Exp Pharmacol** 246: 423–450, 2018. doi:10.1007/164_2017_48.

116. Gazina EV, Leaw BT, Richards KL, Wimmer VC, Kim TH, Aumann TD, Featherby TJ, Churilov L, Hammond VE, Reid CA, Petrou S. 'Neonatal' Nav1.2 reduces neuronal excitability and affects seizure susceptibility and behaviour. **Hum Mol Genet** 24: 1457–1468, 2015. doi:10.1093/hmg/ddu562.

117. Akin EJ, Sole L, Dib-Hajj SD, Waxman SG, Tamkun MM. Preferential targeting of Nav1.6 voltage-gated Na+ channels to the axon initial segment during development. **PLoS One** 10: e0124397, 2015. doi:10.1371/journal.pone.0124397.

118. Boiko T, Van Wart A, Caldwell JH, Levinson SR, Trimmer JS, Matthews G. Functional specialization of the axon initial segment by isoform-specific sodium channel targeting. **J Neurosci** 23: 2306–2313, 2003. doi:10.1523/JNEUROSCI.23-06-02306.2003.

119. Favero M, Sotuyo NP, Lopez E, Kearney JA, Goldberg EM. A transient developmental window of fast-spiking interneuron dysfunction in a mouse model of Dravet syndrome. **J Neurosci** 38: 7912–7927, 2018. doi:10.1523/JNEUROSCI.0193-18.2018.

120. Kress GJ, Dowling MJ, Eisenman LN, Mennerick S. Axonal sodium channel distribution shapes the depolarized action potential threshold of dentate granule neurons. **Hippocampus** 20: 558–571, 2010. doi:10.1002/hipo.20667.

121. Royeck M, Horstmann MT, Remy S, Reitze M, Yaari Y, Beck H. Role of axonal NaV1.6 sodium channels in action potential initiation of CA1 pyramidal neurons. **J Neurophysiol** 100: 2361–2380, 2008. doi:10.1152/jn.90332.2008.

122. Osorio N, Alcaraz G, Padilla F, Couraud F, Delmas P, Crest M. Differential targeting and functional specialization of sodium channels in cultured cerebellar granule cells. **J Physiol** 569: 801–816, 2005. doi:10.1113/jphysiol.2005.097022.

123. Wang C, Derderian KD, Hamada E, Zhou X, Nelson AD, Kyoung H, Ahituv N, Bouvier G, Bender KJ. Impaired cerebellar plasticity hypersensitizes sensory reflexes in SCN2A-associated ASD. **Neuron** 112: 1444–1455.e5, 2024. doi:10.1016/j.neuron.2024.01.029.

124. Wimmer VC, Reid CA, Mitchell S, Richards KL, Scaf BB, Leaw BT, Hill EL, Royeck M, Horstmann MT, Cromer BA, Davies PJ, Xu R, Lerche H, Berkovic SF, Beck H, Petrou S. Axon initial segment dysfunction in a mouse model of genetic epilepsy with febrile seizures plus. **J Clin Invest** 120: 2661–2671, 2010. doi:10.1172/JCI42219.

125. Scala F, Nenov MN, Crofton EJ, Singh AK, Folorunso O, Zhang Y, Chesson BC, Wildburger NC, James TF, Alshammari MA, Alshammari TK, Elfrink H, Grassi C, Kasper JM, Smith AE, Hommel JD, Lichti CF, Rudra JS, D'Ascenzo M, Green TA, Laezza F. Environmental enrichment and social isolation mediate neuroplasticity of medium spiny neurons through the GSK3 pathway. **Cell Rep** 23: 555–567, 2018. doi:10.1016/j.celrep.2018.03.062.

126. Yang J, Xiao Y, Li L, He Q, Li M, Shu Y. Biophysical properties of somatic and axonal voltage-gated sodium channels in midbrain dopaminergic neurons. **Front Cell Neurosci** 13: 317, 2019. doi:10.3389/fncel.2019.00317.

127. Rush AM, Dib-Hajj SD, Waxman SG. Electrophysiological properties of two axonal sodium channels, Nav1.2 and Nav1.6, expressed in mouse spinal sensory neurones. **J Physiol** 564: 803–815, 2005. doi:10.1113/jphysiol.2005.083089.

128. Spratt PW, Ben-Shalom R, Keeshen CM, Burke KJ Jr, Clarkson RL, Sanders SJ, Bender KJ. The autism-associated gene Scn2a contributes to dendritic excitability and synaptic function in the prefrontal cortex. **Neuron** 103: 673–685.e5, 2019. doi:10.1016/j.neuron.2019.05.037.

129. Kroon T, van Hugte E, van Linge L, Mansvelder HD, Meredith RM. Early postnatal development of pyramidal neurons across layers of the mouse medial prefrontal cortex. **Sci Rep** 9: 5037, 2019. doi:10.1038/s41598-019-41661-9.

130. Thompson CH, Ben-Shalom R, Bender KJ, George AL. Alternative splicing potentiates dysfunction of early-onset epileptic encephalopathy SCN2A variants. **J Gen Physiol** 152: e201912442, 2020. doi:10.1085/jgp.201912442.

131. Liang L, Fazel Darbandi S, Pochareddy S, Gulden FO, Gilson MC, Sheppard BK, Sahagun A, An JY, Werling DM, Rubenstein JL, Sestan N, Bender KJ, Sanders SJ. Developmental dynamics of voltage-gated sodium channel isoform expression in the human and mouse brain. **Genome Med** 13: 135, 2021. doi:10.1186/s13073-021-00949-0.

132. Shvartsman A, Kotler O, Stoler O, Khrapunsky Y, Melamed I, Fleidervish IA. Subcellular distribution of persistent sodium conductance in cortical pyramidal neurons. **J Neurosci** 41: 6190–6201, 2021. doi:10.1523/JNEUROSCI.2989-20.2021.

133. Baranauskas G, David Y, Fleidervish IA. Spatial mismatch between the Na+ flux and spike initiation in axon initial segment. **Proc Natl Acad Sci USA** 110: 4051–4056, 2013. doi:10.1073/pnas.1215125110.

134. Astman N, Gutnick MJ, Fleidervish IA. Persistent sodium current in layer 5 neocortical neurons is primarily generated in the proximal axon. **J Neurosci** 26: 3465–3473, 2006. doi:10.1523/JNEUROSCI.4907-05.2006.

135. Drouillas B, Brocard C, Zanella S, Bos R, Brocard F. Persistent Nav1.1 and Nav1.6 currents drive spinal locomotor functions through nonlinear dynamics. **Cell Rep** 42: 113085, 2023. doi:10.1016/j.celrep.2023.113085.

136. Kotler O, Khrapunsky Y, Shvartsman A, Dai H, Plant LD, Goldstein SA, Fleidervish I. SUMOylation of Na(V)1.2 channels regulates the velocity of backpropagating action potentials in cortical pyramidal neurons. **eLife** 12: e81463, 2023. doi:10.7554/eLife.81463.

137. Echevarria-Cooper DM, Hawkins NA, Misra SN, Huffman AM, Thaxton T, Thompson CH, Ben-Shalom R, Nelson AD, Lipkin AM, George AL Jr, Bender KJ, Kearney JA. Cellular and behavioral effects of altered NaV1.2 sodium channel ion permeability in Scn2aK1422E mice. **Hum Mol Genet** 31: 2964–2988, 2022. doi:10.1093/hmg/ddac087.

138. Liu H, Wang HG, Pitt G, Liu Z. Direct observation of compartment-specific localization and dynamics of voltage-gated sodium channels. **J Neurosci** 42: 5482–5498, 2022. doi:10.1523/JNEUROSCI.0086-22.2022.

139. Ahuja S, Mukund S, Deng L, Khakh K, Chang E, Ho H, et al. Structural basis of Nav1.7 inhibition by an isoform-selective small-molecule antagonist. **Science** 350: aac5464, 2015. doi:10.1126/science.aac5464.

140. Goodchild SJ, Shuart NG, Williams AD, Ye W, Parrish RR, Soriano M, Thouta S, Mezeyova J, Waldbrook M, Dean R, Focken T, Ghovanloo MR, Ruben PC, Scott F, Cohen CJ, Empfield J, Johnson JP. Molecular pharmacology of selective Na(V)1.6 and dual Na(V)1.6/Na(V)1.2 channel inhibitors that suppress excitatory neuronal activity ex vivo. **ACS Chem Neurosci** 15: 1169–1184, 2024. doi:10.1021/acschemneuro.3c00757.

141. Colbert CM, Pan E. Ion channel properties underlying axonal action potential initiation in pyramidal neurons. **Nat Neurosci** 5: 533–538, 2002. doi:10.1038/nn0602-857.

142. Colbert CM, Johnston D. Axonal action-potential initiation and Na+ channel densities in the soma and axon initial segment of subicular pyramidal neurons. **J Neurosci** 16: 6676–6686, 1996. doi:10.1523/JNEUROSCI.16-21-06676.1996.

143. Kole MH, Ilschner SU, Kampa BM, Williams SR, Ruben PC, Stuart GJ. Action potential generation requires a high sodium channel density in the axon initial segment. **Nat Neurosci** 11: 178–186, 2008. doi:10.1038/nn2040.

144. Lorincz A, Nusser Z. Molecular identity of dendritic voltage-gated sodium channels. **Science** 328: 906–909, 2010. doi:10.1126/science.1187958.

145. Fleidervish IA, Lasser-Ross N, Gutnick MJ, Ross WN. Na+ imaging reveals little difference in action potential-evoked Na+ influx between axon and soma. **Nat Neurosci** 13: 852–860, 2010. doi:10.1038/nn.2574.

146. Hu W, Bean BP. Differential control of axonal and somatic resting potential by voltage-dependent conductances in cortical layer 5 pyramidal neurons. **Neuron** 97: 1315–1326.e3, 2018. doi:10.1016/j.neuron.2018.02.016.

147. Taddese A, Bean BP. Subthreshold sodium current from rapidly inactivating sodium channels drives spontaneous firing of tuberomammillary neurons. **Neuron** 33: 587–600, 2002. doi:10.1016/s0896-6273(02)00574-3.

148. Ben-Shalom R, Keeshen CM, Berrios KN, An JY, Sanders SJ, Bender KJ. Opposing effects on Na(V)1.2 function underlie differences between SCN2A variants observed in individuals with autism spectrum disorder or infantile seizures. **Biol Psychiatry** 82: 224–232, 2017. doi:10.1016/j.biopsych.2017.01.009.

149. Zang Y, Marder E, Marom S. Sodium channel slow inactivation normalizes firing in axons with uneven conductance distributions. **Curr Biol** 33: 1818–1824.e3, 2023. doi:10.1016/j.cub.2023.03.043.

150. Hu H, Jonas P. A supercritical density of Na(+) channels ensures fast signaling in GABAergic interneuron axons. **Nat Neurosci** 17: 686–693, 2014. doi:10.1038/nn.3678.

151. McCormick DA, Shu Y, Yu Y. Neurophysiology: Hodgkin and Huxley model–still standing? **Nature** 445: E1–E2; 2007. doi:10.1038/nature05523.

152. Yi GS, Wang J, Tsang KM, Wei XL, Deng B. Biophysical insights into how spike threshold depends on the rate of membrane potential depolarization in type I and type II neurons. **PLoS One** 10: e0130250, 2015. doi:10.1371/journal.pone.0130250.

153. Azouz R, Gray CM. Dynamic spike threshold reveals a mechanism for synaptic coincidence detection in cortical neurons in vivo. **Proc Natl Acad Sci USA** 97: 8110–8115, 2000. doi:10.1073/pnas.130200797.

154. Ferragamo MJ, Oertel D. Octopus cells of the mammalian ventral cochlear nucleus sense the rate of depolarization. **J Neurophysiol** 87: 2262–2270, 2002. doi:10.1152/jn.00587.2001.

155. Naundorf B, Wolf F, Volgushev M. Unique features of action potential initiation in cortical neurons. **Nature** 440: 1060–1063, 2006. doi:10.1038/nature04610.

156. Oz P, Huang M, Wolf F. Action potential initiation in a multi-compartmental model with cooperatively gating Na channels in the axon initial segment. **J Comput Neurosci** 39: 63–75, 2015. doi:10.1007/s10827-015-0561-9.

157. Clatot J, Hoshi M, Wan X, Liu H, Jain A, Shinlapawittayatorn K, Marionneau C, Ficker E, Ha T, Deschenes I. Voltage-gated sodium channels assemble and gate as dimers. **Nat Commun** 8: 2077, 2017. doi:10.1038/s41467-017-02262-0.

158. Selimi Z, Rougier JS, Abriel H, Kucera JP. A detailed analysis of single-channel Na(v) 1.5 recordings does not reveal any cooperative gating. **J Physiol** 601: 3847–3868, 2023. doi:10.1113/JP284861.

159. Iamshanova O, Hammerli AF, Ramaye E, Seljmani A, Ross-Kaschitza D, Scharz N, Essers M, Guichard S, Rougier JS, Abriel H. The dispensability of 14-3-3 proteins for the regulation of human cardiac sodium channel Nav1.5. **PLoS One** 19: e0298820, 2024. doi:10.1371/journal.pone.0298820.

160. Brette R. Sharpness of spike initiation in neurons explained by compartmentalization. **PLoS Comput Biol** 9: e1003338, 2013. doi:10.1371/journal.pcbi.1003338.

161. Telenczuk M, Fontaine B, Brette R. The basis of sharp spike onset in standard biophysical models. **PLoS One** 12: e0175362, 2017. doi:10.1371/journal.pone.0175362.

162. Pathak D, Guan D, Foehring RC. Roles of specific Kv channel types in repolarization of the action potential in genetically identified subclasses of pyramidal neurons in mouse neocortex. **J Neurophysiol** 115: 2317–2329, 2016. doi:10.1152/jn.01028.2015.

163. Dumenieu M, Oule M, Kreutz MR, Lopez-Rojas J. The segregated expression of voltage-gated potassium and sodium channels in neuronal membranes: functional implications and regulatory mechanisms. **Front Cell Neurosci** 11: 115, 2017. doi:10.3389/fncel.2017.00115.

164. Kole MH, Letzkus JJ, Stuart GJ. Axon initial segment Kv1 channels control axonal action potential waveform and synaptic efficacy. **Neuron** 55: 633–647, 2007. doi:10.1016/j.neuron.2007.07.031.

165. Shu Y, Yu Y, Yang J, McCormick DA. Selective control of cortical axonal spikes by a slowly inactivating K+ current. **Proc Natl Acad Sci USA** 104: 11453–11458, 2007. doi:10.1073/pnas.0702041104.

166. Rama S, Zbili M, Fekete A, Tapia M, Benitez MJ, Boumedine N, Garrido JJ, Debanne D. The role of axonal Kv1 channels in CA3 pyramidal cell excitability. **Sci Rep** 7: 315, 2017. doi:10.1038/s41598-017-00388-1.

167. Iwakura A, Uchigashima M, Miyazaki T, Yamasaki M, Watanabe M. Lack of molecular-anatomical evidence for GABAergic influence on axon initial segment of cerebellar Purkinje cells by the pinceau formation. **J Neurosci** 32: 9438–9448, 2012. doi:10.1523/JNEUROSCI.1651-12.2012.

168. Goldberg EM, Clark BD, Zagha E, Nahmani M, Erisir A, Rudy B. K+ channels at the axon initial segment dampen near-threshold excitability of neocortical fast-spiking GABAergic interneurons. **Neuron** 58: 387–400, 2008. doi:10.1016/j.neuron.2008.03.003.

169. Campanac E, Gasselin C, Baude A, Rama S, Ankri N, Debanne D. Enhanced intrinsic excitability in basket cells maintains excitatory-inhibitory balance in hippocampal circuits. **Neuron** 77: 712–722, 2013. doi:10.1016/j.neuron.2012.12.020.

170. King AN, Manning CF, Trimmer JS. A unique ion channel clustering domain on the axon initial segment of mammalian neurons. **J Comp Neurol** 522: 2594–2608, 2014. doi:10.1002/cne.23551.

171. Fox PD, Haberkorn CJ, Akin EJ, Seel PJ, Krapf D, Tamkun MM. Induction of stable ER-plasma-membrane junctions by Kv2.1 potassium channels. **J Cell Sci** 128: 2096–2105, 2015. doi:10.1242/jcs.166009.

172. Irie T. Essential role of somatic Kv2 channels in high-frequency firing in cartwheel cells of the dorsal cochlear nucleus. **eNeuro** 8: ENEURO.0515-20.2021, 2021. doi:10.1523/ENEURO.0515-20.2021.

173. Battefeld A, Tran BT, Gavrilis J, Cooper EC, Kole MH**.** Heteromeric Kv7.2/7.3 channels differentially regulate action potential initiation and conduction in neocortical myelinated axons. **J Neurosci** 34: 3719–3732, 2014. doi:10.1523/JNEUROSCI.4206-13.2014.

174. Devaux JJ, Kleopa KA, Cooper EC, Scherer SS**.** KCNQ2 is a nodal K+ channel. **J Neurosci** 24: 1236–1244, 2004. doi:10.1523/JNEUROSCI.4512-03.2004.

175. Klinger F, Gould G, Boehm S, Shapiro MS**.** Distribution of M-channel subunits KCNQ2 and KCNQ3 in rat hippocampus. **Neuroimage** 58: 761–769, 2011. doi:10.1016/j.neuroimage.2011.07.003.

176. Wen H, Levitan IB**.** Calmodulin is an auxiliary subunit of KCNQ2/3 potassium channels. **J Neurosci** 22: 7991–8001, 2002. doi:10.1523/JNEUROSCI.22-18-07991.2002.

177. Vervaeke K, Gu N, Agdestein C, Hu H, Storm JF**.** Kv7/KCNQ/M-channels in rat glutamatergic hippocampal axons and their role in regulation of excitability and transmitter release. **J Physiol** 576: 235–256, 2006. doi:10.1113/jphysiol.2006.111336.

178. Shah MM, Migliore M, Valencia I, Cooper EC, Brown DA**.** Functional significance of axonal Kv7 channels in hippocampal pyramidal neurons. **Proc Natl Acad Sci USA** 105: 7869–7874, 2008. doi:10.1073/pnas.0802805105.

179. Abiraman K, Tzingounis AV, Lykotrafitis G**.** K(Ca)2 channel localization and regulation in the axon initial segment. **FASEB J** 32: 1794–1805, 2018. doi:10.1096/fj.201700605R.

180. Yu Y, Maureira C, Liu X, McCormick D**.** P/Q and N channels control baseline and spike-triggered calcium levels in neocortical axons and synaptic boutons. **J Neurosci** 30: 11858–11869, 2010. doi:10.1523/JNEUROSCI.2651-10.2010.

181. Filipis L, Blomer LA, Montnach J, Loussouarn G, De Waard M, Canepari M**.** Nav1.2 and BK channel interaction shapes the action potential in the axon initial segment. **J Physiol** 601: 1957–1979, 2023. doi:10.1113/JP283801.

182. Luque-Fernández V, Vanspauwen SK, Landra-Willm A, Arvedsen E, Besquent M, Sandoz G, Rasmussen HB**.** An ankyrin G–binding motif mediates TRAAK periodic localization at axon initial segments of hippocampal pyramidal neurons. **Proc Natl Acad Sci USA** 121: e2310120121, 2024. doi:10.1073/pnas.2310120121.

183. Escobedo G Jr, Wu Y, Ogawa Y, Ding X, Rasband MN**.** An evolutionarily conserved ankyrinG-dependent motif clusters axonal K2P K+ channels. **J Cell Biol** 223, 2024. doi:10.1083/jcb.202401140.

184. Kanda H, Ling J, Tonomura S, Noguchi K, Matalon S, Gu JG**.** TREK-1 and TRAAK are principal K(+) channels at the nodes of Ranvier for rapid action potential conduction on mammalian myelinated afferent nerves. **Neuron** 104: 960–971.e7, 2019. doi:10.1016/j.neuron.2019.08.042.

185. Callewaert G, Eilers J, Konnerth A**.** Axonal calcium entry during fast 'sodium' action potentials in rat cerebellar Purkinje neurones. **J Physiol** 495: 641–647, 1996. doi:10.1113/jphysiol.1996.sp021622.

186. Schiller J, Helmchen F, Sakmann B**.** Spatial profile of dendritic calcium transients evoked by action potentials in rat neocortical pyramidal neurones. **J Physiol** 487: 583–600, 1995. doi:10.1113/jphysiol.1995.sp020902.

187. Yang S, Ben-Shalom R, Ahn M, Liptak AT, van Rijn RM, Whistler JL, Bender KJ**.** beta-Arrestin-dependent dopaminergic regulation of calcium channel activity in the axon initial segment. **Cell Rep** 16: 1518–1526, 2016. doi:10.1016/j.celrep.2016.06.098.

188. Bender KJ, Trussell LO**.** Axon initial segment Ca2+ channels influence action potential generation and timing. **Neuron** 61: 259–271, 2009. doi:10.1016/j.neuron.2008.12.004.

189. Bender KJ, Uebele VN, Renger JJ, Trussell LO**.** Control of firing patterns through modulation of axon initial segment T-type calcium channels. **J Physiol** 590: 109–118, 2012. doi:10.1113/jphysiol.2011.218768.

190. Dumenieu M, Senkov O, Mironov A, Bourinet E, Kreutz MR, Dityatev A, Heine M, Bikbaev A, Lopez-Rojas J**.** The low-threshold calcium channel Cav3.2 mediates burst firing of mature dentate granule cells. **Cereb Cortex** 28: 2594–2609, 2018. doi:10.1093/cercor/bhy084.

191. Martinello K, Huang Z, Lujan R, Tran B, Watanabe M, Cooper EC, Brown DA, Shah MM**.** Cholinergic afferent stimulation induces axonal function plasticity in adult hippocampal granule cells. **Neuron** 85: 346–363, 2015. doi:10.1016/j.neuron.2014.12.030.

192. Clarkson RL, Liptak AT, Gee SM, Sohal VS, Bender KJ**.** D3 receptors regulate excitability in a unique class of prefrontal pyramidal cells. **J Neurosci** 37: 5846–5860, 2017. doi:10.1523/JNEUROSCI.0310-17.2017.

193. Zhang W, Fu Y, Peng L, Ogawa Y, Ding X, Rasband A, Zhou X, Shelly M, Rasband MN, Zou P**.** Immunoproximity biotinylation reveals the axon initial segment proteome. **Nat Commun** 14: 8201, 2023. doi:10.1038/s41467-023-44015-2.

194. Anton-Fernandez A, Rubio-Garrido P, DeFelipe J, Munoz A**.** Selective presence of a giant saccular organelle in the axon initial segment of a subpopulation of layer V pyramidal neurons. **Brain Struct Funct** 220: 869–884, 2015. doi:10.1007/s00429-013-0689-1.

195. Hanemaaijer NA, Popovic MA, Wilders X, Grasman S, Pavon Arocas O, Kole MH**.** Ca^{2+} entry through Na_V channels generates submillisecond axonal Ca^{2+} signaling. **eLife** 9: e54566, 2020. doi:10.7554/eLife.54566.

196. Benedeczky I, Molnar E, Somogyi P**.** The cisternal organelle as a Ca (2+)-storing compartment associated with GABAergic synapses in the axon initial segment of hippocampal pyramidal neurones. **Exp Brain Res** 101: 216–230, 1994. doi:10.1007/BF00228742.

197. Hund TJ, Koval OM, Li J, Wright PJ, Qian L, Snyder JS, Gudmundsson H, Kline CF, Davidson NP, Cardona N, Rasband MN, Anderson ME, Mohler PJ**.** A beta(IV)-spectrin/CaMKII signaling complex is essential for membrane excitability in mice. **J Clin Invest** 120: 3508–3519, 2010. doi:10.1172/JCI43621.

198. Sanchez-Ponce D, DeFelipe J, Garrido JJ, Munoz A**.** In vitro maturation of the cisternal organelle in the hippocampal neuron's axon initial segment. **Mol Cell Neurosci** 48: 104–116, 2011. doi:10.1016/j.mcn.2011.06.010.

199. Schultz C, Konig HG, Del Turco D, Politi C, Eckert GP, Ghebremedhin E, Prehn JH, Kogel D, Deller T**.** Coincident enrichment of phosphorylated IkappaBalpha, activated IKK, and phosphorylated p65 in the axon initial segment of neurons. **Mol Cell Neurosci** 33: 68–80, 2006. doi:10.1016/j.mcn.2006.06.008.

200. Chow RH**.** Cadmium block of squid calcium currents. Macroscopic data and a kinetic model. **J Gen Physiol** 98: 751–770, 1991. doi:10.1085/jgp.98.4.751.

201. Shibuya I, Douglas WW**.** Calcium channels in rat melanotrophs are permeable to manganese, cobalt, cadmium, and lanthanum, but not to nickel: evidence provided by fluorescence changes in fura-2-loaded cells. **Endocrinology** 131: 1936–1941, 1992. doi:10.1210/endo.131.4.1327724.

202. McDonough SI, Mintz IM, Bean BP. Alteration of P-type calcium channel gating by the spider toxin omega-Aga-IVA. **Biophys J** 72: 2117–2128, 1997. doi:10.1016/S0006-3495(97)78854-4.

203. McDonough SI, Swartz KJ, Mintz IM, Boland LM, Bean BP. Inhibition of calcium channels in rat central and peripheral neurons by omega-conotoxin MVIIC. **J Neurosci** 16: 2612–2623, 1996. doi:10.1523/JNEUROSCI.16-08-02612.1996.

204. Francois A, Kerckhove N, Meleine M, Alloui A, Barrere C, Gelot A, Uebele VN, Renger JJ, Eschalier A, Ardid D, Bourinet E. State-dependent properties of a new T-type calcium channel blocker enhance CaV3.2 selectivity and support analgesic effects. **Pain** 154: 283–293, 2013. doi:10.1016/j.pain.2012.10.023.

205. Dreyfus FM, Tscherter A, Errington AC, Renger JJ, Shin HS, Uebele VN, Crunelli V, Lambert RC, Leresche N. Selective T-type calcium channel block in thalamic neurons reveals channel redundancy and physiological impact of I(T)window. **J Neurosci** 30: 99–109, 2010. doi:10.1523/JNEUROSCI.4305-09.2010.

206. Shah MM. Cortical HCN channels: function, trafficking and plasticity. **J Physiol** 592: 2711–2719, 2014. doi:10.1113/jphysiol.2013.270058.

207. Dembrow NC, Chitwood RA, Johnston D. Projection-specific neuromodulation of medial prefrontal cortex neurons. **J Neurosci** 30: 16922–16937, 2010. doi:10.1523/JNEUROSCI.3644-10.2010.

208. Roth FC, Hu H. An axon-specific expression of HCN channels catalyzes fast action potential signaling in GABAergic interneurons. **Nat Commun** 11: 2248, 2020. doi:10.1038/s41467-020-15791-y.

209. Elgueta C, Kohler J, Bartos M. Persistent discharges in dentate gyrus perisoma-inhibiting interneurons require hyperpolarization-activated cyclic nucleotide-gated channel activation. **J Neurosci** 35: 4131–4139, 2015. doi:10.1523/JNEUROSCI.3671-14.2015.

210. Ko KW, Rasband MN, Meseguer V, Kramer RH, Golding NL. Serotonin modulates spike probability in the axon initial segment through HCN channels. **Nat Neurosci** 19: 826–834, 2016. doi:10.1038/nn.4293.

211. Bakken TE, Jorstad NL, Hu Q, Lake BB, Tian W, Kalmbach BE, et al. Comparative cellular analysis of motor cortex in human, marmoset and mouse. **Nature** 598: 111–119, 2021. doi:10.1038/s41586-021-03465-8.

212. Compans B, Burrone J. Chandelier cells shine a light on the formation of GABAergic synapses. **Curr Opin Neurobiol** 80: 102697, 2023. doi:10.1016/j.conb.2023.102697.

213. Gallo NB, Paul A, Van Aelst L. Shedding light on chandelier cell development, connectivity, and contribution to neural disorders. **Trends Neurosci** 43: 565–580, 2020. doi:10.1016/j.tins.2020.05.003.

214. Jung K, Choi Y, Kwon HB. Cortical control of chandelier cells in neural codes. **Front Cell Neurosci** 16: 992409, 2022. doi:10.3389/fncel.2022.992409.

215. Szabadics J, Varga C, Molnar G, Olah S, Barzo P, Tamas G. Excitatory effect of GABAergic axo-axonic cells in cortical microcircuits. **Science** 311: 233–235, 2006. doi:10.1126/science.1121325.

216. Price GD, Trussell LO. Estimate of the chloride concentration in a central glutamatergic terminal: a gramicidin perforated-patch study on the calyx of Held. **J Neurosci** 26: 11432–11436, 2006. doi:10.1523/JNEUROSCI.1660-06.2006.

217. Christie JM, Jahr CE. Selective expression of ligand-gated ion channels in L5 pyramidal cell axons. **J Neurosci** 29: 11441–11450, 2009. doi:10.1523/JNEUROSCI.2387-09.2009.

218. Kramer PF, Twedell EL, Shin JH, Zhang R, Khaliq ZM. Axonal mechanisms mediating gamma-aminobutyric acid receptor type A (GABA-A) inhibition of striatal dopamine release. **eLife** 9: e55729, 2020. doi:10.7554/eLife.55729.

219. Glickfeld LL, Roberts JD, Somogyi P, Scanziani M. Interneurons hyperpolarize pyramidal cells along their entire somatodendritic axis. **Nat Neurosci** 12: 21–23, 2009. doi:10.1038/nn.2230.

220. Rinetti-Vargas G, Phamluong K, Ron D, Bender KJ. Periadolescent maturation of GABAergic hyperpolarization at the axon initial segment. **Cell Rep** 20: 21–29, 2017. doi:10.1016/j.celrep.2017.06.030.

221. Dudok B, Szoboszlay M, Paul A, Klein PM, Liao Z, Hwaun E, Szabo GG, Geiller T, Vancura B, Wang BS, McKenzie S, Homidan J, Klaver LM, English DF, Huang ZJ, Buzsaki G, Losonczy A, Soltesz I. Recruitment and inhibitory action of hippocampal axo-axonic cells during behavior. **Neuron** 109: 3838–3850.e8, 2021. doi:10.1016/j.neuron.2021.09.033.

222. Lu J, Tucciarone J, Padilla-Coreano N, He M, Gordon JA, Huang ZJ. Selective inhibitory control of pyramidal neuron ensembles and cortical subnetworks by chandelier cells. **Nat Neurosci** 20: 1377–1383, 2017. doi:10.1038/nn.4624.

223. Lipkin AM, Bender KJ. Axon initial segment GABA inhibits action potential generation throughout periadolescent development. **J Neurosci** 43: 6357–6368, 2023. doi:10.1523/JNEUROSCI.0605-23.2023.

224. Seignette K, Jamann N, Papale P, Terra H, Porneso RO, de Kraker L, van der Togt C, van der Aa M, Neering P, Ruimschotel E, Roelfsema PR, Montijn JS, Self MW, Kole MH, Levelt CN. Experience shapes chandelier cell function and structure in the visual cortex. **eLife** 12: RP91153, 2024. doi:10.7554/eLife.91153.

225. Zhao R, Ren B, Xiao Y, Tian J, Zou Y, Wei J, Qi Y, Hu A, Xie X, Huang ZJ, Shu Y, He M, Lu J, Tai Y. Axo-axonic synaptic input drives homeostatic plasticity by tuning the axon initial segment structurally and functionally (Preprint). **bioRxiv** 2024.04.11.589005, 2024. doi:10.1101/2024.04.11.589005.

226. Pan-Vazquez A, Wefelmeyer W, Gonzalez Sabater V, Neves G, Burrone J. Activity-dependent plasticity of axo-axonic synapses at the axon initial segment. **Neuron** 106: 265–276.e6, 2020. doi:10.1016/j.neuron.2020.01.037.

227. Wen W, Turrigiano GG. Keeping your brain in balance: homeostatic regulation of network function. **Annu Rev Neurosci** 47: 41–61 2024. doi:10.1146/annurev-neuro-092523-110001.

228. Magee JC, Grienberger C. Synaptic plasticity forms and functions. **Annu Rev Neurosci** 43: 95–117, 2020. doi:10.1146/annurev-neuro-090919-022842.

229. Burke KJ Jr, Bender KJ. Modulation of ion channels in the axon: mechanisms and function. **Front Cell Neurosci** 13: 221, 2019. doi:10.3389/fncel.2019.00221.

230. Lovinger DM, Mateo Y, Johnson KA, Engi SA, Antonazzo M, Cheer JF. Local modulation by presynaptic receptors controls neuronal communication and behaviour. **Nat Rev Neurosci** 23: 191–203, 2022. doi:10.1038/s41583-022-00561-0.

231. Jin X, Chen Q, Song Y, Zheng J, Xiao K, Shao S, Fu Z, Yi M, Yang Y, Huang Z. Dopamine D2 receptors regulate the action potential threshold by modulating T-type calcium channels in stellate cells of the medial entorhinal cortex. **J Physiol** 597: 3363–3387, 2019. doi:10.1113/JP277976.

232. Blesneac I, Chemin J, Bidaud I, Huc-Brandt S, Vandermoere F, Lory P. Phosphorylation of the Cav3.2 T-type calcium channel directly

regulates its gating properties. **Proc Natl Acad Sci USA** 112: 13705–13710, 2015. doi:10.1073/pnas.1511740112.

233. Bender KJ, Ford CP, Trussell LO**.** Dopaminergic modulation of axon initial segment calcium channels regulates action potential initiation. **Neuron** 68: 500–511, 2010. doi:10.1016/j.neuron.2010.09.026.

234. Schamiloglu S, Lewis E, Keeshen CM, Hergarden AC, Bender KJ, Whistler JL**.** Arrestin-3 agonism at dopamine D(3) receptors defines a subclass of second-generation antipsychotics that promotes drug tolerance. **Biol Psychiatry** 94: 531–542, 2023. doi:10.1016/j.biopsych.2023.03.006.

235. Cho EY, Cho DI, Park JH, Kurose H, Caron MG, Kim KM**.** Roles of protein kinase C and actin-binding protein 280 in the regulation of intracellular trafficking of dopamine D3 receptor. **Mol Endocrinol** 21: 2242–2254, 2007. doi:10.1210/me.2007-0202.

236. Thompson D, Whistler JL**.** Dopamine D(3) receptors are down-regulated following heterologous endocytosis by a specific interaction with G protein-coupled receptor-associated sorting protein-1. **J Biol Chem** 286: 1598–1608, 2011. doi:10.1074/jbc.M110.158345.

237. Yin L, Rasch MJ, He Q, Wu S, Dou F, Shu Y**.** Selective modulation of axonal sodium channel subtypes by 5-HT1A receptor in cortical pyramidal neuron. **Cereb Cortex** 27: 509–521, 2017. doi:10.1093/cercor/bhv245.

238. Cotel F, Exley R, Cragg SJ, Perrier JF**.** Serotonin spillover onto the axon initial segment of motoneurons induces central fatigue by inhibiting action potential initiation. **Proc Natl Acad Sci USA** 110: 4774–4779, 2013. doi:10.1073/pnas.1216150110.

239. Laedermann CJ, Abriel H, Decosterd I**.** Post-translational modifications of voltage-gated sodium channels in chronic pain syndromes. **Front Pharmacol** 6: 263, 2015. doi:10.3389/fphar.2015.00263.

240. Zybura A, Hudmon A, Cummins TR**.** Distinctive properties and powerful neuromodulation of Na(v)1.6 sodium channels regulates neuronal excitability. **Cells** 10: 1595, 2021. doi:10.3390/cells10071595.

241. Pei Z, Pan Y, Cummins TR**.** Posttranslational modification of sodium channels. **Handb Exp Pharmacol** 246: 101–124, 2018. doi:10.1007/164_2017_69.

242. Garrido JJ, Giraud P, Carlier E, Fernandes F, Moussif A, Fache MP, Debanne D, Dargent B**.** A targeting motif involved in sodium channel clustering at the axonal initial segment. **Science** 300: 2091–2094, 2003. doi:10.1126/science.1085167.

243. Lemaillet G, Walker B, Lambert S**.** Identification of a conserved ankyrin-binding motif in the family of sodium channel alpha subunits. **J Biol Chem** 278: 27333–27339, 2003. doi:10.1074/jbc.M303327200.

244. Brechet A, Fache MP, Brachet A, Ferracci G, Baude A, Irondelle M, Pereira S, Leterrier C, Dargent B**.** Protein kinase CK2 contributes to the organization of sodium channels in axonal membranes by regulating their interactions with ankyrin G. **J Cell Biol** 183: 1101–1114, 2008. doi:10.1083/jcb.200805169.

245. Evans MD, Sammons RP, Lebron S, Dumitrescu AS, Watkins TB, Uebele VN, Renger JJ, Grubb MS**.** Calcineurin signaling mediates activity-dependent relocation of the axon initial segment. **J Neurosci** 33: 6950–6963, 2013. doi:10.1523/JNEUROSCI.0277-13.2013.

246. Zybura AS, Baucum AJ 2nd, Rush AM, Cummins TR, Hudmon A**.** CaMKII enhances voltage-gated sodium channel Nav1.6 activity and neuronal excitability. **J Biol Chem** 295: 11845–11865, 2020. doi:10.1074/jbc.RA120.014062.

247. Schmidt JW, Catterall WA**.** Palmitylation, sulfation, and glycosylation of the alpha subunit of the sodium channel. Role of post-translational modifications in channel assembly. **J Biol Chem** 262: 13713–13723, 1987.

248. Pan Y, Xiao Y, Pei Z, Cummins TR**.** S-Palmitoylation of the sodium channel Nav1.6 regulates its activity and neuronal excitability. **J Biol Chem** 295: 6151–6164, 2020. doi:10.1074/jbc.RA119.012423.

249. Bouza AA, Philippe JM, Edokobi N, Pinsky AM, Offord J, Calhoun JD, Lopez-Floran M, Lopez-Santiago LF, Jenkins PM, Isom LL**.** Sodium channel beta1 subunits are post-translationally modified by tyrosine phosphorylation, S-palmitoylation, and regulated intramembrane proteolysis. **J Biol Chem** 295: 10380–10393, 2020. doi:10.1074/jbc.RA120.013978.

250. Shimell JJ, Globa A, Sepers MD, Wild AR, Matin N, Raymond LA, Bamji SX**.** Regulation of hippocampal excitatory synapses by the Zdhhc5 palmitoyl acyltransferase. **J Cell Sci** 134: jcs254276, 2021. doi:10.1242/jcs.254276.

251. Grubb MS, Burrone J**.** Activity-dependent relocation of the axon initial segment fine-tunes neuronal excitability. **Nature** 465: 1070–1074, 2010. doi:10.1038/nature09160.

252. Tippens AL, Pare JF, Langwieser N, Moosmang S, Milner TA, Smith Y, Lee A**.** Ultrastructural evidence for pre- and postsynaptic localization of Cav1.2 L-type Ca2+ channels in the rat hippocampus. **J Comp Neurol** 506: 569–583, 2008. doi:10.1002/cne.21567.

253. Kuba H, Oichi Y, Ohmori H**.** Presynaptic activity regulates Na(+) channel distribution at the axon initial segment. **Nature** 465: 1075–1078, 2010. doi:10.1038/nature09087.

254. Koppl C**.** Phase locking to high frequencies in the auditory nerve and cochlear nucleus magnocellularis of the barn owl, Tyto alba. **J Neurosci** 17: 3312–3321, 1997. doi:10.1523/JNEUROSCI.17-09-03312.1997.

255. Evans MD, Dumitrescu AS, Kruijssen DL, Taylor SE, Grubb MS**.** Rapid modulation of axon initial segment length influences repetitive spike firing. **Cell Rep** 13: 1233–1245, 2015. doi:10.1016/j.celrep.2015.09.066.

256. Thome C, Janssen JM, Karabulut S, Acuna C, D'Este E, Soyka SJ, Baum K, Bock M, Lehmann N, Roos J, Stevens NA, Hasegawa M, Ganea DA, Benoit CM, Gründemann J, Min L, Bird KM, Schultz C, Bennett V, Jenkins PM, Engelhardt M**.** Live imaging of excitable axonal microdomains in ankyrin-G-GFP mice (Preprint). **bioRxiv** 2023.2002.2001.525891, 2024. doi:10.1101/2023.02.01.525891.

257. Kuba H, Yamada R, Ishiguro G, Adachi R**.** Redistribution of Kv1 and Kv7 enhances neuronal excitability during structural axon initial segment plasticity. **Nat Commun** 6: 8815, 2015. doi:10.1038/ncomms9815.

258. Morgan PJ, Bourboulou R, Filippi C, Koenig-Gambini J, Epsztein J**.** Kv1.1 contributes to a rapid homeostatic plasticity of intrinsic excitability in CA1 pyramidal neurons in vivo. **eLife** 8: e49915, 2019. doi:10.7554/eLife.49915.

259. Zbili M, Rama S, Benitez MJ, Fronzaroli-Molinieres L, Bialowas A, Boumedine-Guignon N, Garrido JJ, Debanne D**.** Homeostatic regulation of axonal Kv1.1 channels accounts for both synaptic and intrinsic modifications in the hippocampal CA3 circuit. **Proc Natl Acad Sci USA** 118: e2110601118, 2021.

260. Evans MD, Tufo C, Dumitrescu AS, Grubb MS**.** Myosin II activity is required for structural plasticity at the axon initial segment. **Eur J Neurosci** 46: 1751–1757, 2017. doi:10.1111/ejn.13597.

261. Berger SL, Leo-Macias A, Yuen S, Khatri L, Pfennig S, Zhang Y, Agullo-Pascual E, Caillol G, Zhu MS, Rothenberg E, Melendez-Vasquez CV, Delmar M, Leterrier C, Salzer JL. Localized myosin II activity regulates assembly and plasticity of the axon initial segment. **Neuron** 97: 555–570.e6, 2018. doi:10.1016/j.neuron.2017.12.039.

262. Micinski D, Hotulainen P. Actin polymerization and longitudinal actin fibers in axon initial segment plasticity. **Front Mol Neurosci** 17: 1376997, 2024. doi:10.3389/fnmol.2024.1376997.

263. Jahan I, Adachi R, Egawa R, Nomura H, Kuba H. CDK5/p35-dependent microtubule reorganization contributes to homeostatic shortening of the axon initial segment. **J Neurosci** 43: 359–372, 2023. doi:10.1523/JNEUROSCI.0917-22.2022.

264. Lezmy J, Lipinsky M, Khrapunsky Y, Patrich E, Shalom L, Peretz A, Fleidervish IA, Attali B. M-current inhibition rapidly induces a unique CK2-dependent plasticity of the axon initial segment. **Proc Natl Acad Sci USA** 114: E10234–E10243, 2017. doi:10.1073/pnas.1708700114.

265. Feng L, Li AP, Wang MP, Sun DN, Wang YL, Long LL, Xiao B. Plasticity at axon initial segment of hippocampal CA3 neurons in rat after status epilepticus induced by lithium-pilocarpine. **Acta Neurochir (Wien)** 155: 2373–2380, 2013. doi:10.1007/s00701-013-1836-4.

266. Harty RC, Kim TH, Thomas EA, Cardamone L, Jones NC, Petrou S, Wimmer VC. Axon initial segment structural plasticity in animal models of genetic and acquired epilepsy. **Epilepsy Res** 105: 272–279, 2013. doi:10.1016/j.eplepsyres.2013.03.004.

267. Liu TT, Feng L, Liu HF, Shu Y, Xiao B. Altered axon initial segment in hippocampal newborn neurons, associated with recurrence of temporal lobe epilepsy in rats. **Mol Med Rep** 16: 3169–3178, 2017. doi:10.3892/mmr.2017.7017.

268. Hinman JD, Rasband MN, Carmichael ST. Remodeling of the axon initial segment after focal cortical and white matter stroke. **Stroke** 44: 182–189, 2013. doi:10.1161/STROKEAHA.112.668749.

269. Stoler O, Fleidervish IA. Functional implications of axon initial segment cytoskeletal disruption in stroke. **Acta Pharmacol Sin** 37: 75–81, 2016. doi:10.1038/aps.2015.107.

270. Vascak M, Sun J, Baer M, Jacobs KM, Povlishock JT. Mild traumatic brain injury evokes pyramidal neuron axon initial segment plasticity and diffuse presynaptic inhibitory terminal loss. **Front Cell Neurosci** 11: 157, 2017. doi:10.3389/fncel.2017.00157.

271. Sohn PD, Huang CT, Yan R, Fan L, Tracy TE, Camargo CM, Montgomery KM, Arhar T, Mok SA, Freilich R, Baik J, He M, Gong S, Roberson ED, Karch CM, Gestwicki JE, Xu K, Kosik KS, Gan L. Pathogenic tau impairs axon initial segment plasticity and excitability homeostasis. **Neuron** 104: 458–470.e5, 2019. doi:10.1016/j.neuron.2019.08.008.

272. Anton-Fernandez A, Leon-Espinosa G, DeFelipe J, Munoz A. Pyramidal cell axon initial segment in Alzheimer s disease. **Sci Rep** 12: 8722, 2022. doi:10.1038/s41598-022-12700-9.

273. Caspi Y, Mazar M, Kushnir Y, Mazor Y, Katz B, Lev S, Binshtok AM. Structural plasticity of axon initial segment in spinal cord neurons underlies inflammatory pain. **Pain** 164: 1388–1401, 2023. doi:10.1097/j.pain.0000000000002829.

274. Harley P, Kerins C, Gatt A, Neves G, Riccio F, Machado CB, Cheesbrough A, R'Bibo L, Burrone J, Lieberam I. Aberrant axon initial segment plasticity and intrinsic excitability of ALS hiPSC motor neurons. **Cell Rep** 42: 113509, 2023. doi:10.1016/j.celrep.2023.113509.

275. Dumitrescu AS, Evans MD, Grubb MS. Evaluating tools for live imaging of structural plasticity at the axon initial segment. **Front Cell Neurosci** 10: 268, 2016. doi:10.3389/fncel.2016.00268.

276. Jamann N, Dannehl D, Lehmann N, Wagener R, Thielemann C, Schultz C, Staiger J, Kole MH, Engelhardt M. Sensory input drives rapid homeostatic scaling of the axon initial segment in mouse barrel cortex. **Nat Commun** 12: 23, 2021. doi:10.1038/s41467-020-20232-x.

277. Gutzmann A, Ergül N, Grossmann R, Schultz C, Wahle P, Engelhardt M. A period of structural plasticity at the axon initial segment in developing visual cortex. **Front Neuroanat** 8: 11, 2014. doi:10.3389/fnana.2014.00011.

278. Nozari M, Suzuki T, Rosa MG, Yamakawa K, Atapour N. The impact of early environmental interventions on structural plasticity of the axon initial segment in neocortex. **Dev Psychobiol** 59: 39–47, 2017. doi:10.1002/dev.21453.

279. Jungenitz T, Bird A, Engelhardt M, Jedlicka P, Schwarzacher SW, Deller T. Structural plasticity of the axon initial segment in rat hippocampal granule cells following high frequency stimulation and LTP induction. **Front Neuroanat** 17: 1125623, 2023. doi:10.3389/fnana.2023.1125623.

280. Ding Y, Chen T, Wang Q, Yuan Y, Hua T. Axon initial segment plasticity accompanies enhanced excitation of visual cortical neurons in aged rats. **NeuroReport** 29: 1537–1543, 2018. doi:10.1097/WNR.0000000000001145.

281. Atapour N, Rosa MG. Age-related plasticity of the axon initial segment of cortical pyramidal cells in marmoset monkeys. **Neurobiol Aging** 57: 95–103, 2017. doi:10.1016/j.neurobiolaging.2017.05.013.

282. Chand AN, Galliano E, Chesters RA, Grubb MS. A distinct subtype of dopaminergic interneuron displays inverted structural plasticity at the axon initial segment. **J Neurosci** 35: 1573–1590, 2015. doi:10.1523/JNEUROSCI.3515-14.2015.

283. Thome C, Kelly T, Yanez A, Schultz C, Engelhardt M, Cambridge SB, Both M, Draguhn A, Beck H, Egorov AV. Axon-carrying dendrites convey privileged synaptic input in hippocampal neurons. **Neuron** 83: 1418–1430, 2014. doi:10.1016/j.neuron.2014.08.013.

284. Höfflin F, Jack A, Riedel C, Mack-Bucher J, Roos J, Corcelli C, Schultz C, Wahle P, Engelhardt M. Heterogeneity of the axon initial segment in interneurons and pyramidal cells of rodent visual cortex. **Front Cell Neurosci** 11: 332, 2017. doi:10.3389/fncel.2017.00332.

285. Wahle P, Sobierajski E, Gasterstädt I, Lehmann N, Weber S, Lübke JH, Engelhardt M, Distler C, Meyer G. Neocortical pyramidal neurons with axons emerging from dendrites are frequent in non-primates, but rare in monkey and human. **eLife** 11: e76101, 2022. doi:10.7554/eLife.76101.

286. Lehmann N, Markovic S, Thome C, Engelhardt M. Axon onset remodeling in response to network activity in mouse cortical neurons (Preprint). **bioRxiv** 2023.2007.2031.551236, 2023. doi:10.1101/2023.07.31.551236.

287. Rusina E, Simonti M, Duprat F, Cestele S, Mantegazza M. Voltage-gated sodium channels in genetic epilepsy: up and down of excitability. **J Neurochem** 168: 3872–3890, 2024. doi:10.1111/jnc.15947.

288. Wimmer VC, Reid CA, So EY, Berkovic SF, Petrou S. Axon initial segment dysfunction in epilepsy. **J Physiol** 588: 1829–1840, 2010. doi:10.1113/jphysiol.2010.188417.

289. Meisler MH, Hill SF, Yu W. Sodium channelopathies in neurodevelopmental disorders. **Nat Rev Neurosci** 22: 152–166, 2021. doi:10.1038/s41583-020-00418-4.

290. Hsu WC, Nilsson CL, Laezza F**.** Role of the axonal initial segment in psychiatric disorders: function, dysfunction, and intervention. **Front Psychiatry** 5: 109, 2014. doi:10.3389/fpsyt.2014.00109.

291. Buffington SA, Rasband MN**.** The axon initial segment in nervous system disease and injury. **Eur J Neurosci** 34: 1609–1619, 2011. doi:10.1111/j.1460-9568.2011.07875.x.

292. Encinas AC, Watkins JC, Longoria IA, Johnson JP Jr, Hammer MF**.** Variable patterns of mutation density among NaV1.1, NaV1.2 and NaV1.6 point to channel-specific functional differences associated with childhood epilepsy. **PLoS One** 15: e0238121, 2020. doi:10.1371/journal.pone.0238121.

293. Sánchez-Ponce D, DeFelipe J, Garrido JJ, Muñoz A**.** Developmental expression of Kv potassium channels at the axon initial segment of cultured hippocampal neurons. **PLoS One** 7: e48557, 2012. doi:10.1371/journal.pone.0048557.

294. Gazina EV, Richards KL, Mokhtar MB, Thomas EA, Reid CA, Petrou S**.** Differential expression of exon 5 splice variants of sodium channel alpha subunit mRNAs in the developing mouse brain. **Neuroscience** 166: 195–200, 2010. doi:10.1016/j.neuroscience.2009.12.011.

295. Thomas EA, Hawkins RJ, Richards KL, Xu R, Gazina EV, Petrou S**.** Heat opens axon initial segment sodium channels: a febrile seizure mechanism? **Ann Neurol** 66: 219–226, 2009. doi:10.1002/ana.21712.

296. Allen NM, Weckhuysen S, Gorman K, King MD, Lerche H**.** Genetic potassium channel-associated epilepsies: clinical review of the K_v family. **Eur J Paediatr Neurol** 24: 105–116, 2020. doi:10.1016/j.ejpn.2019.12.002.

297. Lory P, Nicole S, Monteil A**.** Neuronal Cav3 channelopathies: recent progress and perspectives. **Pflugers Arch** 472: 831–844, 2020. doi:10.1007/s00424-020-02429-7.

298. Wallace RH, Wang DW, Singh R, Scheffer IE, George AL Jr, Phillips HA, Saar K, Reis A, Johnson EW, Sutherland GR, Berkovic SF, Mulley JC**.** Febrile seizures and generalized epilepsy associated with a mutation in the Na+-channel beta1 subunit gene SCN1B. **Nat Genet** 19: 366–370, 1998. doi:10.1038/1252.

299. Audenaert D, Claes L, Ceulemans B, Löfgren A, Van Broeckhoven C, De Jonghe P**.** A deletion in SCN1B is associated with febrile seizures and early-onset absence epilepsy. **Neurology** 61: 854–856, 2003. doi:10.1212/01.wnl.0000080362.55784.1c.

300. Patino GA, Claes LR, Lopez-Santiago LF, Slat EA, Dondeti RS, Chen C, O'Malley HA, Gray CB, Miyazaki H, Nukina N, Oyama F, De Jonghe P, Isom LL**.** A functional null mutation of SCN1B in a patient with Dravet syndrome. **J Neurosci** 29: 10764–10778, 2009. doi:10.1523/JNEUROSCI.2475-09.2009.

301. Ramadan W, Patel N, Anazi S, Kentab AY, Bashiri FA, Hamad MH, Jad L, Salih MA, Alsaif H, Hashem M, Faqeih E, Shamseddin HE, Alkuraya FS**.** Confirming the recessive inheritance of SCN1B mutations in developmental epileptic encephalopathy. **Clin Genet** 92: 327–331, 2017. doi:10.1111/cge.12999.

302. Aeby A, Sculier C, Bouza AA, Askar B, Lederer D, Schoonjans AS, Vander Ghinst M, Ceulemans B, Offord J, Lopez-Santiago LF, Isom LL**.** SCN1B-linked early infantile developmental and epileptic encephalopathy. **Ann Clin Transl Neurol** 6: 2354–2367, 2019. doi:10.1002/acn3.50921.

303. Hull JM, Denomme N, Yuan Y, Booth V, Isom LL**.** Heterogeneity of voltage gated sodium current density between neurons decorrelates spiking and suppresses network synchronization in Scn1b null mouse models. **Sci Rep** 13: 8887, 2023. doi:10.1038/s41598-023-36036-0.

304. Reid CA, Leaw B, Richards KL, Richardson R, Wimmer V, Yu C, Hill-Yardin EL, Lerche H, Scheffer IE, Berkovic SF, Petrou S**.** Reduced dendritic arborization and hyperexcitability of pyramidal neurons in a Scn1b-based model of Dravet syndrome. **Brain** 137: 1701–1715, 2014. doi:10.1093/brain/awu077.

305. Goldfarb M, Schoorlemmer J, Williams A, Diwakar S, Wang Q, Huang X, Giza J, Tchetchik D, Kelley K, Vega A, Matthews G, Rossi P, Ornitz DM, D'Angelo E**.** Fibroblast growth factor homologous factors control neuronal excitability through modulation of voltage-gated sodium channels. **Neuron** 55: 449–463, 2007. doi:10.1016/j.neuron.2007.07.006.

306. Siekierska A, Isrie M, Liu Y, Scheldeman C, Vanthillo N, Lagae L, de Witte PA, Van Esch H, Goldfarb M, Buyse GM**.** Gain-of-function FHF1 mutation causes early-onset epileptic encephalopathy with cerebellar atrophy. **Neurology** 86: 2162–2170, 2016. doi:10.1212/WNL.0000000000002752.

307. Oda Y, Uchiyama Y, Motomura A, Fujita A, Azuma Y, Harita Y, Mizuguchi T, Yanagi K, Ogata H, Hata K, Kaname T, Matsubara Y, Wakui K, Matsumoto N**.** Entire FGF12 duplication by complex chromosomal rearrangements associated with West syndrome. **J Hum Genet** 64: 1005–1014, 2019. doi:10.1038/s10038-019-0641-1.

308. Furia F, Levy AM, Theunis M, Bamshad MJ, Bartos MN, Bijlsma EK, et al**.** The phenotypic and genotypic spectrum of individuals with mono- or biallelic ANK3 variants. **Clin Genet** 106: 574–584, 2024. doi:10.1111/cge.14587.

309. Iqbal Z, Vandeweyer G, van der Voet M, Waryah AM, Zahoor MY, Besseling JA, Roca LT, Vulto-van Silfhout AT, Nijhof B, Kramer JM, Van der Aa N, Ansar M, Peeters H, Helsmoortel C, Gilissen C, Vissers LE, Veltman JA, de Brouwer AP, Frank Kooy R, Riazuddin S, Schenck A, van Bokhoven H, Rooms L**.** Homozygous and heterozygous disruptions of ANK3: at the crossroads of neurodevelopmental and psychiatric disorders. **Hum Mol Genet** 22: 1960–1970, 2013. doi:10.1093/hmg/ddt043.

310. Lopez AY, Wang X, Xu M, Maheshwari A, Curry D, Lam S, Adesina AM, Noebels JL, Sun QQ, Cooper EC**.** Ankyrin-G isoform imbalance and interneuronopathy link epilepsy and bipolar disorder. **Mol Psychiatry** 22: 1464–1472, 2017. doi:10.1038/mp.2016.233.

311. Wolff M, Johannesen KM, Hedrich UB, Masnada S, Rubboli G, Gardella E, et al**.** Genetic and phenotypic heterogeneity suggest therapeutic implications in SCN2A-related disorders. **Brain** 140: 1316–1336, 2017. doi:10.1093/brain/awx054.

312. Larsen J, Carvill GL, Gardella E, Kluger G, Schmiedel G, Barisic N, et al**.** The phenotypic spectrum of SCN8A encephalopathy. **Neurology** 84: 480–489, 2015. doi:10.1212/WNL.0000000000001211.

313. Sanders SJ, Campbell AJ, Cottrell JR, Moller RS, Wagner FF, Auldridge AL, Bernier RA, Catterall WA, Chung WK, Empfield JR, George AL Jr, Hipp JF, Khwaja O, Kiskinis E, Lal D, Malhotra D, Millichap JJ, Otis TS, Petrou S, Pitt G, Schust LF, Taylor CM, Tjernagel J, Spiro JE, Bender KJ**.** Progress in understanding and treating SCN2A-mediated disorders. **Trends Neurosci** 41: 442–456, 2018. doi:10.1016/j.tins.2018.03.011.

314. Sundaram SK, Chugani HT, Tiwari VN, Huq AH**.** SCN2A mutation is associated with infantile spasms and bitemporal glucose hypometabolism. **Pediatr Neurol** 49: 46–49, 2013. doi:10.1016/j.pediatrneurol.2013.03.002.

315. Anderson PA, Greenberg RM**.** Phylogeny of ion channels: clues to structure and function. **Comp Biochem Physiol B Biochem Mol Biol** 129: 17–28, 2001. doi:10.1016/s1096-4959(01)00376-1.

316. Heinemann SH, Terlau H, Stuhmer W, Imoto K, Numa S. Calcium channel characteristics conferred on the sodium channel by single mutations. **Nature** 356: 441–443, 1992. doi:10.1038/356441a0.

317. Schlief T, Schonherr R, Imoto K, Heinemann SH. Pore properties of rat brain II sodium channels mutated in the selectivity filter domain. **Eur Biophys J** 25: 75–91, 1996. doi:10.1007/s002490050020.

318. Nelson AD, Bender KJ. Dendritic integration dysfunction in neurodevelopmental disorders. **Dev Neurosci** 43: 201–221, 2021. doi:10.1159/000516657.

319. Berg AT, Palac H, Wilkening G, Zelko F, Schust Meyer L. SCN2A-developmental and epileptic encephalopathies: challenges to trial-readiness for non-seizure outcomes. **Epilepsia** 62: 258–268, 2021. doi:10.1111/epi.16750.

320. Brennan KC, Pietrobon D. A systems neuroscience approach to migraine. **Neuron** 97: 1004–1021, 2018. doi:10.1016/j.neuron.2018.01.029.

321. Pietrobon D, Brennan KC. Genetic mouse models of migraine. **J Headache Pain** 20: 79, 2019. doi:10.1186/s10194-019-1029-5.

322. Schubert V, Auffenberg E, Biskup S, Jurkat-Rott K, Freilinger T. Two novel families with hemiplegic migraine caused by recurrent SCN1A mutation p.F1499L. **Cephalalgia** 38: 1503–1508, 2018. doi:10.1177/0333102417742365.

323. Auffenberg E, Hedrich UB, Barbieri R, Miely D, Groschup B, Wuttke TV, Vogel N, Luhrs P, Zanardi I, Bertelli S, Spielmann N, Gailus-Durner V, Fuchs H, Hrabe de Angelis M, Pusch M, Dichgans M, Lerche H, Gavazzo P, Plesnila N, Freilinger T. Hyperexcitable interneurons trigger cortical spreading depression in an Scn1a migraine model. **J Clin Invest** 131: e142202, 2021.

324. Dichgans M, Freilinger T, Eckstein G, Babini E, Lorenz-Depiereux B, Biskup S, Ferrari MD, Herzog J, van den Maagdenberg AM, Pusch M, Strom TM. Mutation in the neuronal voltage-gated sodium channel SCN1A in familial hemiplegic migraine. **Lancet** 366: 371–377, 2005. doi:10.1016/S0140-6736(05)66786-4.

325. DeKeyser JM, Thompson CH, George AL Jr. Cryptic prokaryotic promoters explain instability of recombinant neuronal sodium channels in bacteria. **J Biol Chem** 296: 100298, 2021. doi:10.1016/j.jbc.2021.100298.

326. Chen HM, DeLong CJ, Bame M, Rajapakse I, Herron TJ, McInnis MG, O'Shea KS. Transcripts involved in calcium signaling and telencephalic neuronal fate are altered in induced pluripotent stem cells from bipolar disorder patients. **Transl Psychiatry** 4: e375, 2014. doi:10.1038/tp.2014.12.

327. Ferreira MA, O'Donovan MC, Meng YA, Jones IR, Ruderfer DM, Jones L, et al. Collaborative genome-wide association analysis supports a role for ANK3 and CACNA1C in bipolar disorder. **Nat Genet** 40: 1056–1058, 2008. doi:10.1038/ng.209.

328. Hatzimanolis A, Smyrnis N, Avramopoulos D, Stefanis CN, Evdokimidis I, Stefanis NC. Bipolar disorder ANK3 risk variant effect on sustained attention is replicated in a large healthy population. **Psychiatr Genet** 22: 210–213, 2012. doi:10.1097/YPG.0b013e328353ae79.

329. Leussis MP, Madison JM, Petryshen TL. Ankyrin 3: genetic association with bipolar disorder and relevance to disease pathophysiology. **Biol Mood Anxiety Disord** 2: 18, 2012. doi:10.1186/2045-5380-2-18.

330. Muhleisen TW, Leber M, Schulze TG, Strohmaier J, Degenhardt F, Treutlein J, et al. Genome-wide association study reveals two new risk loci for bipolar disorder. **Nat Commun** 5: 3339, 2014. doi:10.1038/ncomms4339.

331. Roussos P, Haroutunian V. Schizophrenia: susceptibility genes and oligodendroglial and myelin related abnormalities. **Front Cell Neurosci** 8: 5, 2014. doi:10.3389/fncel.2014.00005.

332. Craddock N, Sklar P. Genetics of bipolar disorder. **Lancet** 381: 1654–1662, 2013. doi:10.1016/S0140-6736(13)60855-7.

333. Schizophrenia Psychiatric Genome-Wide Association Study Consortium. Genome-wide association study identifies five new schizophrenia loci. **Nat Genet** 43: 969–976, 2011. doi:10.1038/ng.940.

334. Villacres JE, Riveira N, Kim S, Colgin LL, Noebels JL, Lopez AY. Abnormal patterns of sleep and waking behaviors are accompanied by neocortical oscillation disturbances in an Ank3 mouse model of epilepsy-bipolar disorder comorbidity. **Transl Psychiatry** 13: 403, 2023. doi:10.1038/s41398-023-02700-2.

335. Zhu S, Cordner ZA, Xiong J, Chiu CT, Artola A, Zuo Y, Nelson AD, Kim TY, Zaika N, Woolums BM, Hess EJ, Wang X, Chuang DM, Pletnikov MM, Jenkins PM, Tamashiro KL, Ross CA. Genetic disruption of ankyrin-G in adult mouse forebrain causes cortical synapse alteration and behavior reminiscent of bipolar disorder. **Proc Natl Acad Sci USA** 114: 10479–10484, 2017. doi:10.1073/pnas.1700689114.

336. Leussis MP, Berry-Scott EM, Saito M, Jhuang H, de Haan G, Alkan O, Luce CJ, Madison JM, Sklar P, Serre T, Root DE, Petryshen TL. The ANK3 bipolar disorder gene regulates psychiatric-related behaviors that are modulated by lithium and stress. **Biol Psychiatry** 73: 683–690, 2013. doi:10.1016/j.biopsych.2012.10.016.

337. Piguel NH, Yoon S, Gao R, Horan KE, Garza JC, Petryshen TL, Smith KR, Penzes P. Lithium rescues dendritic abnormalities in Ank3 deficiency models through the synergic effects of GSK3towardand cyclic AMP signaling pathways. **Neuropsychopharmacology** 48: 1000–1010, 2023. doi:10.1038/s41386-022-01502-2.

338. Usui N, Tian X, Harigai W, Togawa S, Utsunomiya R, Doi T, Miyoshi K, Shinoda K, Tanaka J, Shimada S, Katayama T, Yoshimura T. Length impairments of the axon initial segment in rodent models of attention-deficit hyperactivity disorder and autism spectrum disorder. **Neurochem Int** 153: 105273, 2022. doi:10.1016/j.neuint.2021.105273.

339. Ma F, Akolkar H, Xu J, Liu Y, Popova D, Xie J, Youssef MM, Benosman R, Hart RP, Herrup K. The amyloid precursor protein modulates the position and length of the axon initial segment. **J Neurosci** 43: 1830–1844, 2023. doi:10.1523/JNEUROSCI.0172-22.2023.

340. Hatch RJ, Wei Y, Xia D, Gotz J. Hyperphosphorylated tau causes reduced hippocampal CA1 excitability by relocating the axon initial segment. **Acta Neuropathol** 133: 717–730, 2017. doi:10.1007/s00401-017-1674-1.

341. Best MN, Lim Y, Ferenc NN, Kim N, Min L, Wang DB, Sharifi K, Wasserman AE, McTavish SA, Siller KH, Jones MK, Jenkins PM, Mandell JW, Bloom GS. Extracellular tau oligomers damage the axon initial segment. **J Alzheimers Dis** 93: 1425–1441, 2023. doi:10.3233/JAD-221284.

342. Sun X, Wu Y, Gu M, Liu Z, Ma Y, Li J, Zhang Y. Selective filtering defect at the axon initial segment in Alzheimer's disease mouse models. **Proc Natl Acad Sci USA** 111: 14271–14276, 2014. doi:10.1073/pnas.1411837111.

343. Sun X, Wu Y, Gu M, Zhang Y. miR-342-5p decreases ankyrin G levels in Alzheimer's disease transgenic mouse models. **Cell Rep** 6: 264–270, 2014. doi:10.1016/j.celrep.2013.12.028.

344. Jorgensen HS, Jensen DB, Dimintiyanova KP, Bonnevie VS, Hedegaard A, Lehnhoff J, Moldovan M, Grondahl L, Meehan CF. Increased axon initial segment length results in increased Na(+)

currents in spinal motoneurones at symptom onset in the G127X SOD1 mouse model of amyotrophic lateral sclerosis. **Neuroscience** 468: 247–264, 2021. doi:10.1016/j.neuroscience.2020.11.016.

345. Sasaki S, Maruyama S**.** Increase in diameter of the axonal initial segment is an early change in amyotrophic lateral sclerosis. **J Neurol Sci** 110: 114–120, 1992. doi:10.1016/0022-510x(92)90017-f.

346. Senol AD, Pinto G, Beau M, Guillemot V, Dupree JL, Stadelmann C, Ranft J, Lubetzki C, Davenne M**.** Alterations of the axon initial segment in multiple sclerosis grey matter. **Brain Commun** 4: fcac284, 2022. doi:10.1093/braincomms/fcac284.

347. Baalman KL, Cotton RJ, Rasband SN, Rasband MN**.** Blast wave exposure impairs memory and decreases axon initial segment length. **J Neurotrauma** 30: 741–751, 2013. doi:10.1089/neu.2012.2478.

348. Schafer DP, Jha S, Liu F, Akella T, McCullough LD, Rasband MN**.** Disruption of the axon initial segment cytoskeleton is a new mechanism for neuronal injury. **J Neurosci** 29: 13242–13254, 2009. doi:10.1523/JNEUROSCI.3376-09.2009.

349. Greer JE, Hanell A, McGinn MJ, Povlishock JT**.** Mild traumatic brain injury in the mouse induces axotomy primarily within the axon initial segment. **Acta Neuropathol** 126: 59–74, 2013. doi:10.1007/s00401-013-1119-4.

350. Harris AC Jr, Sun J, Jacobs KM**.** Concussive head trauma deranges axon initial segment function in axotomized and intact layer 5 pyramidal neurons. **J Neurotrauma** 41: 244–270, 2024. doi:10.1089/neu.2022.0469.

351. Song H, McEwan PP, Ameen-Ali KE, Tomasevich A, Kennedy-Dietrich C, Palma A, Arroyo EJ, Dolle JP, Johnson VE, Stewart W, Smith DH**.** Concussion leads to widespread axonal sodium channel loss and disruption of the node of Ranvier. **Acta Neuropathol** 144: 967–985, 2022. doi:10.1007/s00401-022-02498-1.

352. Tamada H, Kiryu-Seo S, Sawada S, Kiyama H**.** Axonal injury alters the extracellular glial environment of the axon initial segment and allows substantial mitochondrial influx into axon initial segment. **J Comp Neurol** 529: 3621–3632, 2021. doi:10.1002/cne.25212.